Title
THERMAL ANALYSIS OF THE STRIPA HEATER TEST DATA FROM THE FULL SCALE DRIFT

Author
Witherspoon, P.A.

Publication Date
1981-08-01

LBL-13217 c.2
SAC-43
UC-70

SWEDISH-AMERICAN COOPERATIVE PROGRAM ON RADIOACTIVE WASTE STORAGE IN MINED CAVERNS IN CRYSTALLINE ROCK

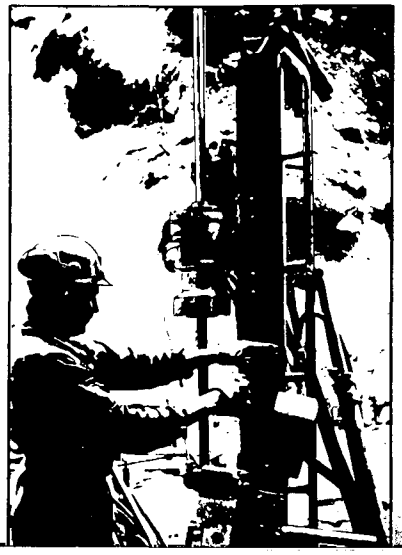

Technical Information Report No. 43

THERMAL ANALYSIS OF THE STRIPA HEATER TEST DATA FROM THE FULL SCALE DRIFT

I. Javandel and P. A. Witherspoon

Lawrence Berkeley Laboratory
University of California
Berkeley, California 94720

August 1981

A Joint Project of

Swedish Nuclear Fuel Supply Co.
Fack 10240 Stockholm, Sweden

Operated for the Swedish
Nuclear Power Utility Industry

Lawrence Berkeley Laboratory
Earth Sciences Division
University of California
Berkeley, California 94720, USA

Operated for the U.S. Department of
Energy under Contract DE-AC03-76SF00098

DISCLAIMER

LBL-13217
SAC 43
UC-70

THERMAL ANALYSIS OF THE STRIPA HEATER TEST DATA FROM THE FULL SCALE DRIFT

Iraj Javandel and Paul A. Witherspoon
Earth Sciences Division
Lawrence Berkeley Laboratory
Berkeley, California 94720

August, 1981

This work was supported by the Assistant Secretary for Nuclear Energy, Office of Waste Isolation of the U.S. Department of Energy under contract DE-AC03-76SF00098 Funding for this project is administered by the Office of Nuclear Waste Isolation at Battelle Memorial Institute.

PREFACE

This report is one of a series documenting the results of the Swedish-American cooperative research program in which the cooperating scientists explore the geological, geophysical, hydrological, geochemical, and structural effects anticipated from the use of a large crystalline rock mass as a geologic repository for nuclear waste. This program has been sponsored by the Swedish Nuclear Power Utilities through the Swedish Nuclear Fuel Supply Company (SKBF), and the U.S. Department of Energy (DOE) through the Lawrence Berkeley Laboratory.

The principal investigators are L.B. Nilsson and O. Degerman for SKBF, and N.G.W. Cook, P.A. Witherspoon, and J.E. Gale for LBL. Other participants will appear as authors of the individual reports.

Previous technical reports in this series are listed below.

1. Swedish-American Cooperative Program on Radioactive Waste Storage in Mined Caverns by P.A. Witherspoon and O. Degerman. (LBL-7049, SAC-01).

2. Large Scale Permeability Test of the Granite in the Stripa Mine and Thermal Conductivity Test by Lars Lundstrom and Haken Stille. (LBL-7052, SAC-02).

3. The Mechanical Properties of the Stripa Granite by Graham Swan. (LBL-7074, SAC-03).

4. Stress Measurements in the Stripa Granite by Hans Carlsson. (LBL-7078, SAC-04).

5. Borehole Drilling and Related Activities at the Stripa Mine by P.J. Kurfurst, T. Hugo-Persson, and G. Rudolph. (LBL-7080, SAC-05).

6. A Pilot Heater Test in the Stripa Granite by Hans Carlsson. (LBL-7086, SAC-06).

7. An Analysis of Measured Values for the State of Stress in the Earth's Crust by Dennis B. Jamison and Neville G.W. Cook. (LBL-7071, SAC-07).

8. Mining Methods Used in the Underground Tunnels and Test Rooms at Stripa by B. Andersson and P.A. Halen. (LBL-7081, SAC-08).

9. Theoretical Temperature Fields for the Stripa Heater Project by T. Chan, Neville G.W. Cook, and C.F. Tsang. (LBL-7082, SAC-09).

10. Mechanical and Thermal Design Considerations for Radioactive Waste Repositories in Hard Rock. Part I: An Appraisal of Hard Rock for Potential Underground Repositories of Radioactive Waste by N.G.W. Cook; Part II: In Situ Heating Experiments in Hard Rock: Their Objectives and Design by N.G.W. Cook and P.A. Witherspoon. (LBL-7073, SAC-10).

11. Full-Scale and Time-Scale Heating Experiments at Stripa: Preliminary Results by N.G.W. Cook and M. Hood. (LBL-7072, SAC-11).

12. Geochemistry and Isotope Hydrology of Groundwaters in the Stripa Granite: Results and Preliminary Interpretation by P. Fritz, J.F. Barker, and J.E. Gale. (LBL-8285, SAC-12).

13. Electrical Heaters for Thermo-Mechanical Tests at the Stripa Mine by R.H. Burleigh, E.P. Binnall, A.O. DuBois, D.O. Norgren, and A.R. Ortiz. (LBL-7063, SAC-13).

14. Data Acquisition, Handling, and Display for the Heater Experiments at Stripa by Maurice B. McEvoy. (LBL-7063, SAC-14).

15. An Approach to the Fracture Hydrology at Stripa: Preliminary Results by J.E. Gale and P.A. Witherspoon. (LBL-7079, SAC-15).

16. Preliminary Report on Geophysical and Mechanical Borehole Measurements at Stripa by P. Nelson, B. Paulsson, R. Rachiele, L. Andersson, T. Schrauf, W. Hustrulid, O. Duran, and K.A. Magnussen. (LBL-8280, SAC-16).

17. Observations of a Potential Size-Effect in Experimental Determination of the Hydraulic Properties of Fractures by P.A. Witherspoon, C.H. Amick, J.E. Gale, and K. Iwai. (LBL-8571, SAC-17).

18. Rock Mass Characterization for Storage in Nucler Waste in Granite by P.A. Witherspoon, P. Nelson, T. Doe, R. Thorpe, B. Paulsson, J.E. Gale, and C. Forster. (LBL-8570, SAC-18).

19. Fracture Detection in Crystalline Rock Using Ultrasonic Shear Waves by K.H. Waters, S.P. Palmer, and W.F. Farrell. (LBL-7051, SAC-19).

20. Characterization of Discontinuities in the Stripa Granite--Time Scale Heater Experiment by R. Thorpe. (LBL-7083, SAC-20).

21. Geology and Fracture System at Stripa by A. Okliewicz, J.E. Gale, R. Thorpe, and B. Paulsson. (LBL-8907, SAC-21).

22. Calculated Thermally Induced Displacements and Stresses for Heater Experiements at Stripa by T. Chan and N.G.W. Cook. (LBL-7061, SAC-22).

23. Validity of Cubic Law for Fluid Flow in a Deformable Rock Fracture by P.A. Witherspoon, J. Wang, K. Iwai, and J.E. Gale. (LBL-9557, SAC-23).

24. Determination of In-Situ Thermal Properties of Stripa Granite from Temperature Measurements in the Full-Scale Heater Experiments: Methods and Primary Results by J. Jeffry, T. Chan, N.G.W. Cook and P.A. Witherspoon. (LBL-8424, SAC-24).

25. Instrumentation Evaluation, Calibration, and Installation for Heater Tests Simulating Nuclear Waste in Crystalline Rock, Sweden by T. Schrauf, H. Pratt, E. Simonson, W. Hustrulid, P. Nelson, A. DuBois, E. Binnall, and R. Haught. (LBL-8313, SAC-25)

26. Part I: Some Results From a Field Investigation of Thermo-Mechanical Loading of a Rock Mass When Heater Canisters are Emplaced in the Rock by M. Hood. Part II: The Application of Field Data from Heater Experiments Conducted at Stripa, Sweden for Repository Design by M. Hood, H. Carlsson, and P.H. Nelson. (LBL-9392, SAC-26).

27. Progress with Field Investigations at Stripa by P.A. Witherspoon, N.G.W. Cook, and J.E. Gale (LBL-10559, SAC-27).

28. A Laboratory Assessment of the Use of Borehole Pressure Transients to Measure the Permeability of Fractured Rock Masses by C.B. Forster and J.E. Gale. (LBL-8674, SAC-28).

29. Thermal and Thermomechanical Data for In Situ Heater Experiments at Stripa, Sweden by T. Chan, E. Binnall, P. Nelson, O. Wan, C. Weaver, K. Ang, J. Braley, and M. McEvoy. (LBL-11477, SAC-29).

30. The Effect of Radon Transport in Groundwater Upon Gamma Ray Borehole Logs by P.H. Nelson, R. Rachiele, and A. Smith. (LBL-11180, SAC-30).

31. Strength and Permeability Tests on Ultra-Large Stripa Granite Core by R. Thorpe, D.J. Watkins, W.E. Ralph, R. Hsu, and S. Flexser. (LBL-11203, SAC-31).

32. Ultrasonic and Acoustic Emission Results from the Stripa Heater Experiments. Part I: A Cross-Hole Investigation of a Rock Mass Subjected to Heating by B.N.P. Paulsson and M.S. King. Part II: Acoustic Emission Monitoring During Cool-Down of the Stripa Heater Experiment by R. Rachiele. (LBL-10975, SAC-32).

33. Numerical Modeling to Assess Possible Influence of the Mine Openings on Far-Field In Situ Stress Measurements at Stripa by T. Chan, V. Guvanasen, and N. Littlestone (LBL-12469, SAC-33).

34. A Field Assessment of the Use of Borehole Pressure Transients to Measure the Permeability of Fractured Rock Masses by C.B. Forster and J.E. Gale. (LBL-11829, SAC-34).

35. Water Inflow into Boreholes During the Stripa Experiments by P.H. Nelson, R. Rachiele, J.S. Remer and H.S. Carlsson (LBL-12547, SAC-35).

36. Petrology and Radiogeology of the Stripa Pluton by H. Wollenberg, S. Flexser, and L. Andersson. (LBL-11654, SAC-36).

37. Geohydrological Data from the Macopermeability Experiment at Stripa, Sweden by C.R. Wilson, J.C.S. Long, R.M. Galbraith, K. Karasaki, H.K. Endo, A.O. DuBois, M.J. McPherson, and G. Ramqvist. (LBL-12520, SAC-37).

38. Characterization of Discontinuities in the Stripa Granite--Full-Scale Heater Experiments by B.N.P. Paulsson, P.H. Nelson, and P.J. Kurfurst. (LBL-9063, SAC-38).

39. Application of Borehole Geophysics at an Experimental Waste Storage Site by P.H. Nelson, K.A. Magnusson, and R. Rachiele. (LBL-11982, SAC-39).

40. Laboratory Investigations of Thermomechanical Properties of Stripa Granite by L. Myer and R. Rachiele. (LBL-13435, SAC-40)

41. Petrologic Changes and Damage in the Stripa Quartz Monzonite in Response to Heater Tests by S. Flexser, H. Wollenberg, and D.E. Wedge. (LBL-14929, SAC-41).

TABLE OF CONTENTS

LIST OF FIGURES

Page

Page

Page

Page

LIST OF TABLES

ABSTRACT

To investigate the thermomechanical behavior of a deep fractured crystalline rock subjected to the thermal loading of buried nuclear waste, two full-scale heater tests, among others, were carried out. These tests were performed at an approximate depth of 340 meters in a granitic rock adjacent to an inactive iron mine at Stripa, Sweden.

Temperature data from these tests have been analyzed and their reliability examined. Possible sources of error have been identified. A finite element code capable of handling nonuniform initial temperature distribution as well as nonlinear heat conduction has been used for predicting the test results; this calculation is in good agreement with the field data.

The temperature data analysis indicates that, as far as the thermal field is concerned, this fractured granite behaves very much like a continuous, homogeneous, and isotropic medium.

1. INTRODUCTION

The thermomechanical behavior of a deep, fractured crystalline rock used for isolation of high-level nuclear waste was tested through a series of experiments conducted in granitic rock at Stripa, Sweden, in a site adjacent to an inactive iron mine (Witherspoon and Degerman, 1978). These tests included two "full-scale" heating experiments and a "time-scaled" heating experiment, all carried out at a depth of approximately 340 m.

The full-scale experiments were designed to study the near-field effects of heating the rock by a nuclear waste canister with two different thermal power levels. One of these experiments was later supplemented by eight peripheral heaters to account for the interaction of the surrounding waste canisters.

The time-scaled experiment, which was based on the assumption of linear conduction of heat flow in solids, was designed to investigate, within a one-year period, the response that the rock would make to heating by several canisters over 10 years (Cook and Witherspoon, 1978).

In this report, we shall concentrate on the analysis of thermal data collected from the two full-scale experiments.

1.1 Site and Setup of the Experiments

The site was excavated in granitic rock intruded by diabase and pegmatite dikes. Mapping of the drifts and core data from boreholes has shown that the rock is highly fractured. At least four sets of joints have been identified

in the test area (Olkiewicz et al., 1979). In addition, fissures, fracture zones and small-scale shear zones have been located. Pegmatite offsets of 1 to 2 meters caused by small local faults have been observed. It is believed that all connected fractures in the site were water-saturated before excavation.

Figure 1 illustrates the location of experimental rooms at Stripa. Figure 2 shows the layout of the two full-scale experiments. Details of the setup have been given in other reports (Witherspoon and Degerman, 1978, and Kurfurst et al., 1978).

Experiment 1 was located at the end of the full-scale drift and was energized by an electrical heater with a constant power of 3.6 kW to represent the initial thermal output of a canister of reprocessed high-level waste after approximately 5 years. This heater, which had a diameter of 0.324 m and a length of 2.60 m was placed in a vertical borehole with a diameter of 0.406 m, identified as H-9 in Fig. 2. Construction details of the heaters are given by Burleigh et al. (1979).

Experiment 2, located close to the the entrance of the full-scale drift, used a main heater with the same dimensions as the first but with a constant power of 5 kW, corresponding to a waste canister approximately 3.5 years old at the time of emplacement. This heater was placed in borehole H-10, of the same diameter as H-9. Center-to-center distance of these two heaters was 22 m, which, in effect, thermally separated the two experiments for the duration of the tests.

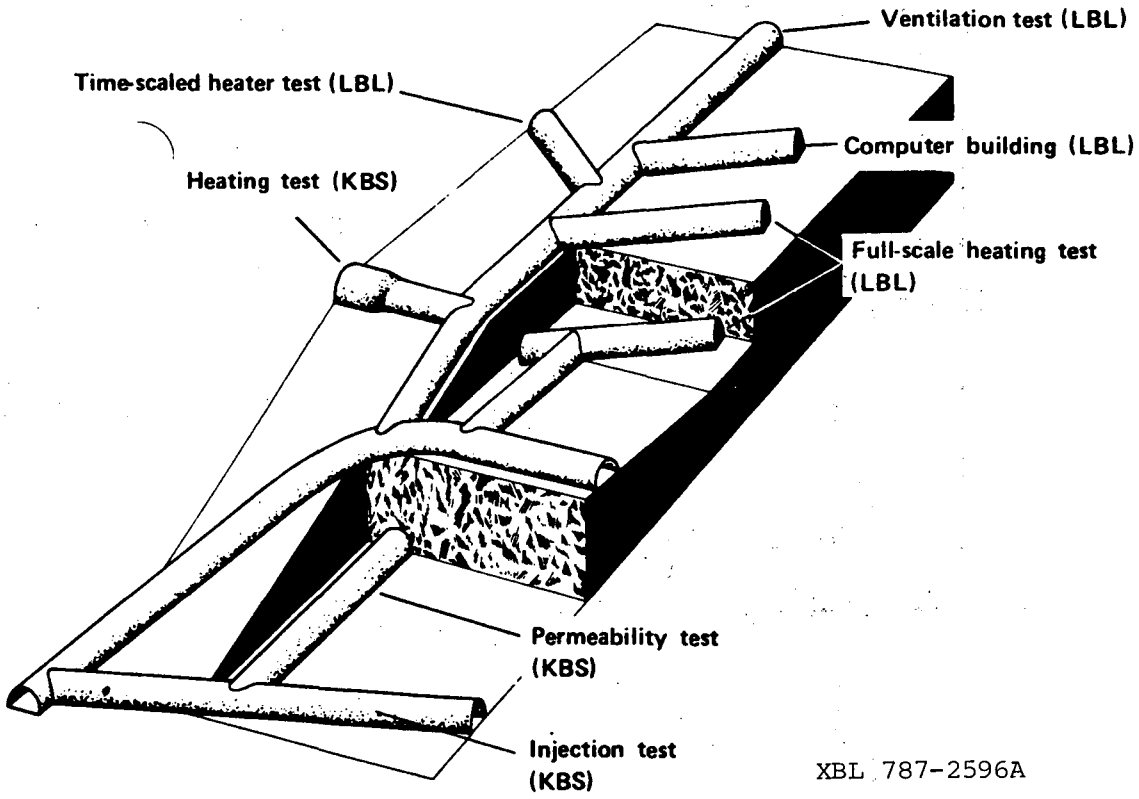

Fig. 1. Location of experimental rooms (from Witherspoon et al., 1978).

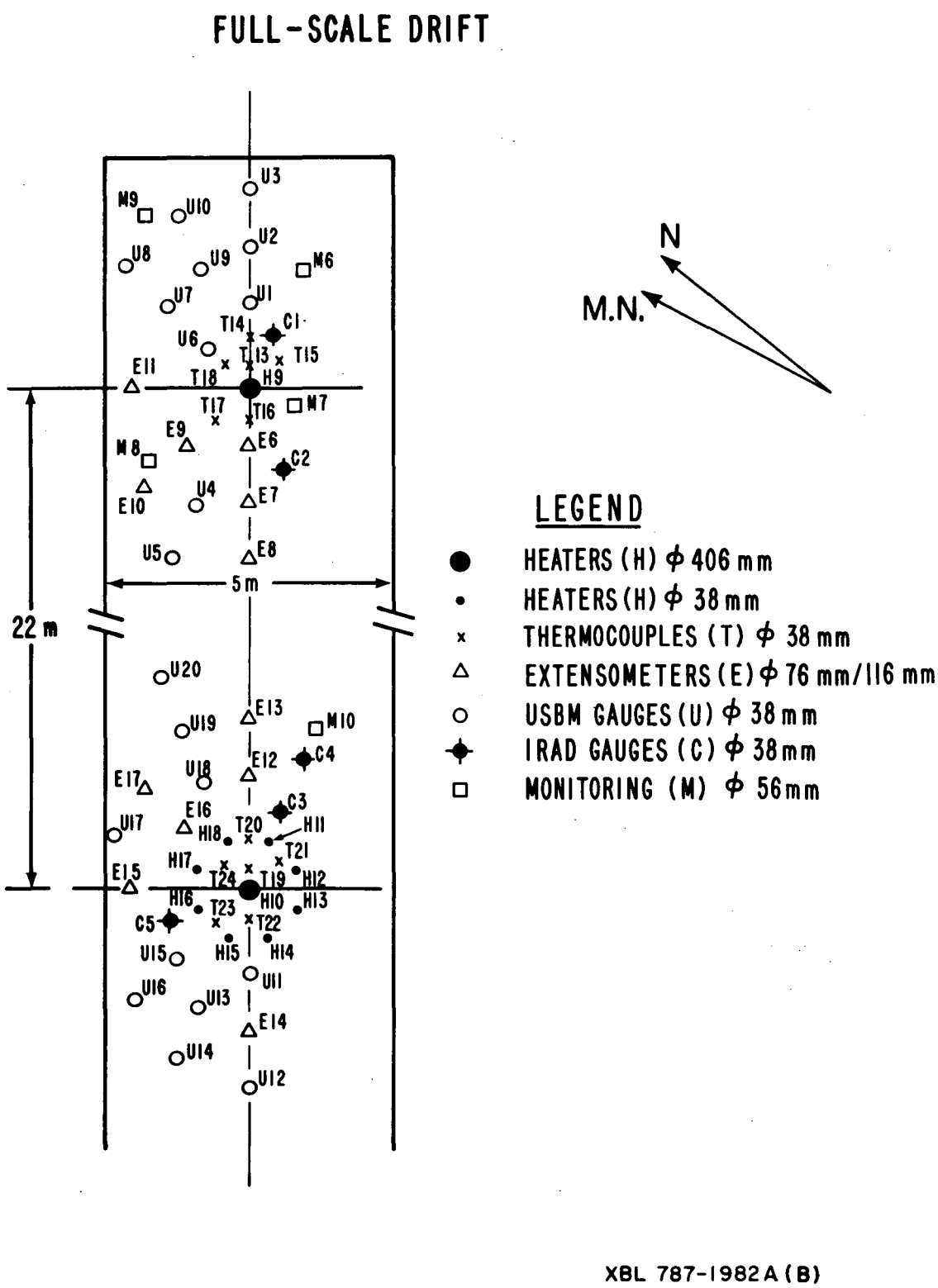

Fig. 2. Layout of the two full-scale experiments (from Kurfurst et al., 1978). The heaters simulating waste canisters are at H9 and H10.

Eight other heaters, each with a diameter of 0.027 m and a length of 4.3 m, were placed in boreholes H-11 through H-18 around the main heater in H-10. The distance between the axis of the main heater and each peripheral heater was 0.9 m. The power of the peripheral heaters was 1 kW each, and they were energized 204 days after the main heater turn-on. After 40 days of operation, power was reduced to 0.85 kW each.

Figure 3 shows a simplified cross section of an emplaced main heater. There is an annular gap of 41 mm of air between the heater wall and the rock. This gap was intended to simulate the spacing between a nuclear waste canister and the rock, since it is believed that such an air gap is unavoidable (Lowry, et al, 1980).

For the peripheral heaters, this gap was only 5.5 mm. Their vertical position was supposed to be such that their midplanes would coincide with that of the main heater.

The two main heaters were set upon a layer of pea gravel. Any volume of water that found its way into the hole should have ended up in the gravel pack, which was drained by a dewatering system. The space above the main heaters was partially filled with vermiculite, an insulating material. No dewatering device or insulating material was provided for the peripheral heaters.

Both experiments were provided with several kinds of measuring devices in both vertical and horizontal holes around the heaters. Details of the installation and calibration of these instruments have been reported by

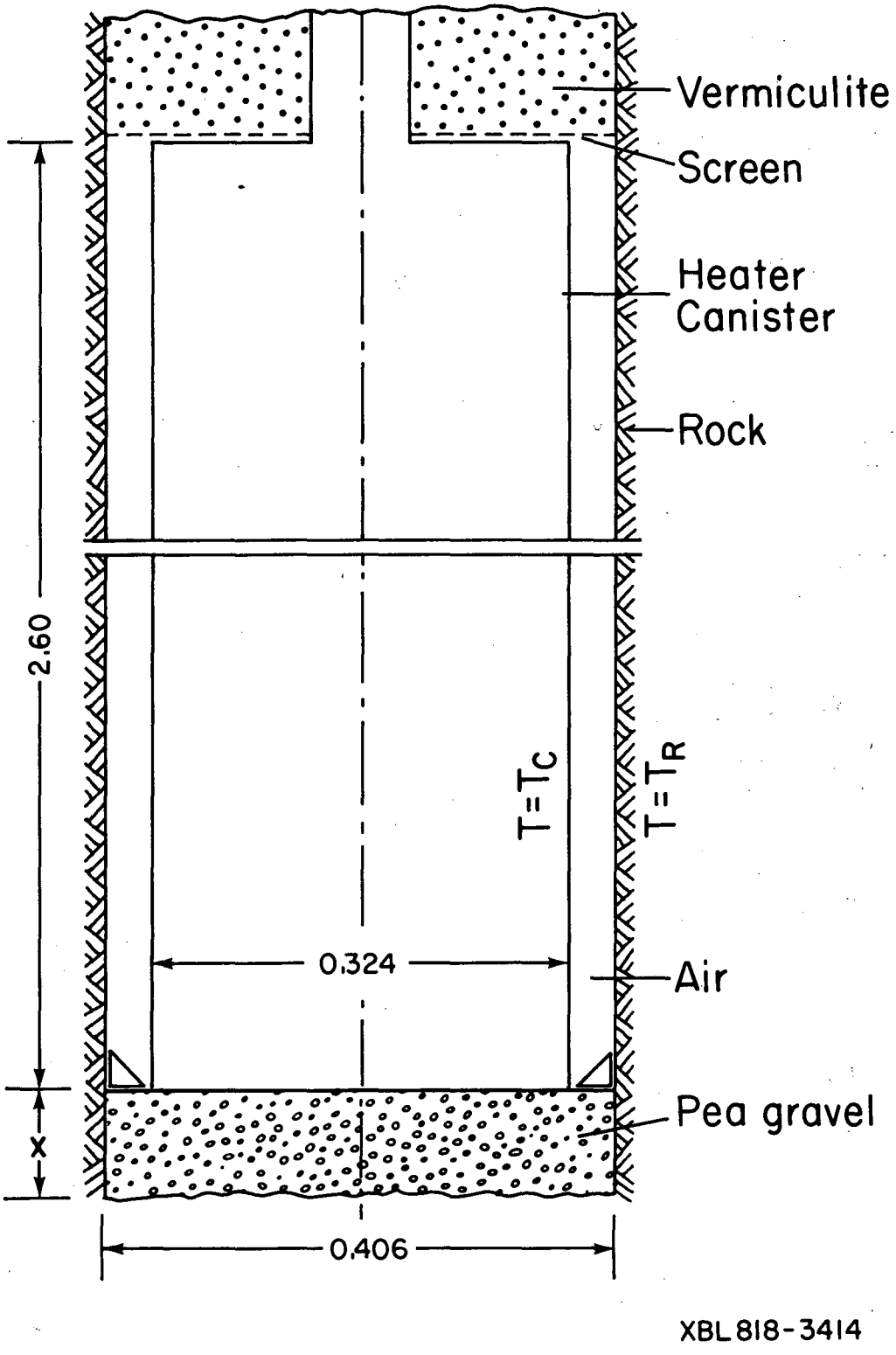

Fig. 3. Simplified cross section of a main heater emplaced in borehole.

Schrauf et al. (1979). In addition to monitoring the heating elements themselves, rock temperature and displacement and stress changes due to thermal loading were the main quantities measured. The design positions of all sensors are also given by Schrauf et al. (1979). (During data analysis, it was found that some of the sensors were not exactly at their design positions; the discriepancies are discussed at length later in this report).

A computer-based data acquisition system stored data from sensors on magnetic tapes. Three data-logger systems were also installed to collect data and provide back-up in case of computer failure. Details are described by McEvoy (1979).

Finally, all these data have been organized and converted into engineering units and are now available in the public domain (Chan et al., 1980a).

1.2 Previous Work

The following is a short review of earlier studies of heat transfer at this site.

Calculations were performed before the experiments to predict the temperature field qenerated by the heaters (Chan et al., 1978). These calculations used a closed-form integral solution derived from theories of finite line sources and Green's function (Carslaw and Jeager, 1959; Saad, 1960). Application of this solution was based on the following assumptions:

(a) the rock medium is continuous, homogeneous, and isotropic;

(b) the radius of the heater is infinitesimal;

(c) conduction is the only mode of heat transfer;

(d) the heaters are in perfect thermal contact with the rock;

(e) initial rock temperature around the heater is uniform;

(f) thermal conductivity of the rock is constant and independent of the temperature;

(g) heat generation along the total length of line source is uniform;

(h) the rock medium is either infinite or semi-infinite.

In the semi-infinite case, the rock was assumed to be bounded above by an imaginary plane coinciding with the floor of the heater drift. The upper plane could be either isothermal or adiabatic. Chan et al. (1978) have also examined the close-form analytic solution that considers a cylindrical rather than a line source. Numerical comparison of these two cases indicated that, except for short periods of time (less than a day), temperature increases in the rock are identical.

Thermal properties of the Stripa granite were determined in the laboratory (Pratt et al., 1977). The density (ρ) and specific heat (c) of the rock sample were found to be independent of the temperature and to be given by:

$$\rho = 2600 \text{ kg/m}^3$$

$$c = 824 \text{ J/kg-°C}$$

However, thermal conductivity was found to be temperature dependent and its value is given by the equation:

$$k(T) = 3.6 - 0.0037T \text{ W/m°C.}$$

Since the analytical solution can handle only constant thermal conductivity, a value of k = 3.2 W/m°C corresponding to T = 108°C was employed for preliminary prediction of the thermal field around the heaters.

Cook and Hood (1978) conducted a preliminary comparison of the predicted temperatures with data from the heater tests. They noticed that measured temperatures at the midplane of the 5kW heater 65 days after turn-on were, in general, slightly lower than predicted. They report no gross evidence of thermal anisotropy or of heat transfer other than by conduction.

A comparison of temperatures calculated by the analytical method and of actual temperature readings after 100 days for the midplane of the 3.6 kW heater seems to confirm the conclusions reached by Cook and Hood (Chan et al., 1980b). However, at other elevations than the midplane, some discrepancies between measured and calculated data for the 3.6 kW heater were reported (Chan et al., 1980b). Several possible causes of these discrepancies have been suggested; these possibilities will be discussed in later chapters.

In situ thermal properties of the Stripa granite have been statistically calculated from data for the 5 kW heater at early times (Jeffry et al., 1979). As far as thermal conductivity is concerned, these results are very close to the values measured in the laboratory.

1.3 Scope of the Present Study

We shall first examine how and where the thermal data have been measured in the full-scale experiments. Then we shall examine the data to see how reliable they are and identify possible sources of error. An attempt will be made to develop a numerical model capable of predicting the thermal field induced by heat from nuclear waste canisters. The results of this model will be verified with the experimental data obtained from the heater tests. We shall also address the shortcomings of the present work.

2. EVALUATION AND INTERPRETATION OF THE MEASURED DATA

In this chapter, we shall describe how and where the thermal data were measured. Then we shall examine the data for reliability and look for possible sources of error.

2.1 Sources of Temperature Data

Thermocouples were placed in different types of holes to measure the temperature not only of the rock but of some instruments. T-holes were dedicated to the measurement of rock temperatures, while thermocouples in E-holes and in C- and U-holes recorded the temperatures of extensometer rods and of stress and borehole-deformation gauges. Each type of hole is discussed below. Output in millivolts was recorded on magnetic tape before conversion into temperature units. A back-up system of data loggers independently recorded temperatures in degrees Celsius. A microprocessor built into each data logger converted the thermocouple voltage output into degrees Celsius. The quality of the measured temperatures will be discussed, and a basis will be set for choosing reliable results.

2.1.1 T-Holes

Six 38-mm T-holes around each of the two full-scale heaters (see Fig. 2) were especially designed for temperature measurement. Five thermocouples were installed in each T-hole. One was at the midplane elevation, a horizontal plane passing through the center of the main heater. The others were placed 1.5 and 3.0 m above and below the midplane. After installing the thermocouples and a dewatering system at the bottom of each hole, the holes were filled with sand. Some 15 cm of fiber glass separated the sand-filled section from the lower part of the hole. A rubber cork at the mouth of each hole separated

the equipment from the open room. Figure 4 shows the typical setup. The T-holes were arranged in different directions at nominal distances of 0.4, 0.5, 0.6, 0.7, 0.8, and 0.9 m from the axis of the main heater.

Although the thermocouples were not directly in contact with the rock (the small gap between the beads of the thermocouple and the rock was filled with sand) each one was supposed to measure rock temperatures at a particular coordinate. This assumption is reasonably correct if conduction is the only mode of heat transfer within the hole. The recorded data, however, show some periods when water coming into the hole through the cracks came in contact with sand heated above 100°C. Under such circumstances, the water will take heat from the sand and vaporize to steam. If a thermocouple is nearby, its temperature will be lowered. The ascending steam will then warm up thermocouples located above that point.

The interesting condition is when the rock temperature itself is over 100°C; no water can then exist in the cracks. Water that approached thermocouples where the rock was above 100°C must therefore have entered the hole from a point above, where the rock was cooler. This suggests that some of the data collected from such thermocouples does not represent the true rock temperature at those times. Although such data may be used for a more detailed analysis, for temperature distribution in the rock itself, they are not admissible, for they do not show the true rock temperature and therefore cannot be compared with temperature fields based on conduction.

Some data from these holes also have been eliminated because of instrument

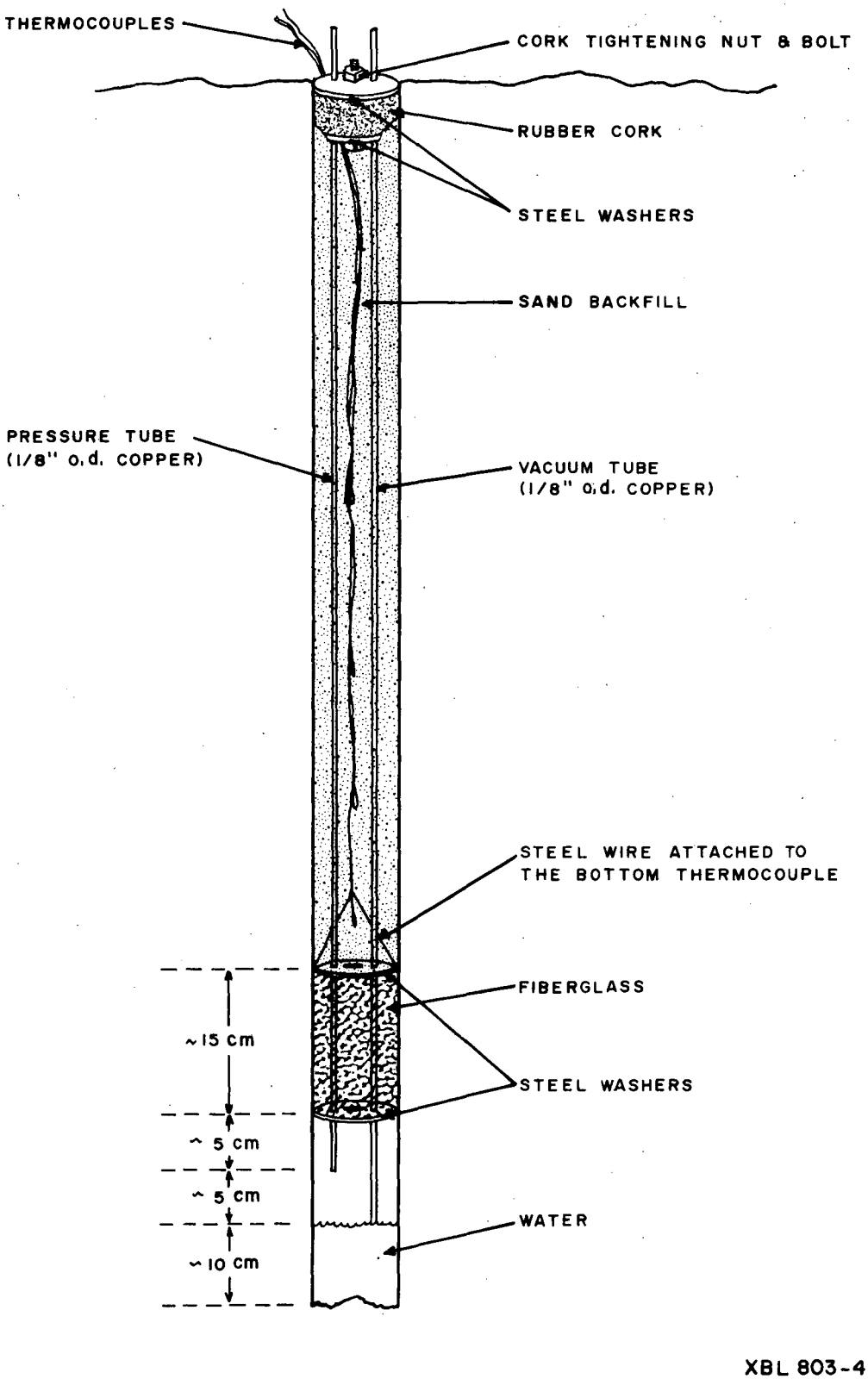

Fig. 4. Arrangement of a thermocouple hole (from Schrauf et al., 1979).

failures. An example is the failure of stainless steel thermocouple sheaths due to corrosion. Although corroded thermocouples were gradually replaced, part of the data they registered had to be separated and eliminated. These data obviously do not match the temperatures predicted by the model.

Inaccurately positioned thermocouples can also be a source of error. Temperatures recorded by thermocouples suspected to have been installed at incorrect coordinates, including some that replaced corroded instruments, have been deleted.

Detecting this type of error can be difficult because thermocouple position cannot be checked after installation without disturbing the setup. For this reason, the instruments were positioned and installed with care to obviate this problem as much as possible. However, since temperatures in the area adjacent to the heater are very sensitive to the position of the thermocouple, we might detect gross dislocations by careful examination of data. The amount of thermocouple dislocation in a horizontal direction could be as much as 1.9 cm from the borehole center line. In the vertical direction it is relatively unlimited.

Another source of error lies in the accuracy of the thermocouples themselves, a matter that has been extensively studied (Binnall and McEvoy, 1982). The output of the thermocouple is in millivolts, which has to be converted into units of temperature. For this reason, all the original thermocouples were carefully calibrated over an applicable temperature range. Binnall and McEvoy (1982) reported that the range of error in this respect

was ± 0.5°C. Although none of the replacement thermocouples was calibrated before installation, most were checked at the end of the experiment, and they did not indicate errors over 2°C.

2.1.2 E-Holes

Six vertical E-holes surrounded each full-scale heater and were located at nominal distances of 1.0, 1.5, 2.0, 2.5, and 3.0 m from the axis of the main heaters (Fig. 2). Four to six thermocouples were placed in each hole. The thermocouples were attached to a Superinvar rod anchored inside the hole for displacement measurement. The main purpose of these thermocouples was to measure the temperature of the rod itself rather than the rock at that position. The rock was separated from the rod by a silicon rubber tube, a flexible conduit, and a layer of air. However, most of the thermocouples were located at an anchor, where the rods were in contact with each other and with the anchor metal, which itself was in a grout with about the same thermal conductivity as rock. Design details of the instrumentation in the E-holes is given by Schrauf et al. (1979).

Because these thermocouples were protected from water and steam, they did not corrode, although they are of the same type that corroded in the T-holes. Moreover, except for one hole, steam did not cause a warming and cooling problem. When steam did find its way into the protective conduit of one hole, it kept the temperature of three thermocouples at about the same temperature above 100°C until several days after turn-off and cooling, when each thermocouple registered the true temperature of its position. Thus these devices

did not actually register the true rock temperature. The exact temperature difference between the rock wall and the rod is not known. Results of some tests performed by Schrauf et al. (1979) indicated a difference of 15°C where vertical temperature gradients were about 90°C per meter.

In addition to the vertical E-holes, nine approximately horizontal E-holes were drilled from the extensometer drift toward each heater hole. Thermocouples were attached to the longest Superinvar rod in each hole.

2.1.3 C- and U-Holes

A total of 13 C-holes and 30 U-holes with diameters of 38 mm were drilled around the H-9 and H-10 heaters. These holes housed the IRAD and USBM gauges that measured stress changes and borehole deformations. Some holes were vertical and were located at half-meter intervals from 1 to 4 m from the axis line of the heaters. Some were approximately horizontal and were drilled from the extensometer drift.

One thermocouple was installed in each hole. In the case of the IRAD gauges, the thermocouples were connected to the dewatering tube close to the gauges but were not in contact with the rock. In the case of the USBM gauges, the thermocouples were connected directly to the gauges which were in contact with the rock.

A general source of error common to all of these temperature data was due to the computer hardware. During the course of the experiments, offsets were observed in the data recorded by the computer (Chan et al., 1980a). Some were due to the interchange of the circuit boards, but some cannot be explained.

Although all these data have been adjusted by comparison with values recorded separately by the back-up system, in order to be on the safe side and avoid any uncertainty, we have based our evaluation on the Autodata-Nine data-logger records, which seem to be quite stable and smooth. Other possible errors in temperature measurement have been fully described in previous reports (Chan et al. 1980a; and Binnall and McEvoy, 1982).

2.2 Evaluation of Thermal Data in the H-9 Area

The "H-9 area" is the volume of rock subjected to a significant temperature rise from the heater in the H-9 hole. Throughout this report, positions will be specified using a local cylindrical coordinate system with the axis of the full-scale main heater as the Z-axis. The plane $Z = 0$ is the design (horizontal) midplane of the heater. Above this plane, $Z > 0$.

The total time span of this experiment, about 1.5 years, may be divided into two consecutive periods, warm-up and cooling.

2.2.1 Warm-up Period (Aug. 24, 1978 to Sept. 26, 1979)

This period, which lasted 398 days, covers the time between heater turn-on and turn-off. To examine the near-field temperature data for this period, semi-log plots of temperature vs. time have been prepared from T-hole data. Figures 5 through 9 show these temperature histories for five elevations. At each level, six temperature sensors provided coverage for distances between 0.4 and 0.9 m from the heater. To avoid crowding in Figs. 5 and 9, the response of only two thermocouples has been plotted. Broken lines indicate periods when thermocouples either failed because of corrosion or were left

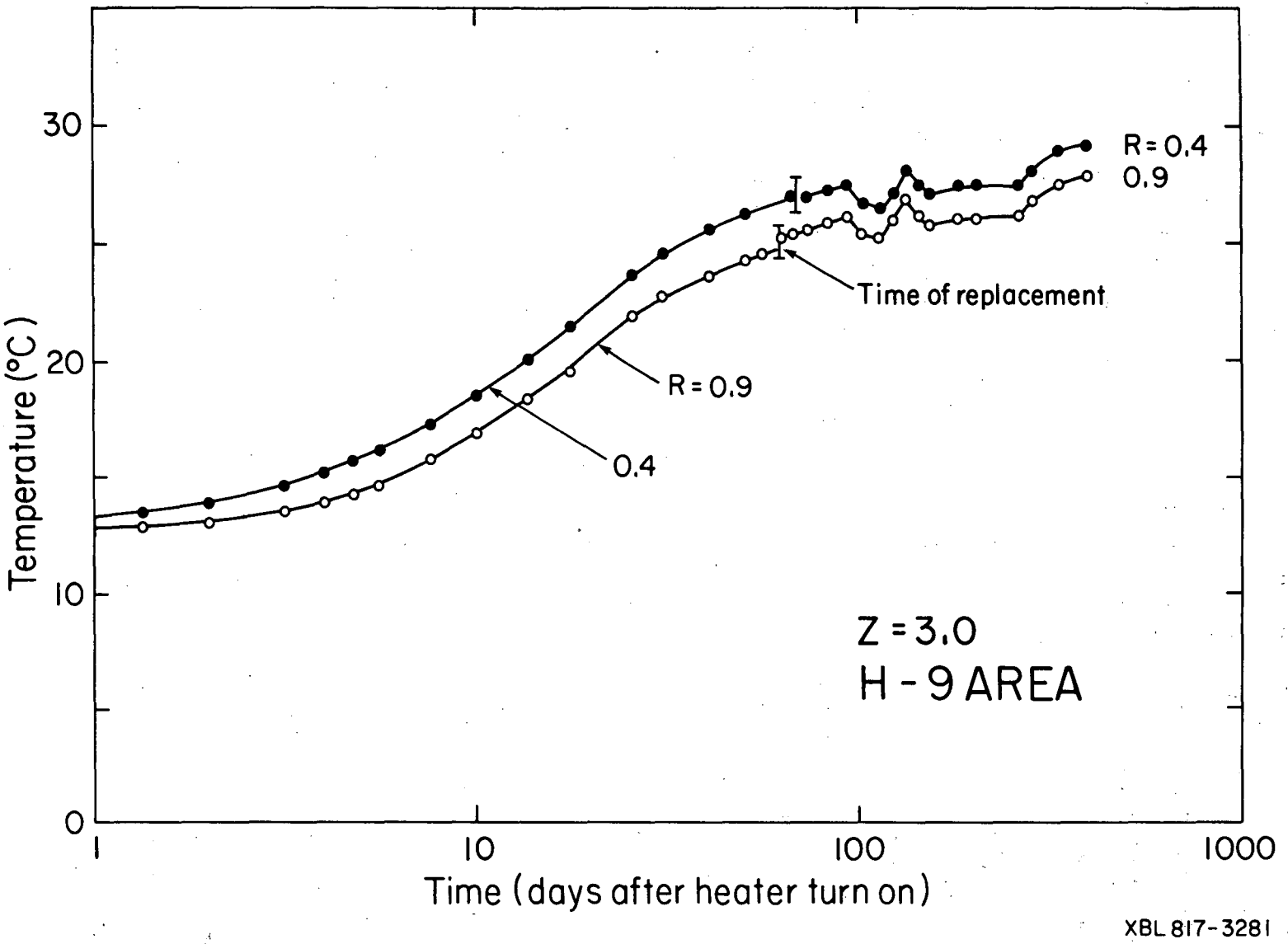

Fig. 5. Semi-log plot of measured temperatures versus time in the T-holes at elevation Z = 3.0 m, H-9 area.

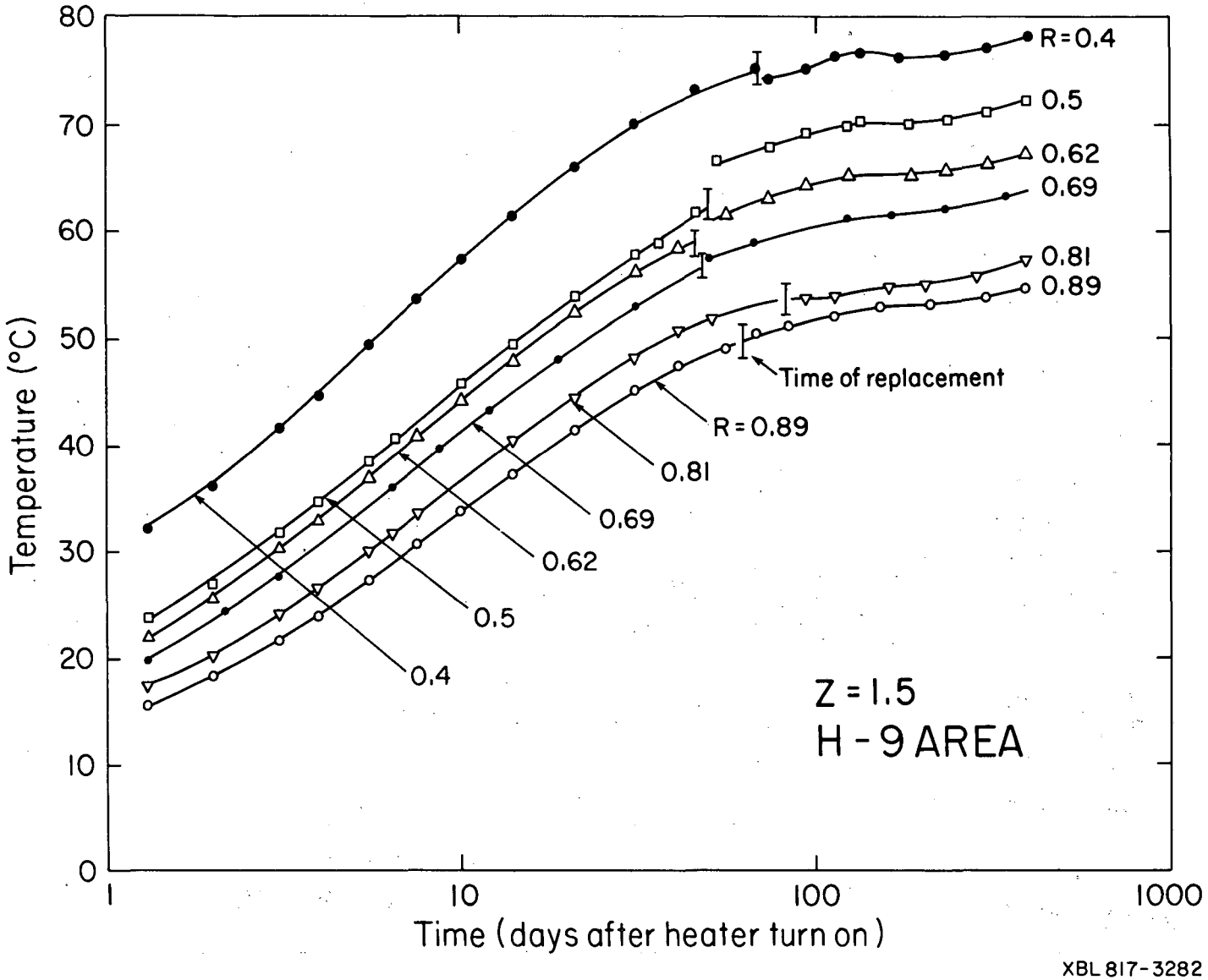

Fig. 6. Semi-log plot of measured temperatures versus time in the T-holes at elevation Z = 1.5 m, H-9 area.

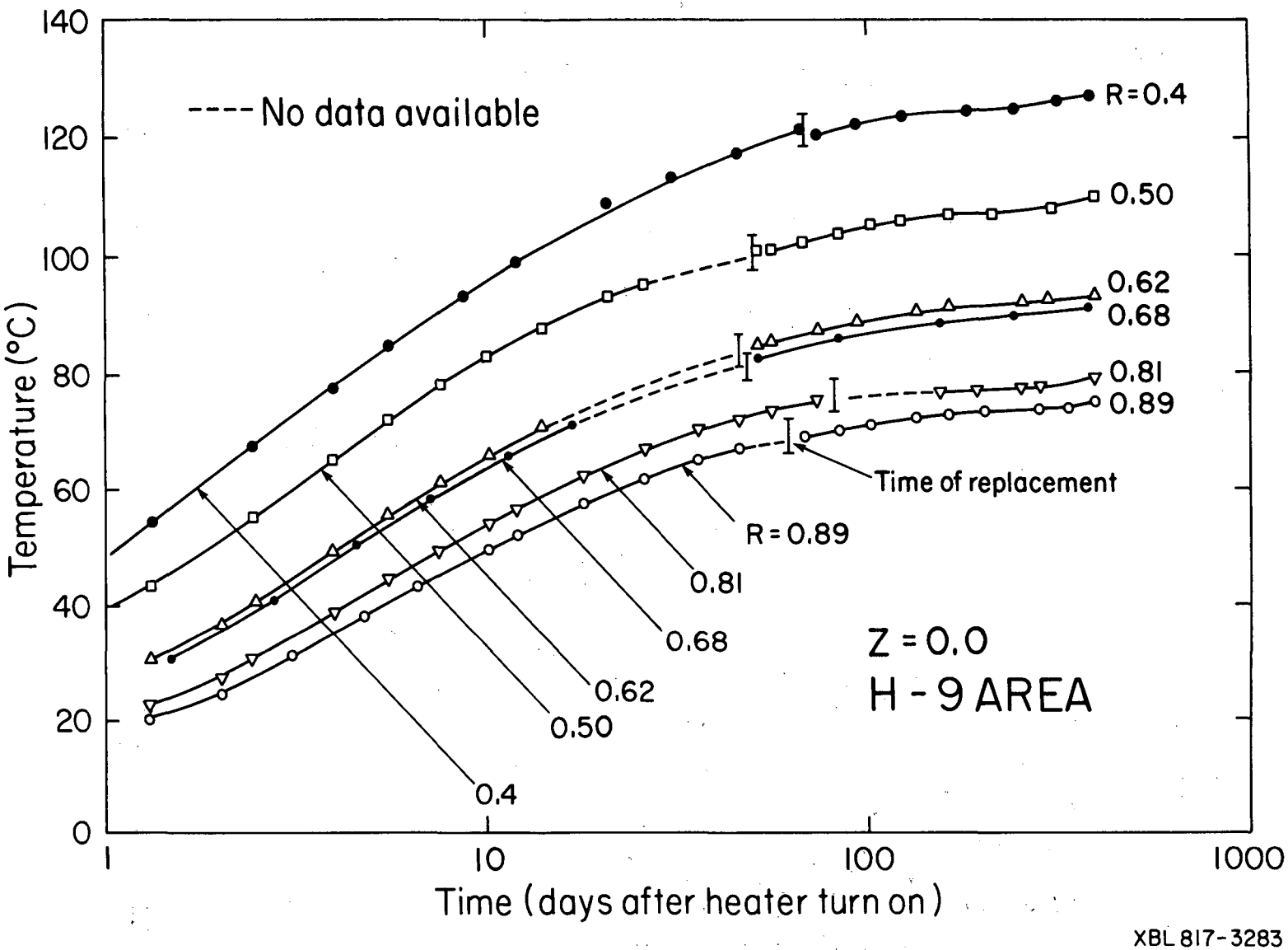

Fig. 7. Semi-log plot of measured temperatures versus time in the T-holes at elevation Z = 0.0, H-9 area.

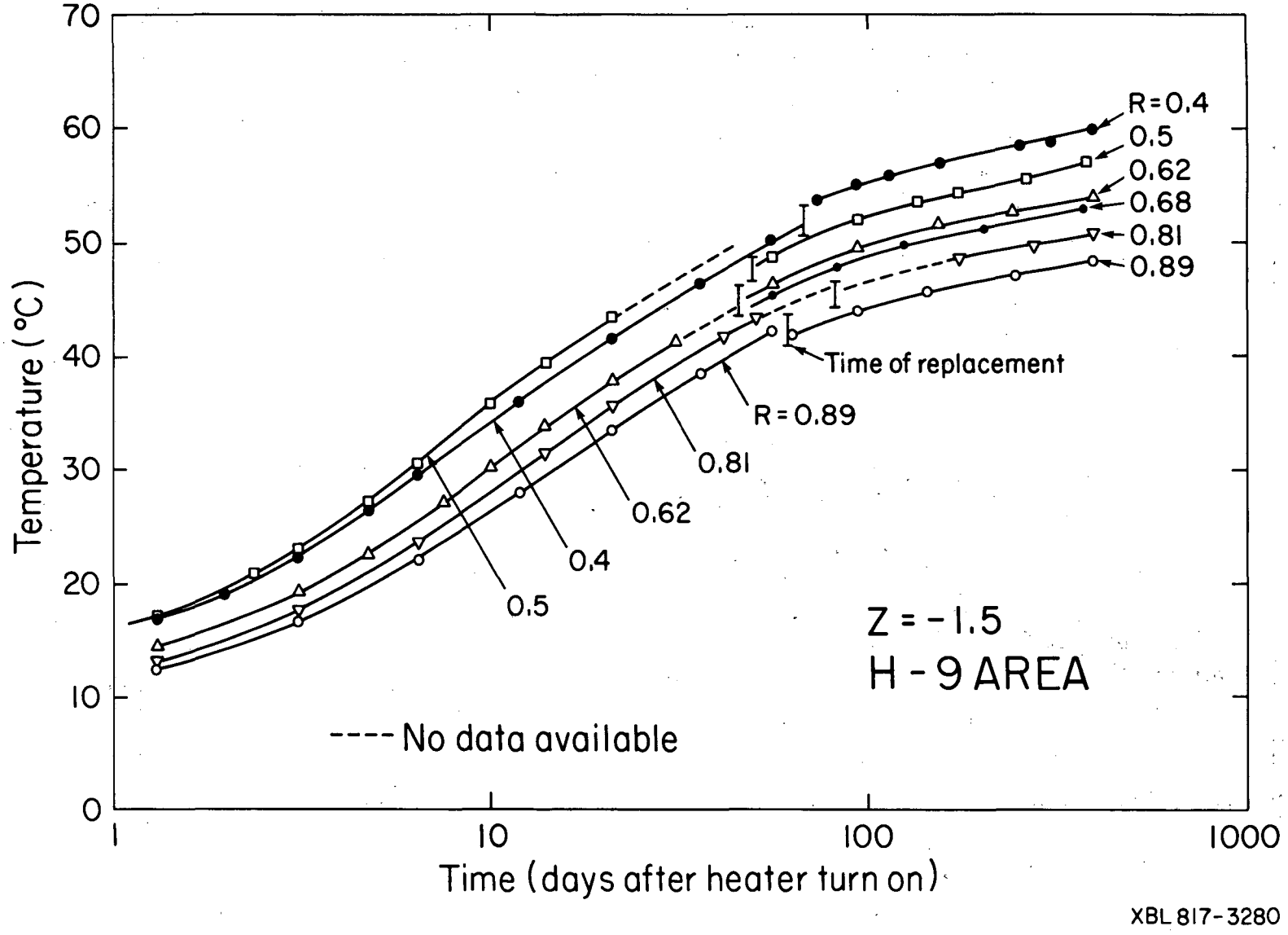

Fig. 8. Semi-log plot of measured temperatures versus time in the T-holes at elevation Z= -1.5 m, H-9 area.

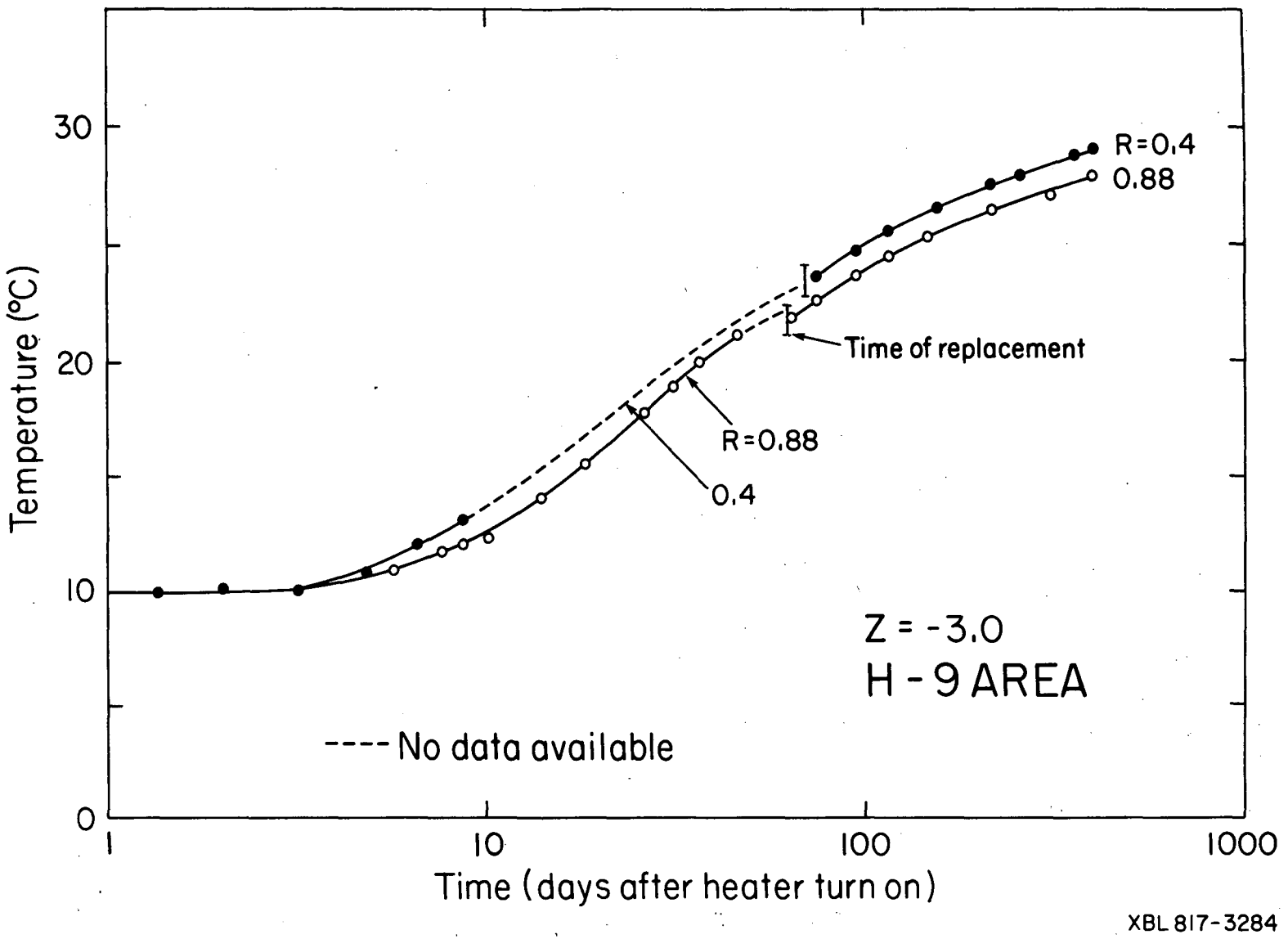

Fig. 9. Semi-log plot of measured temperatures versus time in the T-holes at elevation of Z = -3 m, H-9 area.

disconnected. Vertical bars show when the thermocouples were replaced. These figures reveal that:

- o relatively little data has been lost because of corrosion.
- o data are reasonably smooth and free of oscillation.
- o some small oscillation of temperature at Z = 3 m is due to changes of temperature in the drift. Thermocouples at levels farther away from the drift do not sense this oscillation.

Further information may be obtained from a comparison of Figs. 6 and 8 at Z = $\pm$ 1.5 m, namely that some replacement thermocouples respond differently from their predecessors. To see this, note that at the elevation -1.5 m in Fig. 8, the thermocouple at a distance R = 0.5 m before replacement shows temperatures higher than that at R = 0.4 m, closer to the heater. This is obviously wrong. However, after replacement, relative temperatures of these two thermocouples are reversed, so that the one at R = 0.4 m is now correctly higher than the one at R = 0.5 m.

Now let us consider two other thermocouples in the same holes but at the elevation of Z = 1.5 m (Fig. 6). We see that the thermocouple at R = 0.5 m before replacement not only is not warmer than the one at R = 0.4 m, rather it is much cooler than expected. However, after replacement, the new thermocouple at R = 0.5 m shows temperatures a few degrees warmer, which seems to be more reasonable. Some other thermocouples in this set also show changes as much as one to two degrees after replacement, but these are not significant.

What we may derive from this discussion is that the thermocouple string in the T-hole with R = 0.5 m was a few centimeters above its intended position and that, after replacement, this dislocation was eliminated. The replacement

thermocouple at R = 0.5 m and Z = -1.5 m was thus closer to the midplane of the heater, where it should sense higher temperatures; at the same time, the replacement thermocouple at R = 0.5 m and Z = 1.5 m was moved farther away from the midplane, so that it should sense cooler temperatures. Figure 7 shows no such temperature shift at Z = 0 and R = 0.5 m at thermocouple replacement. This is because the vertical temperature gradient near the midplane was so small that a vertical misplacement of a few centimeters could not change the magnitude of the rock temperature.

We believe this explanation eliminates the possibility that the temperature inversion at R = 0.4 and 0.5 m could be due to anisotropy in the thermal conductivity of the rock.

2.2.2 Cooling Period

It is of great interest to follow the response of the thermocouples after the heater was turned off. Figures 10 through 12 show residual temperatures of the rock as plotted against t/t' where t and t' are elapsed times since the heater turn-on and turn-off, respectively. These figures show the response of six thermocouples that are supposed to be at the same level. Obviously, the actual time increases as the ratio of t/t' decreases.

The following comments may be made:

- The temperature decreases are smooth and no major oscillations are observed.
- No major thermocouple misplacements can be detected.
- At early times after turn off, temperatures at elevation Z = -1.5 m are generally much cooler than the corresponding positions at Z = 1.5 m.

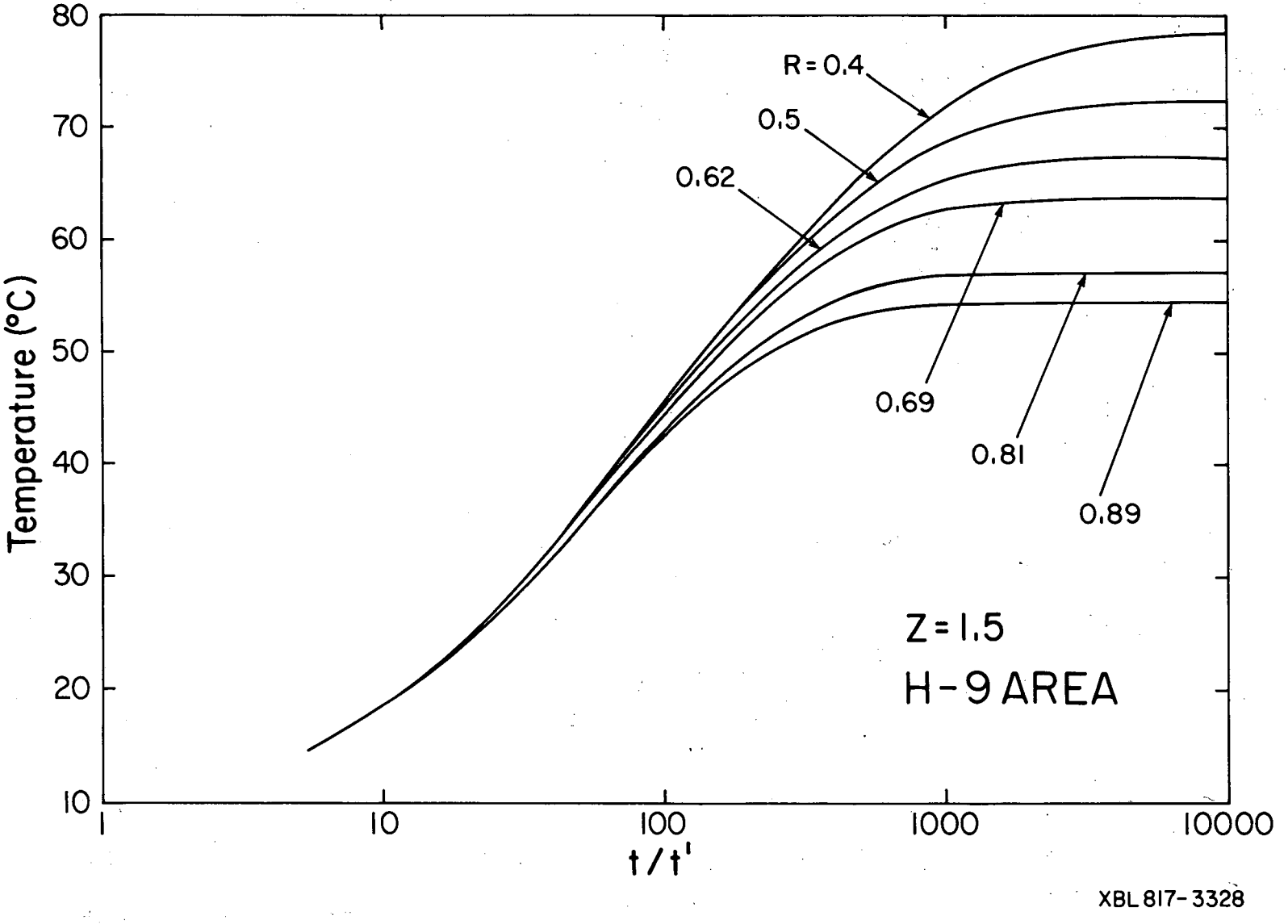

Fig. 10. Semi-log plot of measured residual temperatures versus dimensionless time in the T-holes, at elevation Z = 1.5 m, H-9 area.

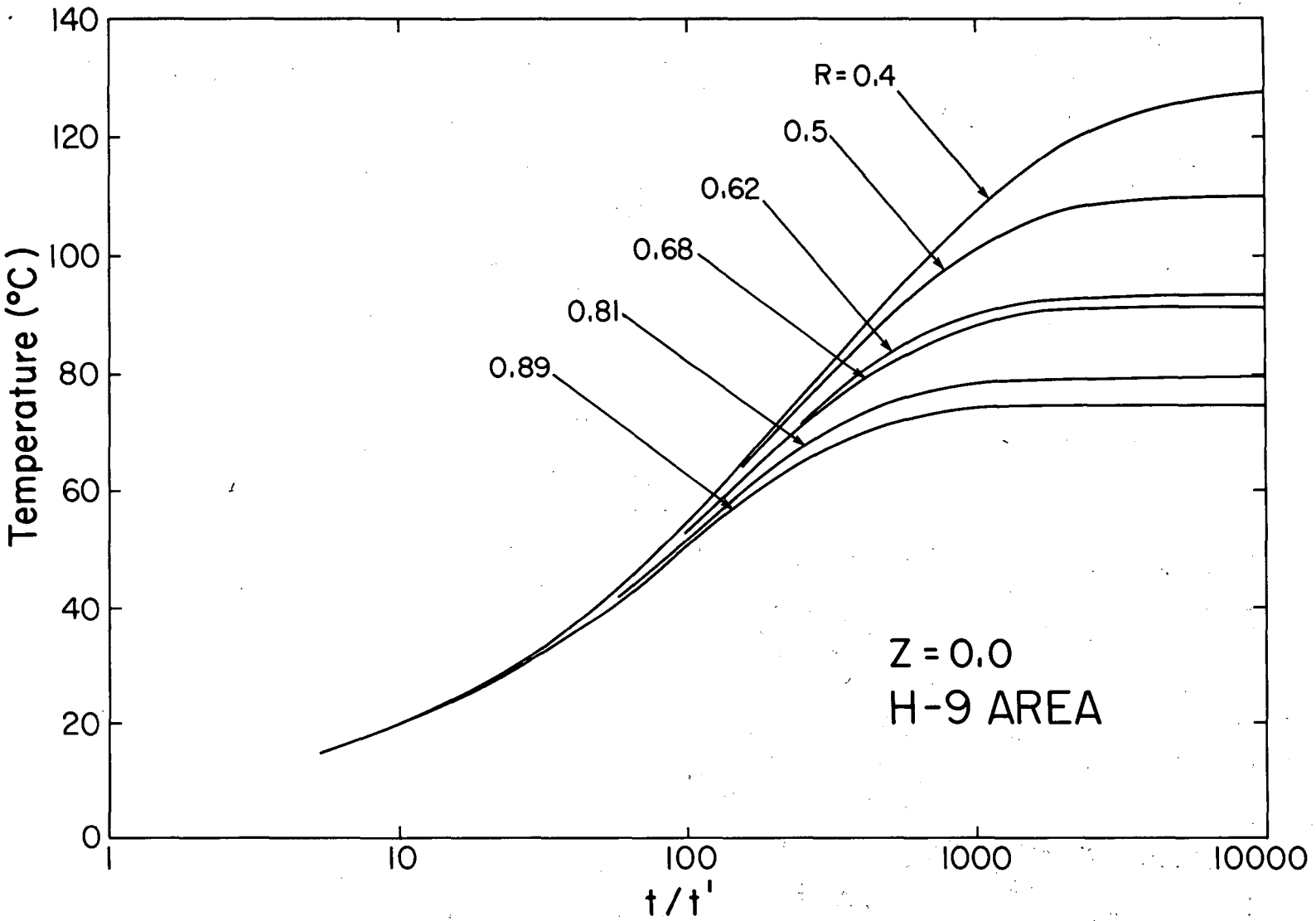

Fig. 11. Semi-log plot of measured residual temperatures versus dimensionless time in the T-holes, at elevation Z = 0.0, H-9 area.

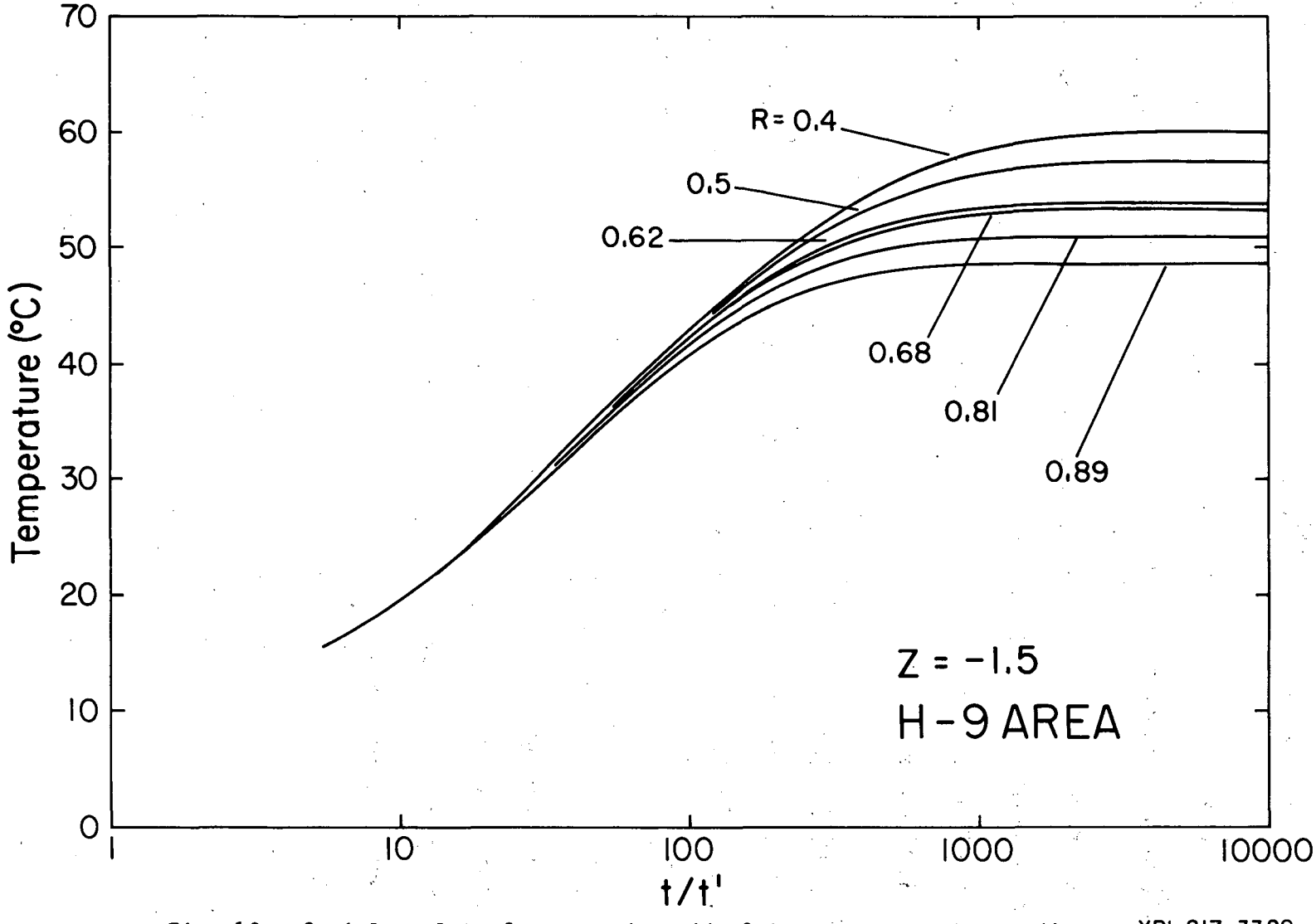

Fig. 12. Semi-log plot of measured residual temperatures versus dimensionless time in the T-holes, at elevation Z = -1.5 m, H-9 area. XBL 817-3329

- Temperature differences between the two thermocouples at R = 0.4 and 0.89 m for Z = 1.5 are approximately twice as much as the temperature differences for the corresponding thermocouples at Z = -1.5.

Note that the nonuniform spacing between the radial distances of the different T-holes has led to a nonuniform separation of the cool-down curves.

Around t/t' = 40, which corresponds to t' = 10 days after heater turn-off, the temperatures of all thermocouples at the same elevation merge. This means isotherms in the near-field area become horizontal, with the highest temperature at the midplane.

2.3 Evaluation Of The Thermal Data In H-10 Area

The H-10 area is the zone affected by the H-10 heater and its corresponding peripheral heaters. To cope with the bulk of the data and avoid confusion, this experiment was divided into four periods, with each one studied separately.

2.3.1 First Period (July 3, 78-...)

This period spans the time between the turn-on of the H-10 heater and the replacement of the corroded thermocouples, which was not the same for all holes. To examine temperature measurements in the near field over this time, we have prepared semi-log plots of families of curves showing temperature versus time as measured in the T-holes. Figures 13 through 17 show these plots for thermocouples that were supposed to be at the same elevation. These plots have also drawn on the data obtained from the Autodata-Nine data logger, which is believed to be stable and trouble-free.

As mentioned earlier, six thermocouples were located on each level at

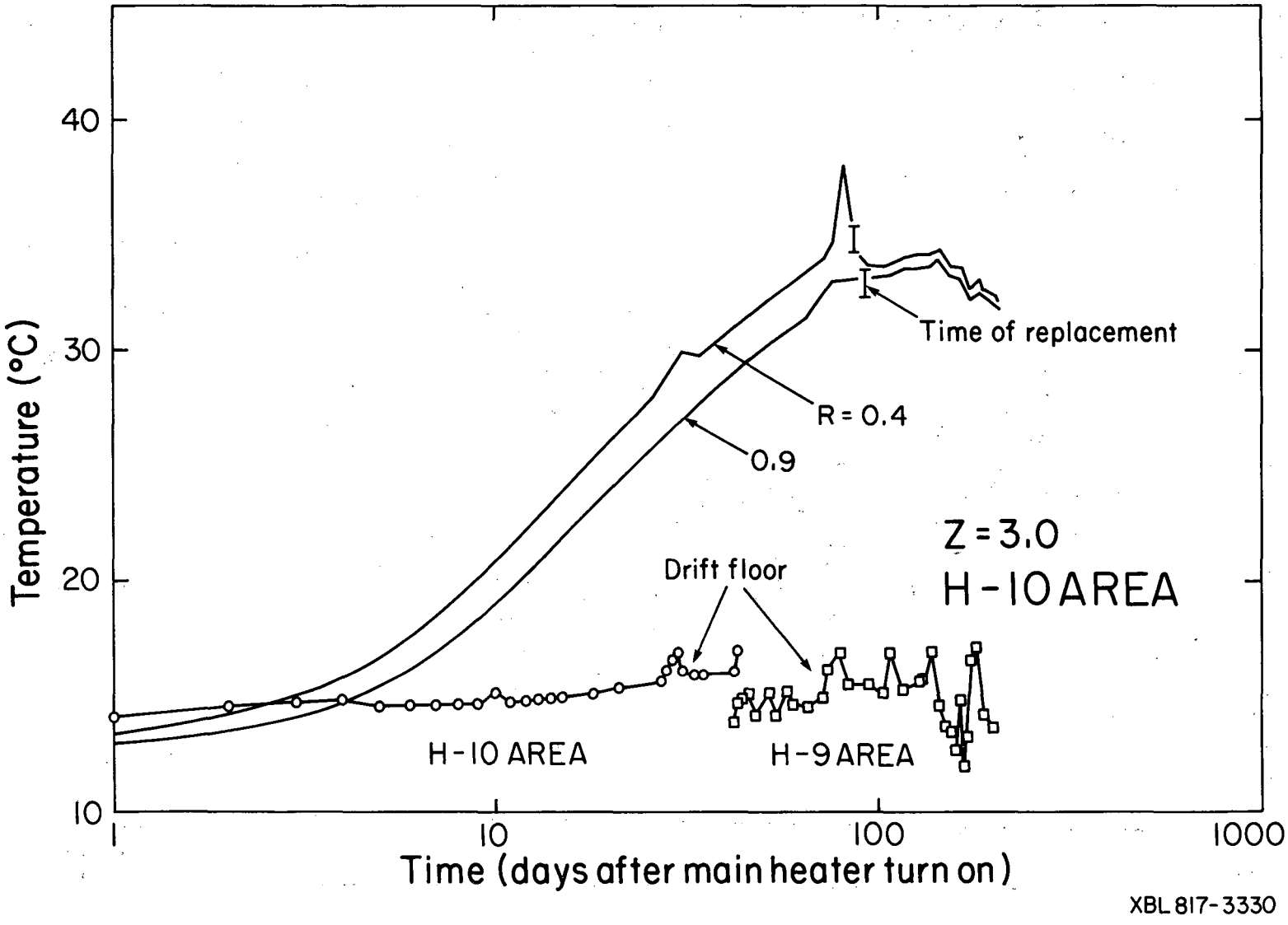

Fig. 13. Semi-log plot of measured temperatures versus time at Z = 3 m, H-10 area, for the first 204 days.

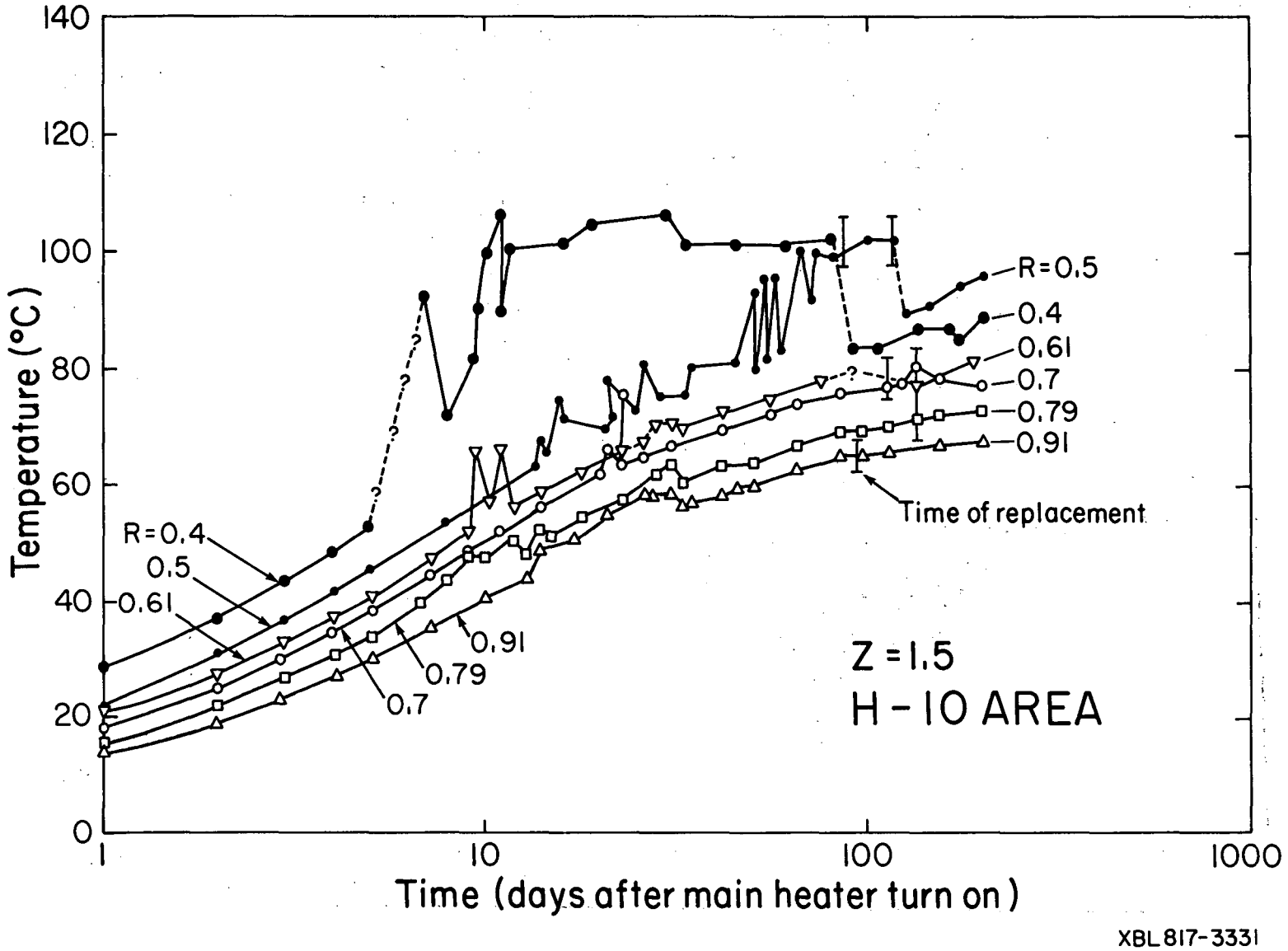

Fig. 14. Semi-log plot of measured temperatures versus time at Z = 1.5 m, H-10 area, for the first 204 days.

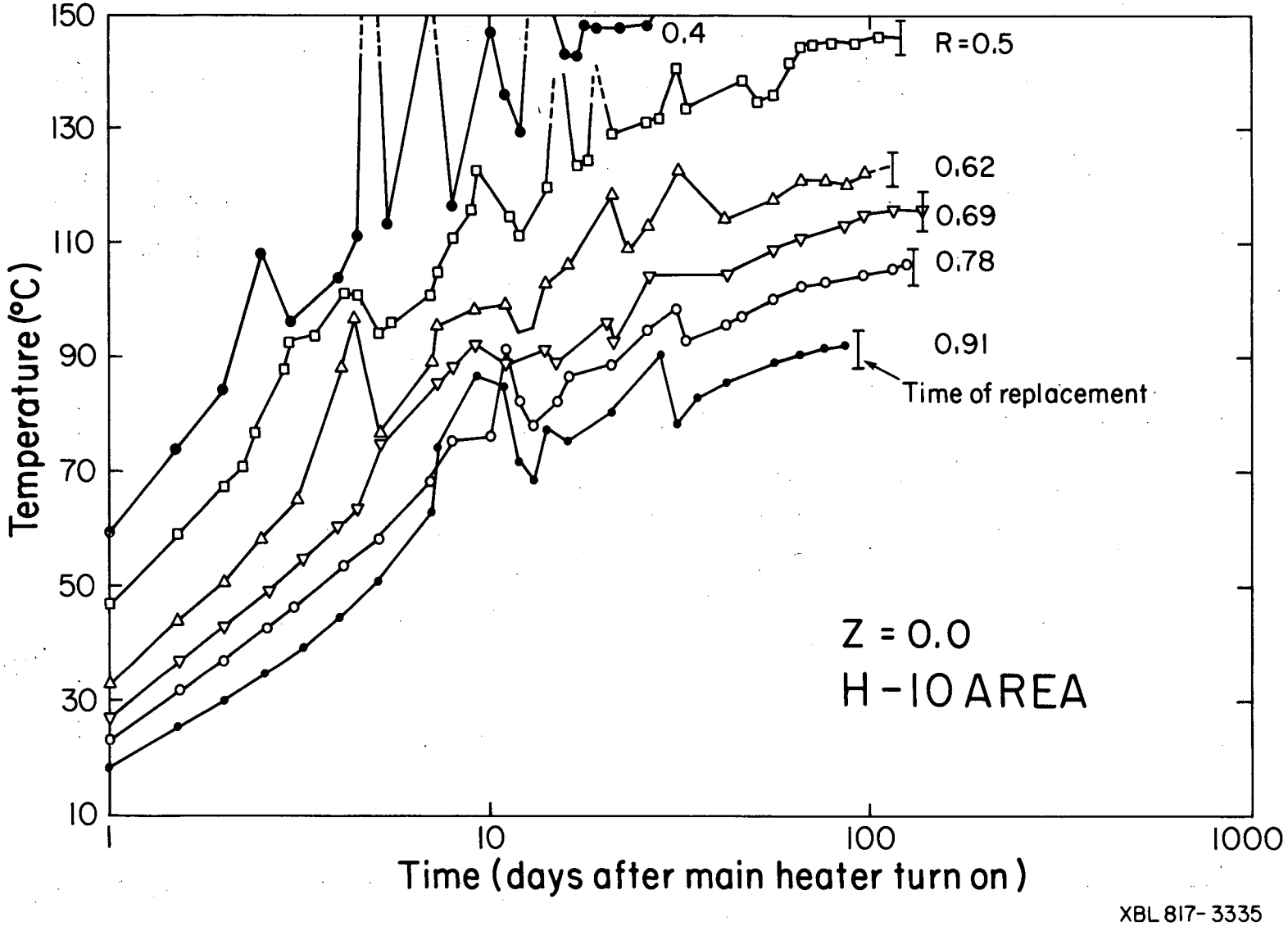

Fig. 15. Semi-log plot of measured temperatures versus time at Z = 0.0, H-10 area, from heater turn-on to thermocouple replacement.

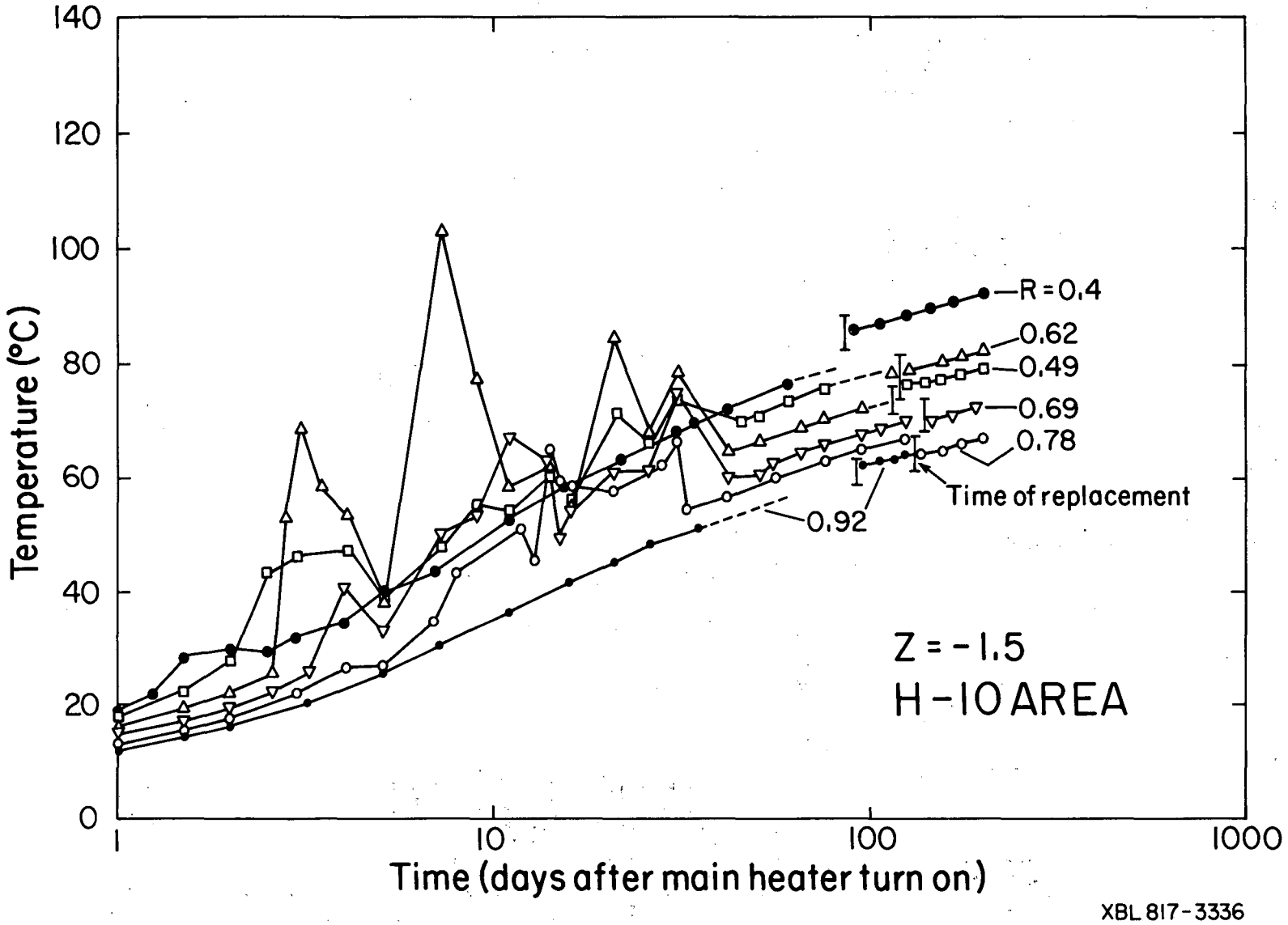

Fig. 16. Semi-log plot of measured temperatures versus time at Z = -1.5 m, H-10 area, first 204 days.

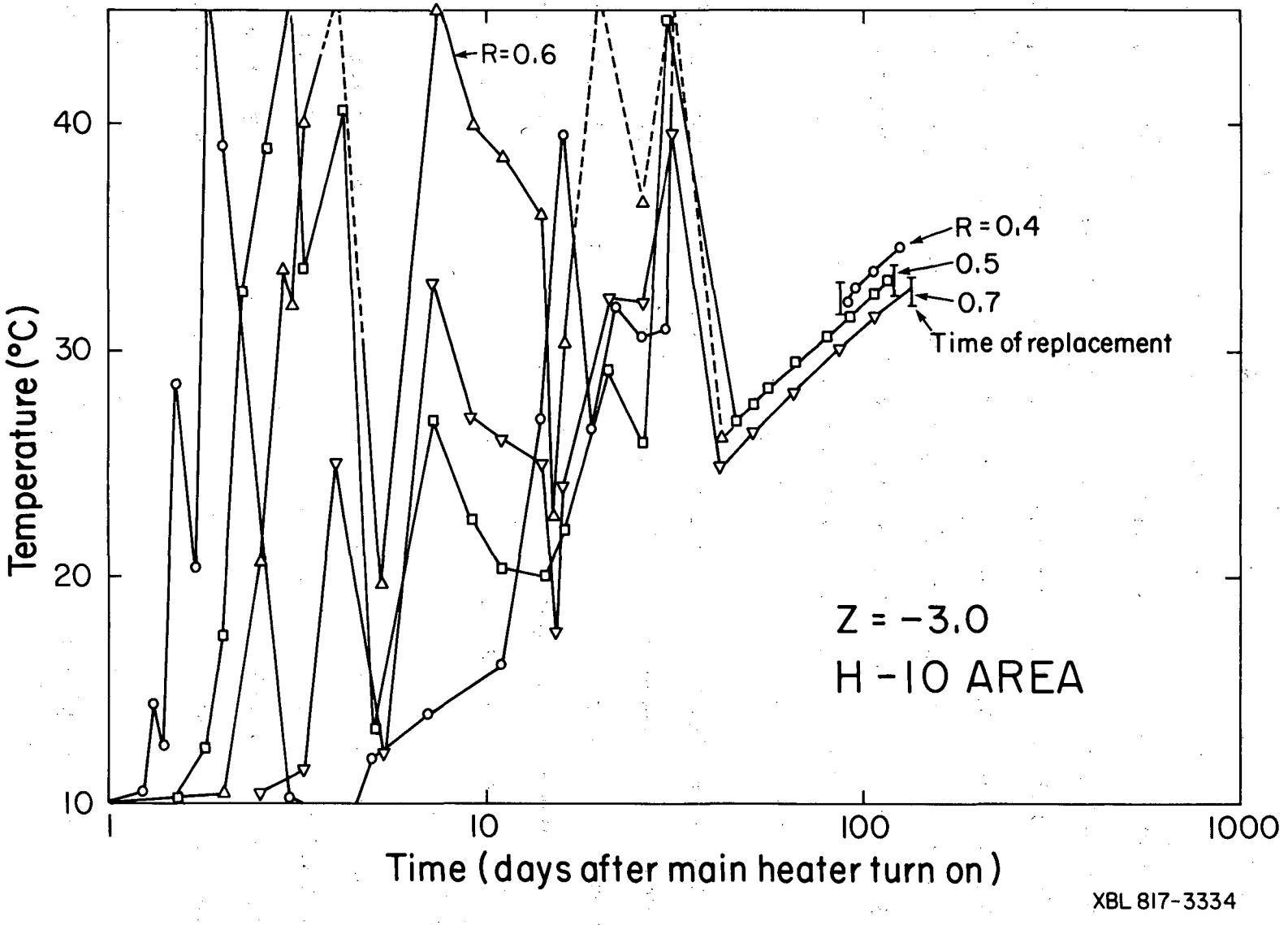

Fig. 17. Semi-log plot of measured temperatures versus time at Z = -3 m, H-10 area, from heater turn-on to thermocouple replacement.

different distances from the axis of the heater, ranging from approximately 0.4 to 0.9 m. To avoid crowding, the responses of some thermocouples have been deleted from Figs. 13 and 17. The replacement time of each thermocouple is also indicated. Figure 13 shows the temperature variation of two limiting thermocouples, i.e., at R = 0.4 and 0.9 at Z = 3.0 m. The temperature decline and the oscillation observed some time after thermocouple replacement was due to a drop and oscillation in air temperature in the full-scale drift. To show this, the variation in air temperature recorded by two thermocouples connected to the collar of instruments in two E-holes has also been plotted in Fig. 13. Thermocouples at lower elevations seem to be too far away to be affected by variations in the drift temperature.

Except for elevation Z = 3 m, which shows a relatively smooth rise of temperature, the thermocouple curves can be divided into three distinct periods. In the first period, which covers the first few days of the experiment, all thermocouples seem to show correct rock temperature. The length of this period decreases with depth, so that, at Z = -3 m, it is slightly less than one day.

The second period shows abnormally high but oscillating temperatures for almost all thermocouples on the lower four levels; this ends shortly after 40 days. These oscillations show that the phenomenon causing them is not a continuous one. The amplitude of the oscillations seems to increase with depth.

During the third period, which starts shortly after 40 days and continues until the thermocouples are replaced, temperatures generally return to their

normal range and their values do not seem to be very far from expected rock temperatures. This raises the question of whether the earlier measurements were correct.

At first, it was believed that the start of oscillation of each thermocouple was an indication of corrosion caused by the combined effect of moisture and heat. It was thus assumed that all temperatures recorded by a thermocouple after the start of its oscillation and before its removal were invalid.

However, the stability of most thermocouples after 40 days prompted us to look for another explanation. At present, we believe the heat treatment of the stainless steel sheaths made the thermocouples vulnerable to corrosion. Moisture and heat corroded the sheaths, but the thermocouple wires remained safe until the corrosion completely penetrated the steel. Other possible mechanisms of corrosion have been presented by Binnall and McEvoy (1982).

Later, when moisture reached them, the thermocouple wires probably established a ground loop, caused by a common ground connection at the data acquisition system, and generated random currents that affected the thermocouple readings. The connection was made between the negative voltage wires of all the thermocouples in this area and a single point electrical grounds. Still later, when the electrical grounds were removed at the data acquisition system, the thermocouples recorded stable temperatures until the time of replacement.

Erratic readings of some thermocouples below the midplane level could also have been caused by moisture temporarily shorting the two wires together

where the protective sheath had corroded away. However, since similar oscillations were not observed in the H-9 area, where the common ground at the data acquisition system was removed prior to turn-on, this explanation seems less likely.

Since thermocouples above the midplane experienced considerably less corrosion, the two thermocouples at Z = 1.5 m that went into oscillation (R = 0.5 and 0.4 m) may have done so because of steam moving up the borehole (the thermocouple at R = 0.4 m comes very close to stabilizing at 100°C).

2.3.2 Second Period (...-Jan. 23, 79)

For each T-hole, this period covers the time between thermocouple replacement and the peripheral heater turn-on. Figures 18 and 19 present semi-log plots of measured temperatures versus time for two different elevations in the T-holes, Z = 1.5 and -1.5 m. Some earlier data have also been included for comparison. We have intentionally deleted the oscillation data to concentrate on more important issues.

Inspection of Fig. 18 for Z = 1.5 m indicates that:

- o After replacement, temperatures recorded by the thermocouple at radial distance R = 0.5 m are consistently warmer than those recorded at R = 0.4 m, which is obviously incorrect. One may notice, from Figs. 14 and 18, that before replacement of the thermocouples, temperatures at R = 0.4 m were correctly warmer than those at R = 0.5 m.
- o Temperatures at R = 0.4, 0.5, and 0.61 m after replacement are much cooler than the corresponding temperatures just before replacement.

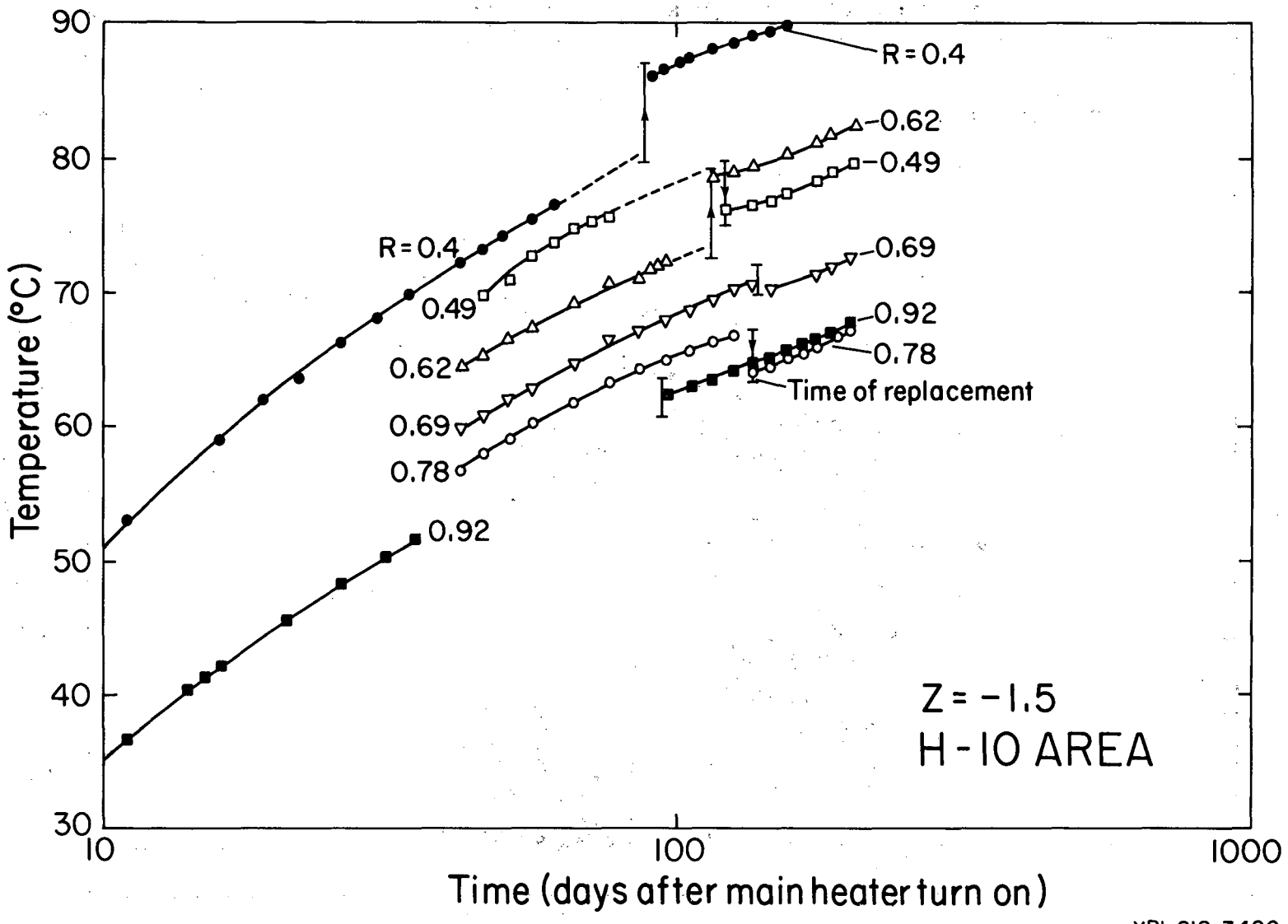

Fig. 18. Semi-log plot of measured temperatures versus time at Z = -1.5 m, H-10 area, before and after thermocouple replacement. XBL 818-3400

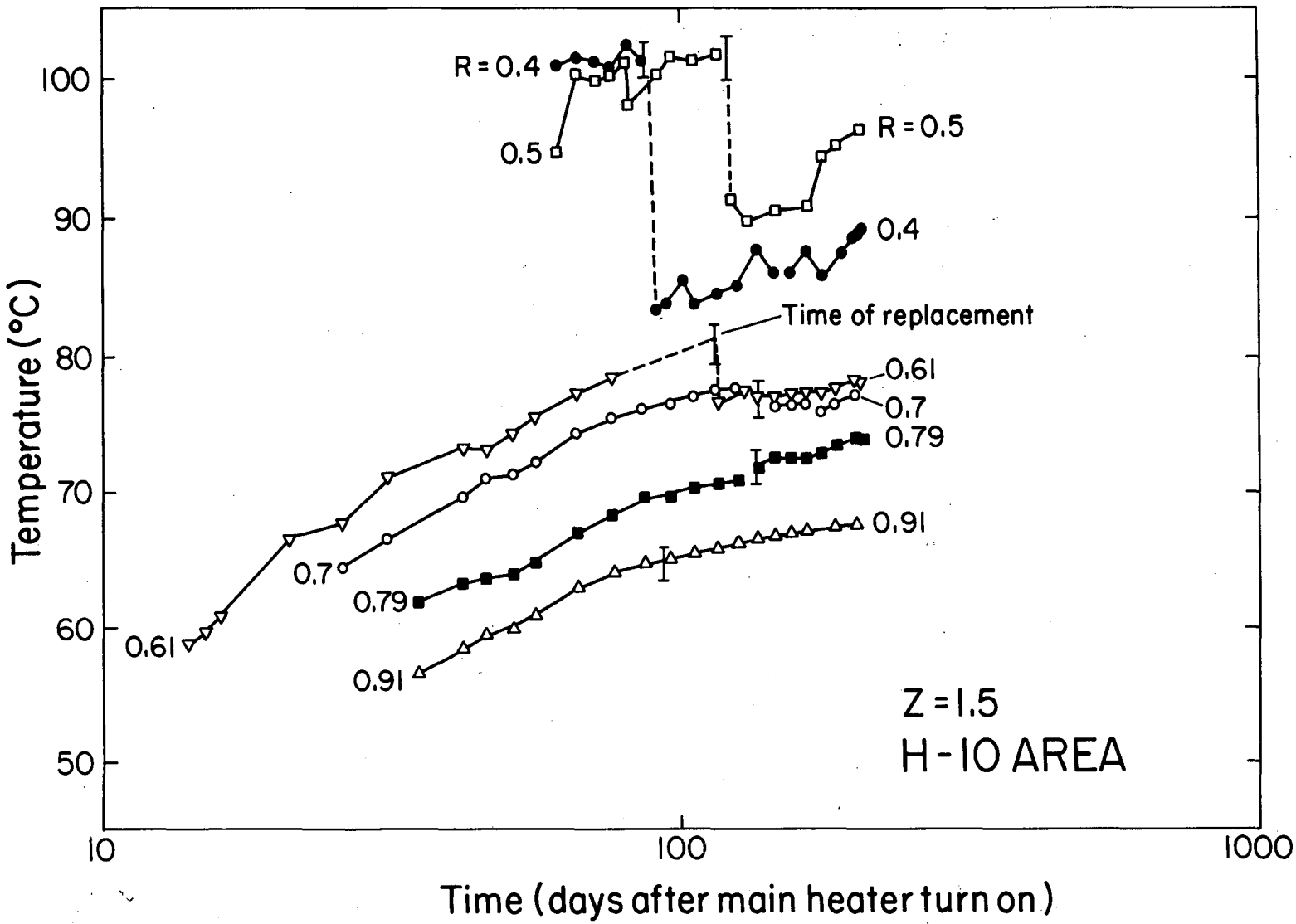

XBL818-3401

Fig. 19. Semi-log plot of measured temperatures versus time at Z = 1.5 m, H-10 area, before and after thermocouple replacement.

- Temperatures at R = 0.91 m do not show any sensible change after replacement.

One would logically expect that at any given elevation during this period, a thermocouple closer to the heater would be warmer than another farther away. This was in fact the case before the replacement, but not afterward. We shall see later that the thermocouple at R = 0.4 and Z = 1.5 m remains cooler than the one at R = 0.5 and Z = 1.5 m all the way to the end of the experiment, even after the heater turn-off, and thus was not a short-term anomaly.

Let us now turn to Fig. 19, which shows temperature variations at Z = -1.5 m. This figure reveals that:

- Measured temperatures at R = 0.49 m after replacement not only are cooler than those at R = 0.4 m, contrary to what was seen at Z = 1.5 m, but are even cooler than those at R = 0.62 m.
- In contrast to Fig. 18, temperatures at R = 0.4 and 0.62 m, are much warmer after replacement than before.
- Temperatures at R = 0.78 m dropped after replacement and were even cooler than those at R = 0.92 m.

Since these observations contradict the laws of heat conduction through solids, they should be thoroughly examined; they can be explained by the same reasoning that was used for the H-9 area.

Leads of the five thermocouples in each T-hole were taped together before installation. The vertical mislocation should therefore be the same in all five. If the string is somewhat higher than its designed position,

the thermocouple at Z = 1.5 m, now farther than intended from the heater midplace, will measure cooler temperatures, and the thermocouple at Z = -1.5 m, now closer, will measure warmer temperatures. This kind of misplacement has been identified for thermocouples in T-holes at R = 0.4 and 0.6 m.* Conversely, if a string of thermocouples is somewhat lower than its designed position, thermocouples above the midplane will register warmer temperatures than expected, and those below it, cooler temperatures. This sort of misplacement occurred in T-holes at R = 0.5 and 0.8 m.

The magnitude of these dislocations is not known at this stage of the study, but an estimate for various T-holes will be given later.

Figure 20 presents semi-log plots of temperature variations in the T-holes at elevation Z = 0. Because the temperature gradient at Z = 0 in the vertical direction was very small, a slight vertical dislocation of the thermocouples should not have lead to much temperature change. However, the temperature gradient in the radial direction has its maximum value at Z = 0. Thus, any temperature change in excess of 1 to 2°C on the midplane cannot be due to vertical dislocation alone. Figure 20 shows that the thermocouple at R = 0.4 m indicates an increase of about 10°C after replacement. A change of this magnitude is probably due mainly to horizontal movement of the sensor.

On the basis of this analysis, four out of the six strings of thermocouples in T-holes around the H-10 heater were somewhat misplaced after the

*Since the holes are not exactly vertical, nominal distances are sometimes used for reference.

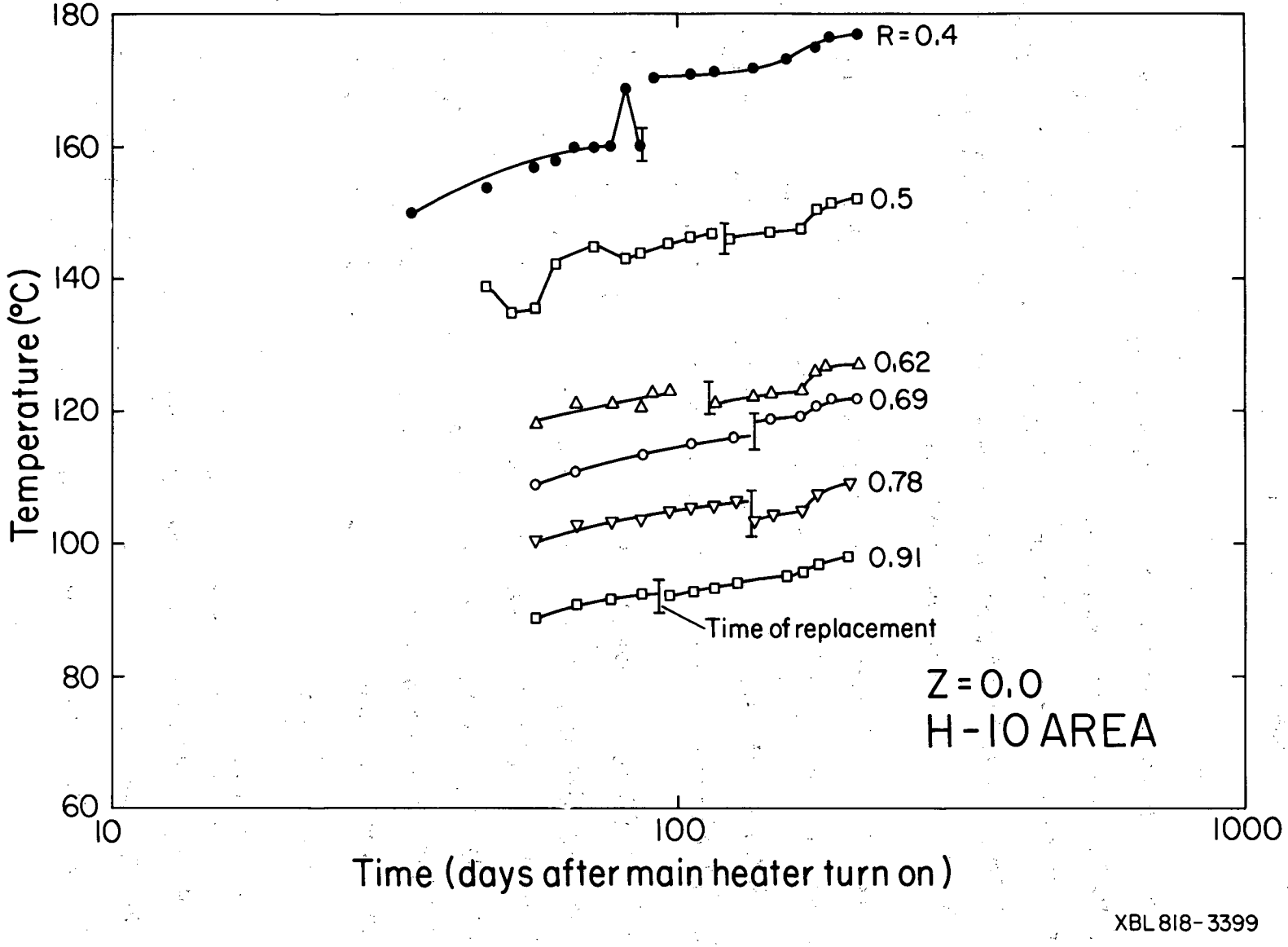

Fig. 20. Semi-log plot of measured temperatures versus time at Z = 0.0 of H-10 area, before and after thermocouple replacement.

original thermocouples were removed. Figure 21 shows schematic positions of T-hole thermocouples in the H-10 area after replacement.

Let us now consider another approach. Figure 22 shows a semi-log plot of variation in temperature versus $1/R^2$ for thermocouples in T-holes, at Z = 1.5 m, before and after replacement. One plot is for t = 5 days, when temperature recordings were still smooth, and before any thermocouple replacement. The other plot is from temperature data recorded 165 days after heater turn-on. By this time, all T-hole thermocouples had been replaced.

Data for t = 5 days fit a straight line, whereas the data at t = 165 days do not. As the straight line drawn on Fig. 22 indicates at t = 165 days, the temperatures recorded at R = 0.4 and 0.6 m are much cooler and those at R = 0.5 m are somewhat warmer than should have been the case.

Figure 23 presents similar plots for elevation Z = -1.5 m. Day 61, after the period of temperature oscillations, was chosen to represent data before replacement. It can be seen that before replacement, the data fit a straight line fairly well. At 150 days (after all replacements), temperatures at R = 0.4 and 0.6 m are too high, while those at R = 0.5 and 0.8 m are too low. Both observations support the hypothesis of a vertical dislocation of some thermocouples in T-holes.

2.3.3 Third Period (Jan 23, 79 to Aug 1, 79)

This period starts when peripheral heaters were turned on (day 204) and ends when all heaters in the H-10 area were turned off (day 394). Recall that each of the eight peripheral heaters initially operated at a power level of

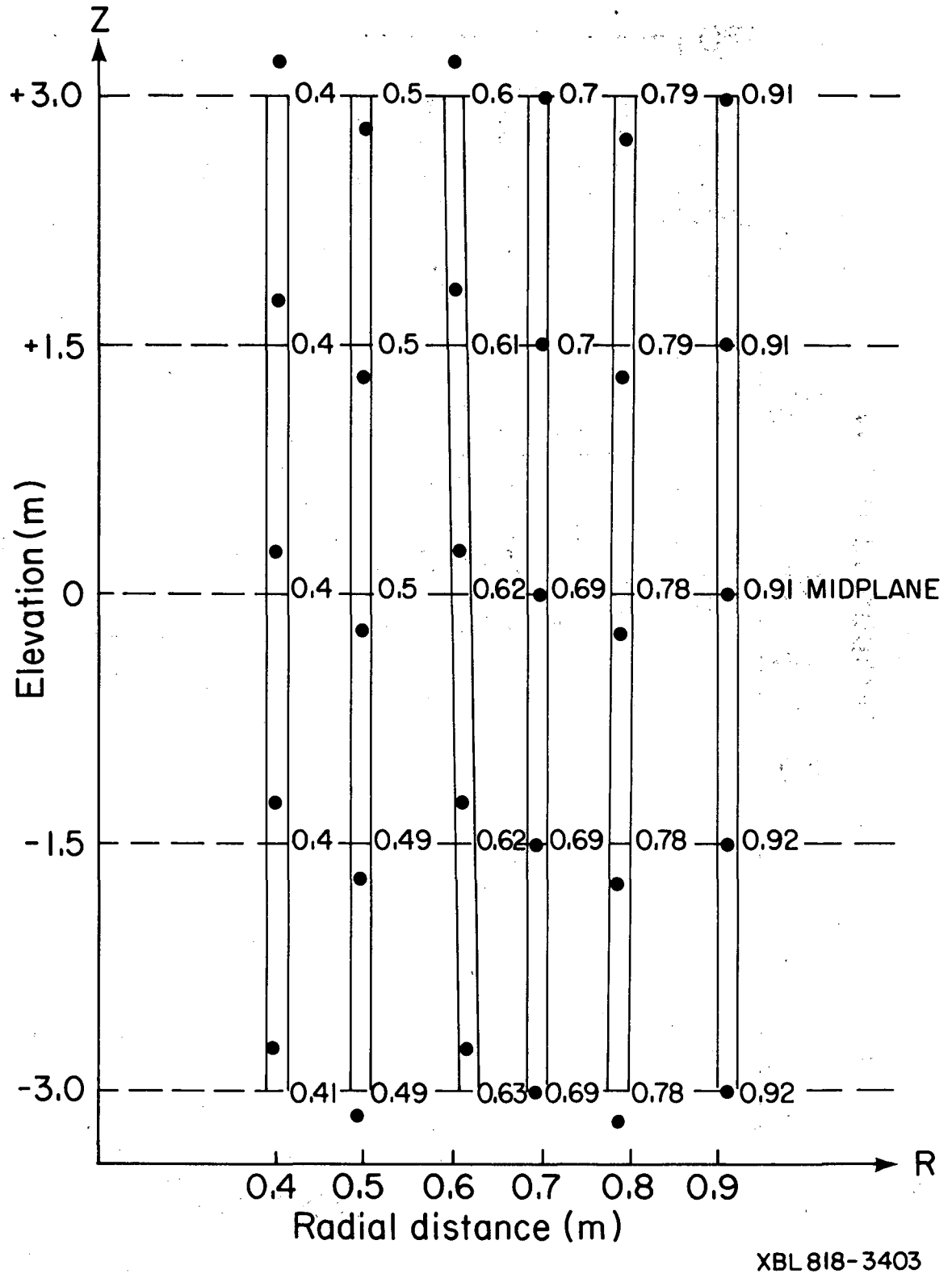

Fig. 21. Schematic positions of the thermocouples in the T-holes around the H-10 heater after replacement.

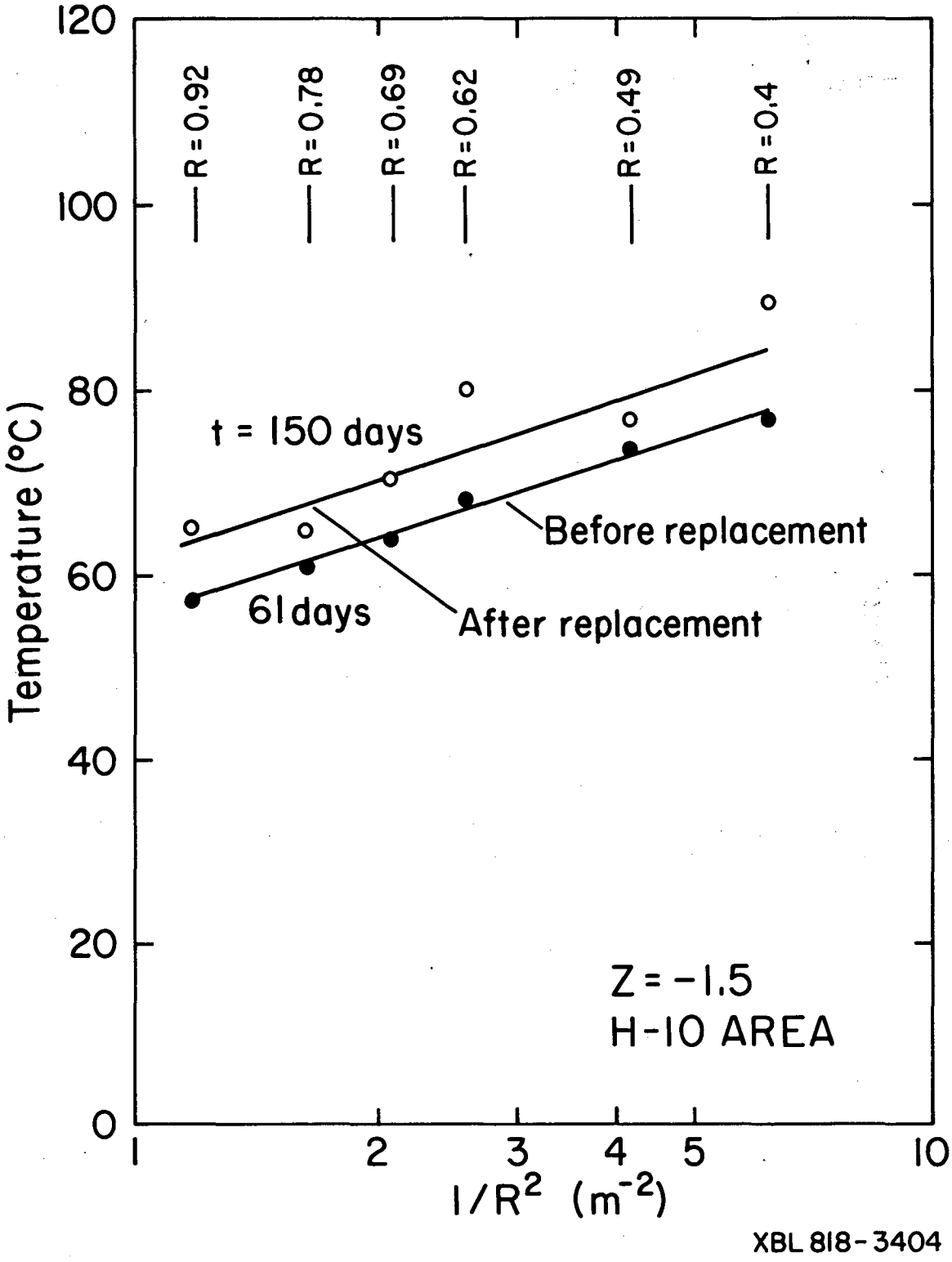

Fig. 22. Semi-log plot of temperature variation versus $1/R^2$ measured by thermocouples in the T-holes at H-10 area at Z = -1.5 m, before and after thermocouple replacement.

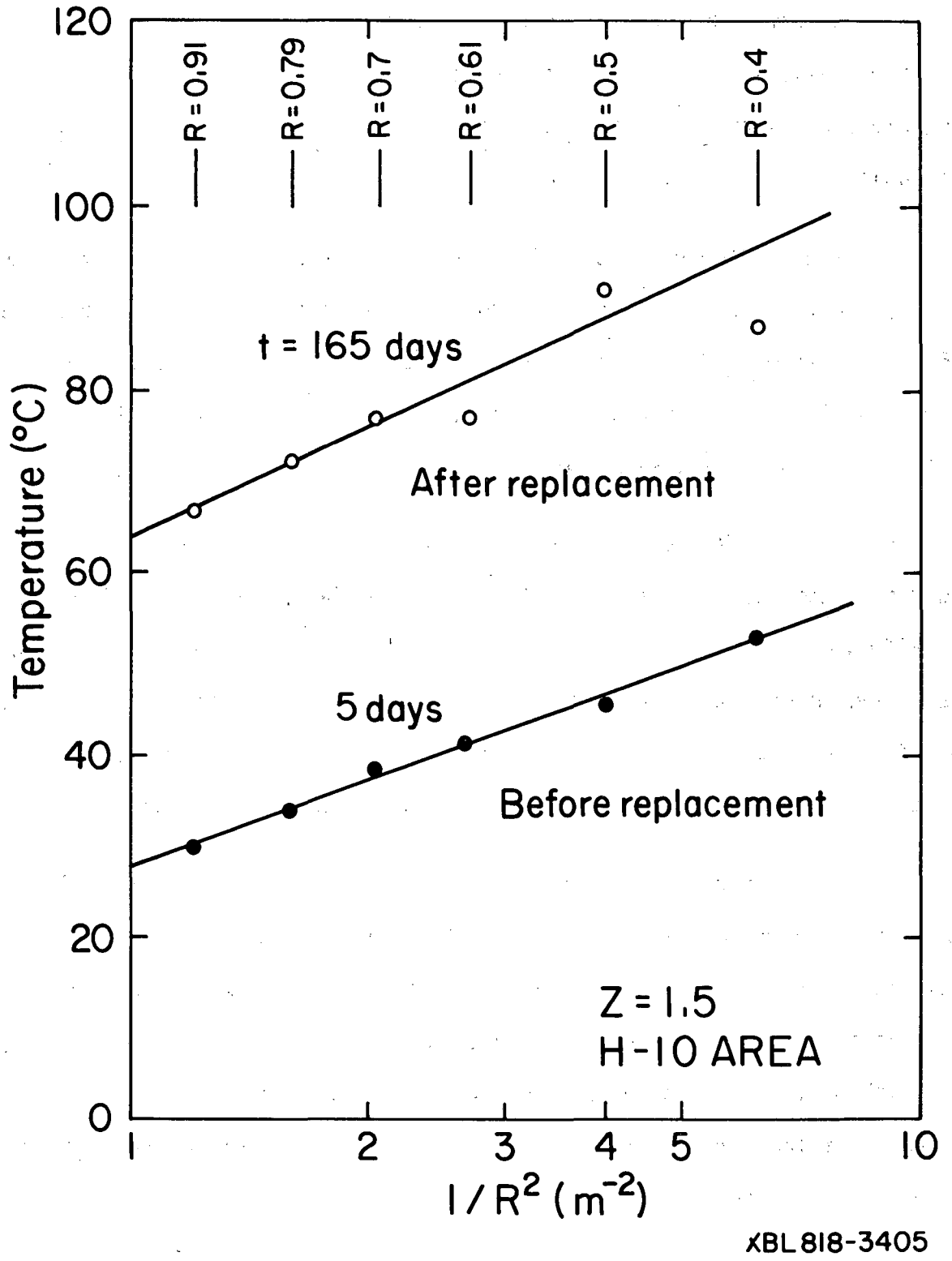

Fig. 23. Semi-log plot of temperature variation versus $1/R^2$ measured by thermocouples in the T-holes at H-10 area at Z = 1.5 m, before and after thermocouple replacement.

1.0 kW and surrounded the main heater at a distance of 0.9 m. After 40 days, the power levels were reduced to 0.85 kW. Figures 24 through 26 present semi-log plots of temperature variations in T-holes as measured at three different elevations: Z = + 1.5, 0.0, and -1.5 m.

In general, temperature variations on the midplane and below were relatively smooth. However, there was considerable oscillation above the midplane (Fig. 24); only during the first day or so, when their temperatures were below 100°C, did the thermocouples show a detectable sequence. Later, the response became mixed, with some oscillations.

As we shall see later, a smooth temperature decline after turn-off rules out any assumption of a malfunction by the thermocouples. These temperature anomalies did not occur in the rock. Rather, they were a local phenomenon caused by water inflow in the T-holes. This is a matter of some importance and will be discussed in a separate report. The simple theory of heat conduction would not be able to predict this temperature behavior.

Figure 25, for the midplane (Z = 0), shows a general increase of temperature until the power level of the peripheral heater was lowered. During the next 150 days, all temperatures drop and then warm up again. However, the maximum temperatures did not rise more than 4°C above those at power reduction. Although heat was reaching each thermocouple from nine different heaters, the sequence of the curves is still the same as they were before the peripheral heaters were turned on.

Figure 26 at Z = -1.5 m shows that temperatures for the thermocouple at

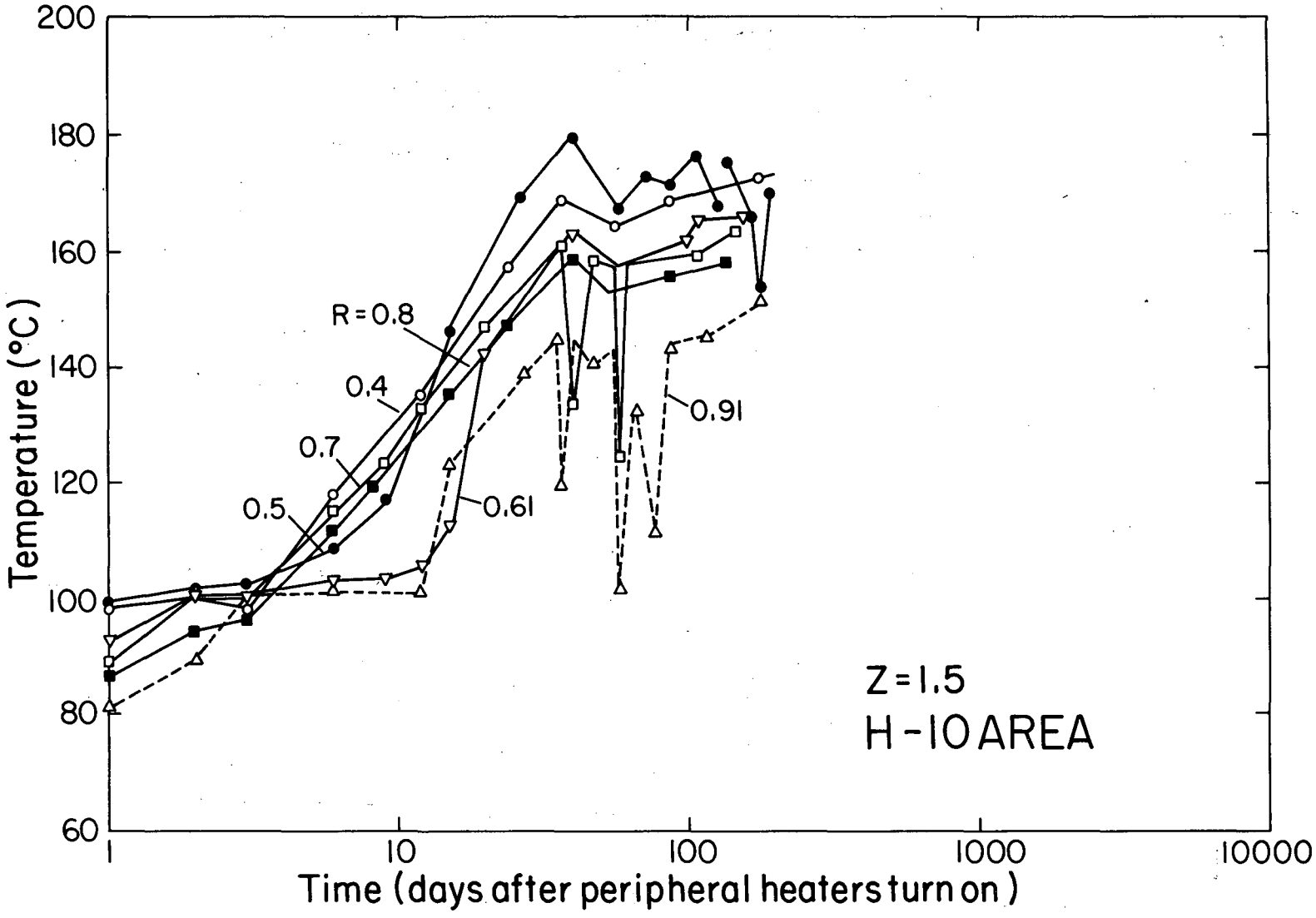

XBL818-3408

Fig. 24. Semi-log plot of temperature variation with time as measured at Z = 1.5 m, in the T-holes, H-10 area, from peripheral-heater turn-on to turn-off.

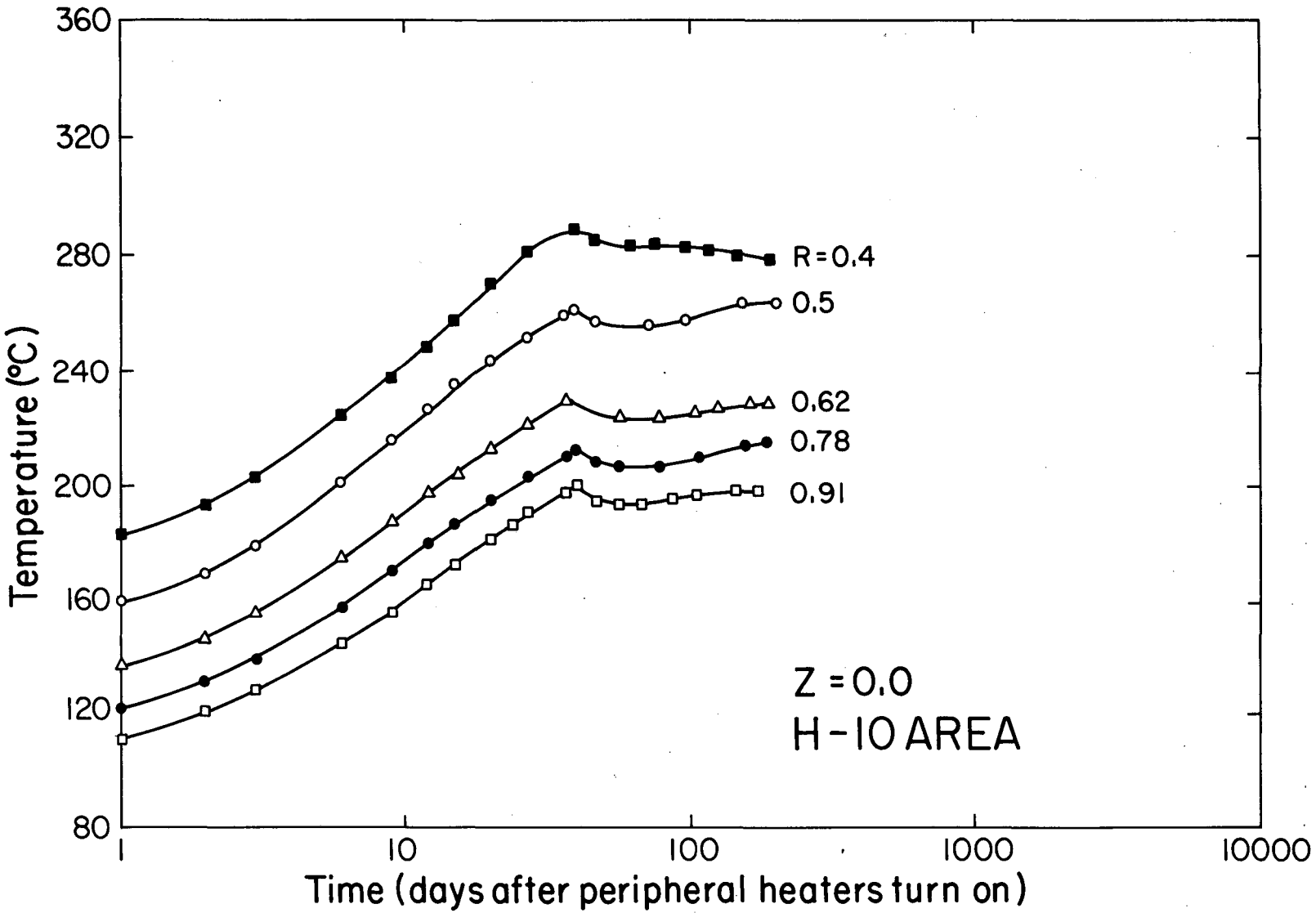

XBL 818-3407

Fig. 25. Semi-log plot of temperature variation with time as measured at Z = 0.0 in the T-holes at H-10 area, from peripheral-heater turn-on to turn-off.

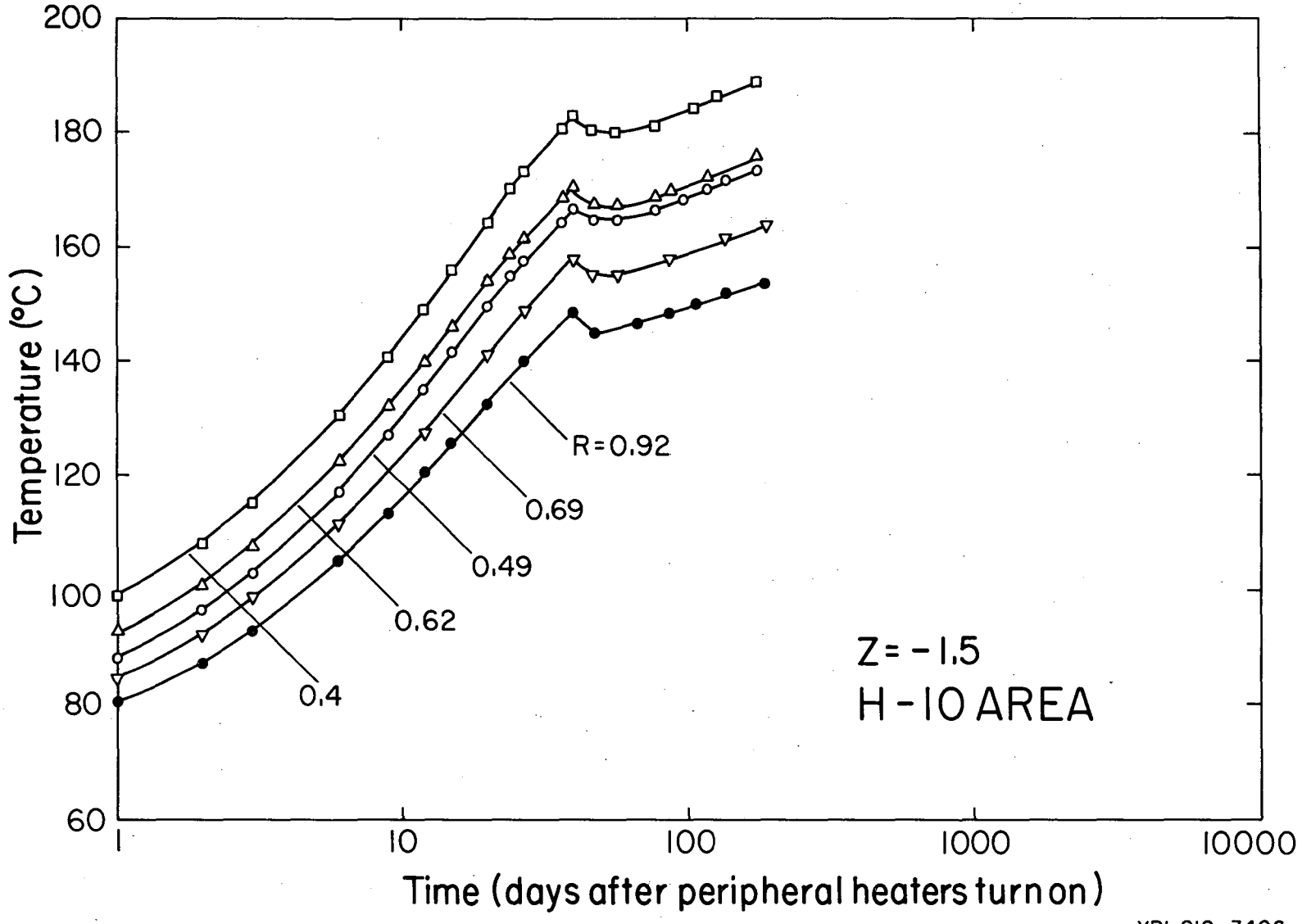

XBL 818-3406

Fig. 26. Semi-log plot of temperature variation with time as measured at Z = -1.5 m in the T-holes at H-10 area, from peripheral-heater turn-on to turn-off.

R = 0.49 m were consistently cooler than those for the thermocouple at R = 0.62 m, farther away. This is due to the vertical misplacement of thermocouples, as discussed earlier.

2.3.4 Fourth Period (Aug. 1, 1979 to Jan. 1, 1980)

This period covers the five months after heater turn-off. All heaters were turned off on August 1, 1979, but temperature recording continued until January 1, 1980. Figures 27 through 31 present semi-log plots of the variation in residual temperatures versus t/t', where t and t' are times elapsed since the main heater turn-on and turn-off, respectively. Each figure shows the response of the thermocouples at a given elevation in the T-holes.

These figures clearly confirm the argument presented earlier regarding vertical misplacement of some thermocouples in the T-holes after replacement. Figures 30 and 31 at elevations Z = -1.5 and -3 m, respectively, show that temperatures recorded for R = 0.62 m are consistently warmer than those for R = 0.49 m.

Another interesting point can be seen in a comparison of Figs. 27 and 31. Figure 27 shows that except for the response of the thermocouple at R = 0.5 m which was exceptionally hot, temperatures recorded at R = 0.79 m were the warmest, while temperatures recorded at R = 0.4 m were the coolest. One might anticipate that thermocouples farther away from the main heater but closer to the peripheral ones should have been warmer. But Fig. 31 does not support this idea. Temperatures at R = 0.41 m are, in fact, warmer than temperatures recorded in other holes, and the temperatures at R = 0.78 m are cooler than

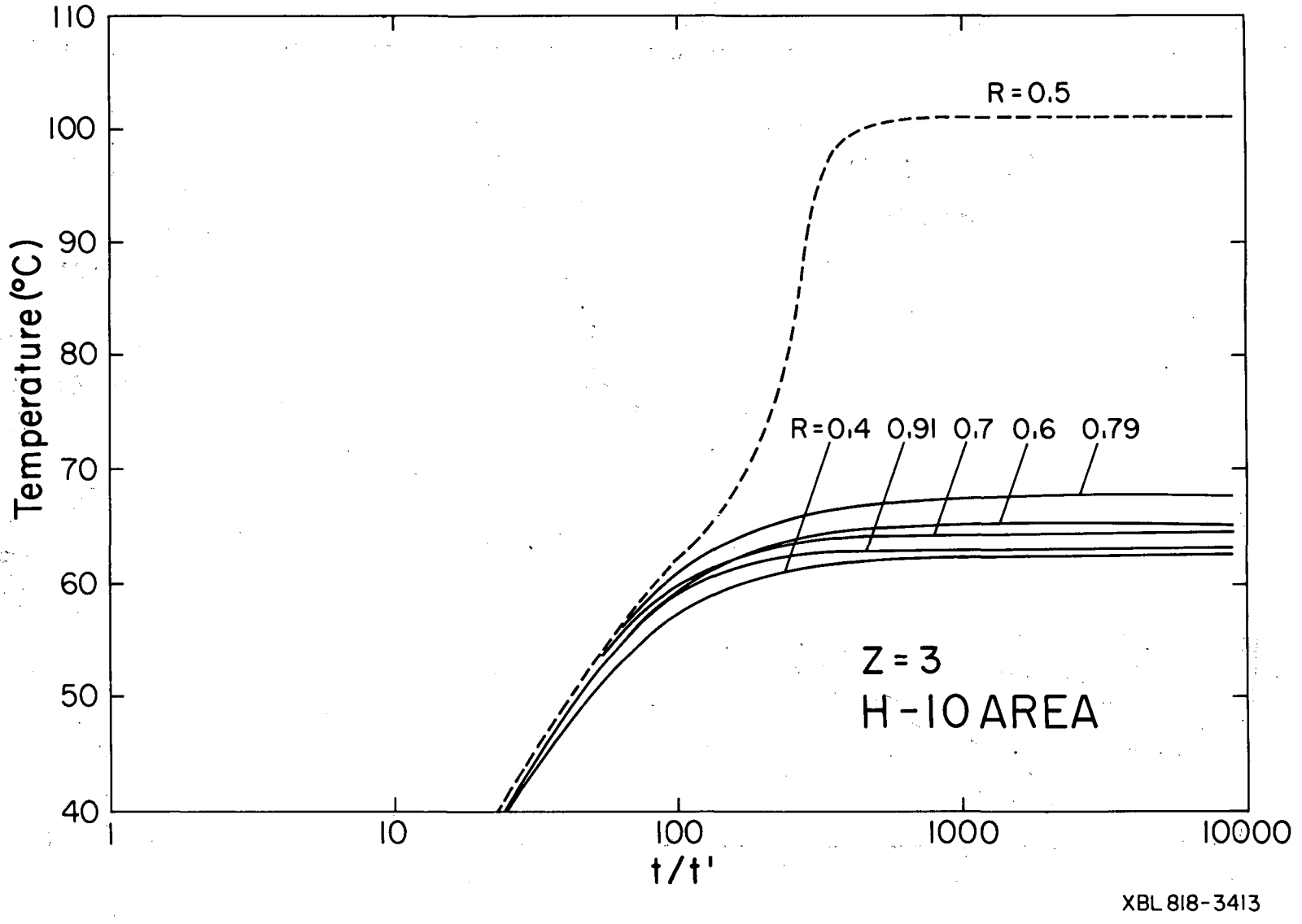

Fig. 27. Semi-log plot of variation in residual temperature versus t/t' as measured at Z = 3 m in the H-10 area.

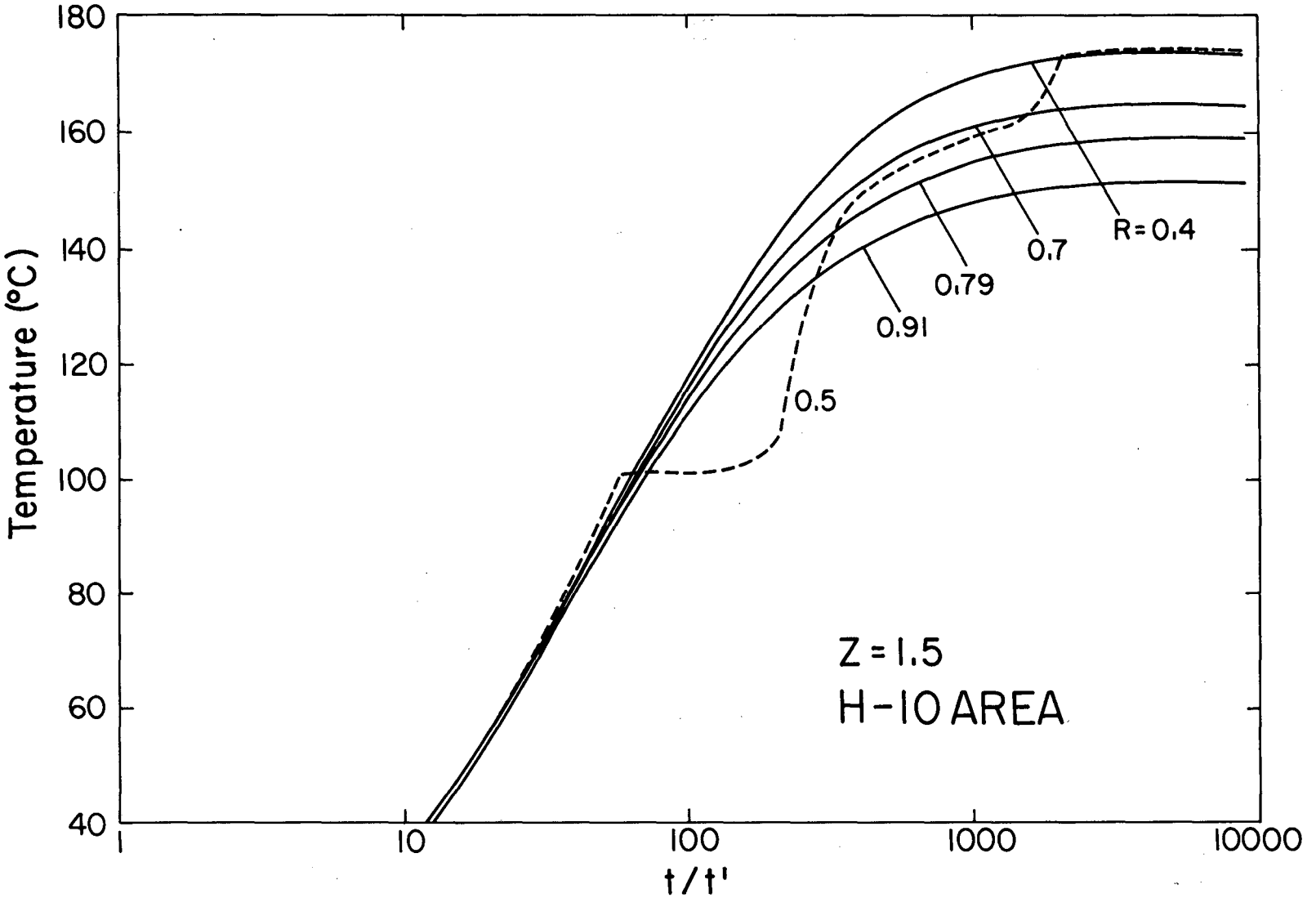

Fig. 28. Semi-log plot of variation in residual temperature versus t/t' as measured at Z = 1.5 m in the H-10 area.

XBL 818-3412

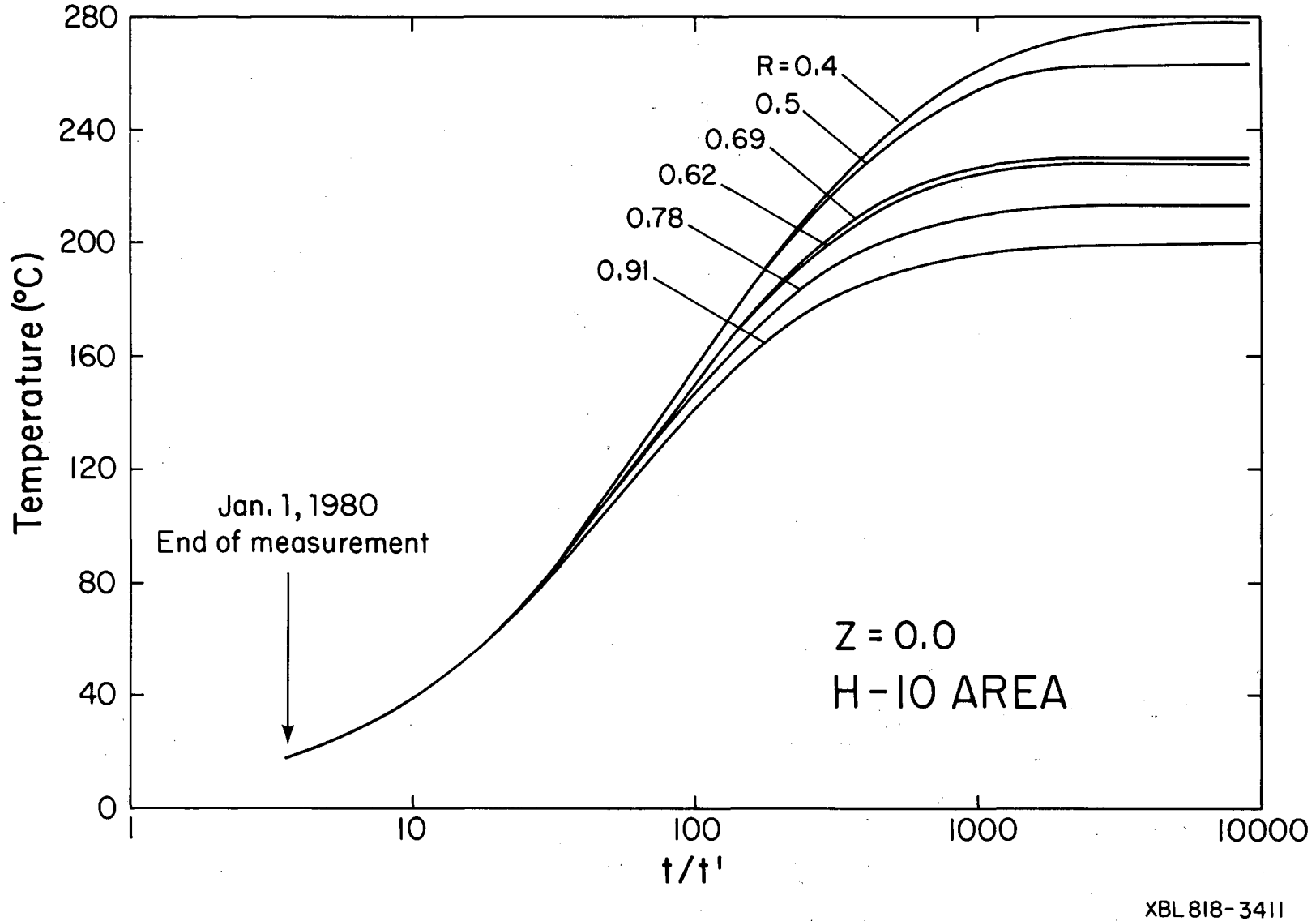

Fig. 29. Semi-log plot of variation in residual temperature versus t/t' as measured at Z = 0.0 in the H-10 area.

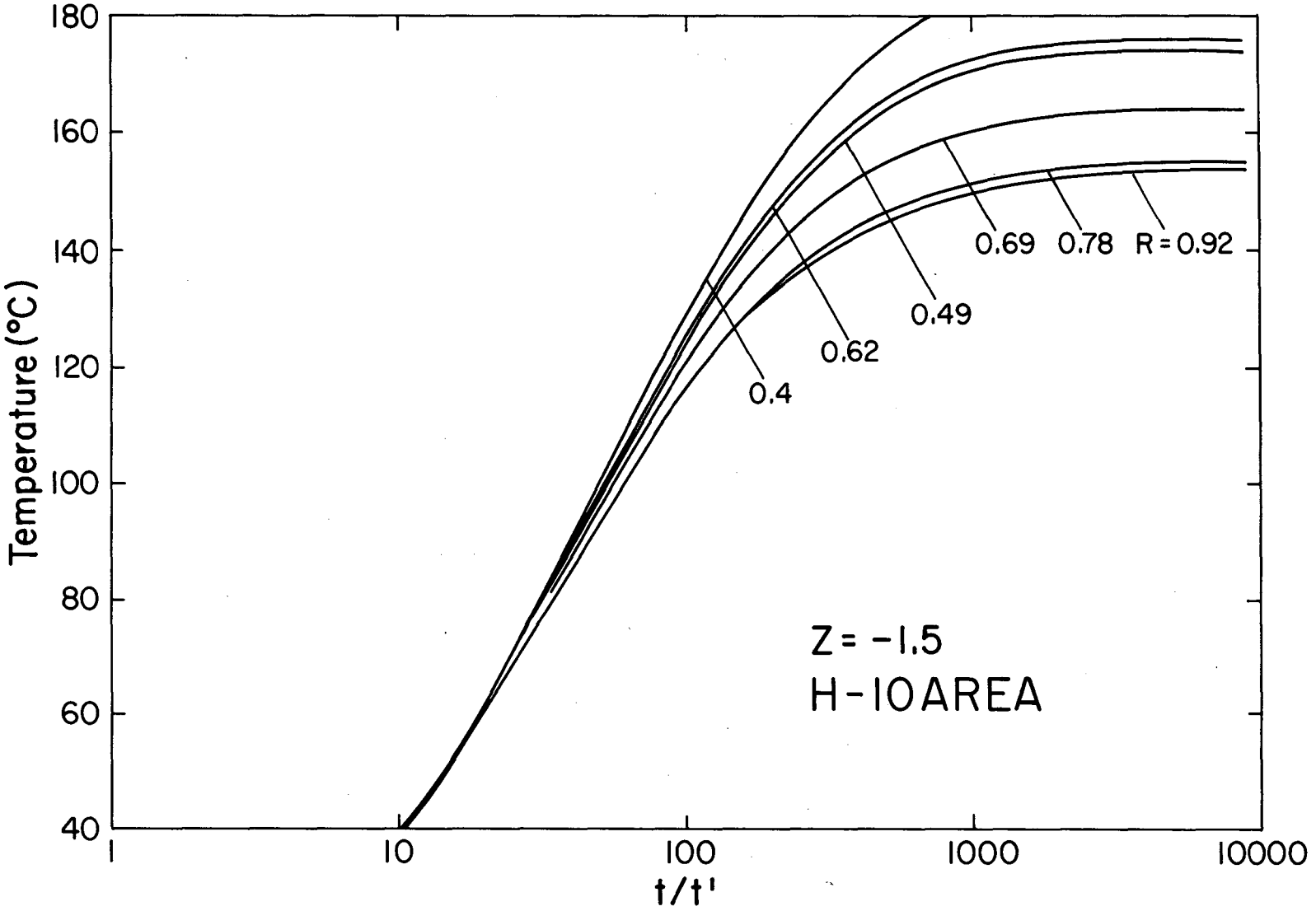

Fig. 30. Semi-log plot of variation in residual temperature versus t/t' as measured at Z = -1.5 m in the H-10 area.

XBL 818-3410

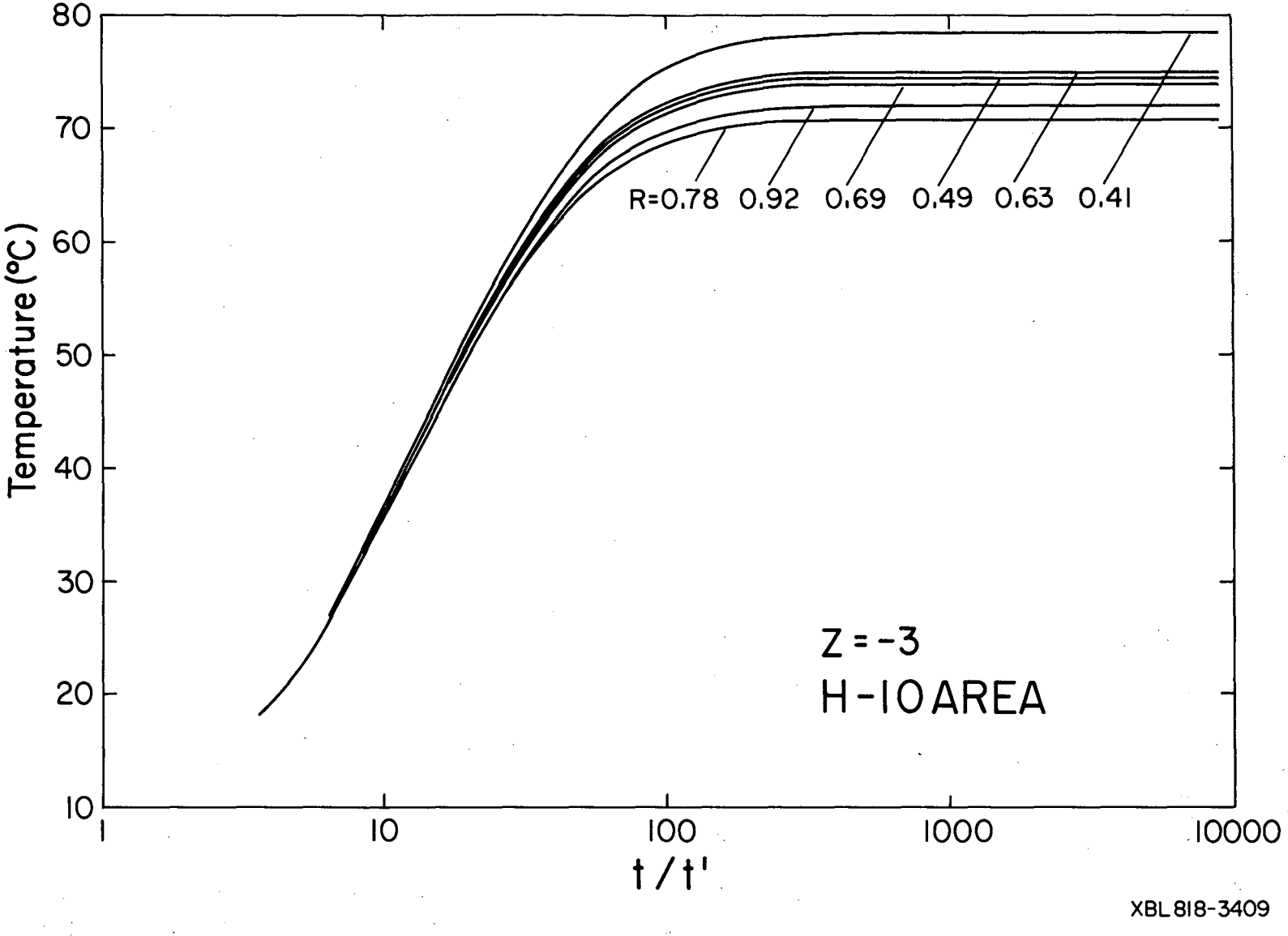

Fig. 31. Semi-log plot of variation in residual temperature versus t/t' as measured at Z = -3 m in the H-10 area.

the rest, exactly the reverse of Fig. 27. The reason for this has been discussed in section 2.3.2. Thermocouples in the T-holes at R = 0.4 m were located somewhat higher than their planned position, and those in the T-hole at R = 0.8 m were somewhat lower. However, the effect is more pronounced at Z = $\pm$ 3 m because the 2.6-m long main heater generated a large vertical gradient around the elevations of $\pm$ 1.5 m. The peripheral heaters are 4.3 m high. Thus the vertical gradient they created at the $\pm$1.5 m elevations was negligible, but was quite significant at the $\pm$3 m elevations.

The effect of vertical displacement on some thermocouples at these elevations has therefore been magnified.

In addition, Figs. 27 and 28 show that the response of the thermocouples above the midplane in the T-hole at R = 0.5 m is not compatible with the responses in other T-holes. Figure 27 shows that the temperature at R = 0.5 m was much hotter than the other thermocouples at this level. In fact, it recorded 101°C until 20 hours after turn-off, corresponding to $t/t' = 400$, while the other thermocouples at the same level were all between 60 to 70°C. Temperatures for this thermocouple drop rapidly for values of t/t' smaller than 400 and converge to the actual rock temperature when $t/t' = 100$, about 3 days after turn-off.

Figure 28 shows that at the time of turn off the thermocouple at elevation Z = 1.5 m in the same hole was recording a lower temperature than expected and continued cooling further. After $t/t' = 400$, the rate of cooling increased and temperatures fell below those of other thermocouples. Some time around $t/t' = 60$, or 6 days after turn-off, temperatures at R = 0.5 m started registering true rock temperatures.

The explanation for this phenomenon is that long before turn-off of the heaters, some amount of water had started flowing into the hole through fractures intersecting the hole at an elevation above Z = 1.5 m. This flow may be related to injection tests that were taking place at the same time in the ventilation drift. Downward flow of water through the sand filling the hole brought water into contact with very hot sand, around 180°C. Evaporation of the water lowered the temperature of the sand around the thermocouple at Z = 1.5 m and sent steam upward. The rising steam brought heat to the upper thermocouple at Z = 3 m, raising its temperature from around 70°C to 101°C.

This phenomenon continued until the rock temperature at the elevation of Z = 1.5 m cooled down and the supply of steam stopped. At this time, the upper thermocouple also cooled down to the actual rock temperature. However, as long as the temperature at the lower thermocouple was above 100°C and capable of generating steam, the presence of steam did not allow the upper thermocouple to register the true rock temperature. A more detailed discussion of this phenomenon will be presented in a separate report.

Finally, temperatures at thermocouples in all T-holes at the same level equalize for values of $t/t' < 30$, which corresponds to 13 days. This means that, at least in the near field after 13 days, there were horizontal planes of isothermals.

3. MODELING

Once the measured data have been evaluated and the faulty portions distinguished, one can examine how well the thermal response of the rock can be predicted for the thermal power supplied by the heaters.

3.1 The "DOT" Code and Its Capabilities

A finite element code called "DOT" developed by Polivka and Wilson (1976), was employed for this study. Its capabilities include the following:

(a) "DOT" can solve steady state or transient heat conduction in the solid with a plane or axisymmetric geometry.

(b) It can handle a nonuniform initial temperature distribution.

(c) It can allow the thermal properties of a solid to be a function of temperature, thus allowing the solution of problems that are non-linear.

d) It can solve problems with convection and radiation as well as isothermal and adiabatic boundary conditions.

e) Boundary conditions can be time dependent.

3.2 Sensitivity Analysis

Some characteristics of the actual field problem had to be simplified in order to make it manageable for this model. In section 1.2 we discussed the assumptions and simplifications that were imposed to obtain solutions by the closed-form analytic method. The DOT finite element code allowed us to relax some of those assumptions. It is of interest, however, to evaluate their influence.

Figure 32 shows a sketch of the two models employed in these investigations. Model A was used in the preliminary study of thermal fields for the full-scale experiments (Chan et al., 1978). Model B represents the geometrical arrangement used in "DOT." In the latter approach, we attempted to incorporate the effects of the drift openings, as well as certain information on initial conditions and material properties that were not available when the first predictions had to be made.

Certain field conditions could not be included in either model. One is the discontinuity of the rock mass. The granite has been intruded by dikes and is highly fractured (Olkiewicz, et al., 1979; Gale and Witherspoon, 1979). It was assumed that the thermal conductivity of the rock was not affected by these fractures. Another condition is the magnitude of heat transfer due to convection of groundwater in the fracture system. Because of the low permeability of the rock mass, this was assumed to be very small (Chan et al., 1980b). A third condition is the mode of heat transfer from the outer surface of the heater to the wall of the borehole. In both models, perfect thermal contact between heater and rock was assumed. We shall examine this assumption below.

Otherwise, however, the effects of factors that were not incorporated in Model A could be examined in Model B. These factors are: (a) a nonuniform initial temperature condition that was not known when the first temperature calculations were made, (b) the temperature-dependent thermal conductivity, also unknown at the beginning, and (c) the drift openings surrounding the heat source. These factors and an analysis of the mechanisms of heat transfer within the heater hole are discussed below.

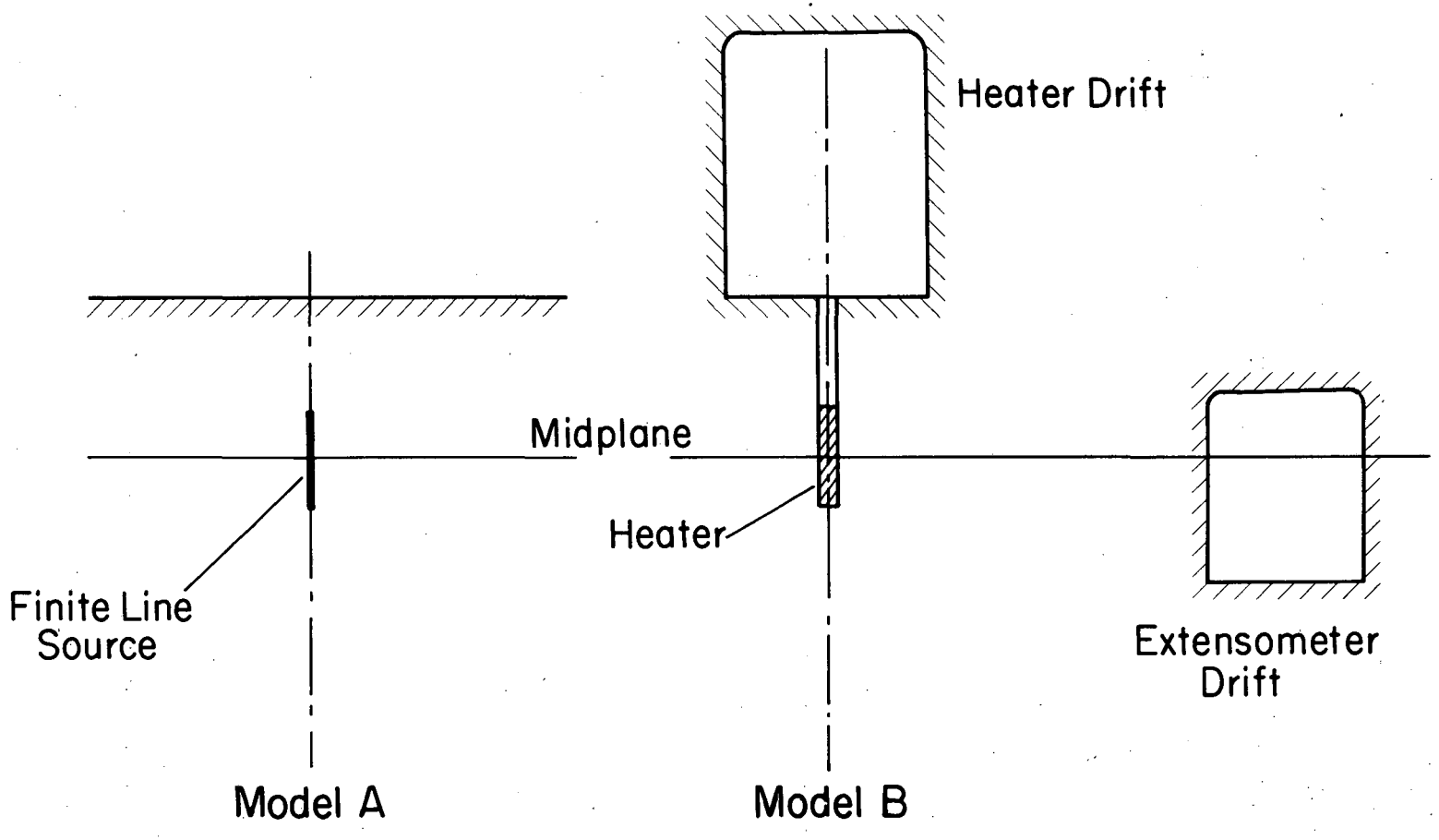

Fig. 32. Cross-sections of Model A, used for the preliminary study, and Model B, which included the position of the heater together with the heater drift and the extensometer drift.

3.2.1 Nonuniform Initial Condition

In the first temperature investigations using Model A, a uniform initial rock temperature of 10°C-- close to the original ambient-- was assumed. Shortly before starting the heater experiments, it was found that temperatures on the floor of the heater room had increased a few degrees above 10°C, and this resulted in the profile shown in Fig. 33. Model B therefore used this nonuniform temperature distribution as the initial condition.

Plots of temperature differences versus time between the two models at radius R = 0.4 m and three different elevations (Z= 0.0, 1.5, and 3.0 m) of the H-9 area are given in Fig. 34; the figure shows that the differences diminish with time. At any point, the maximum error due to the assumption of uniform initial temperature is equal to the difference between the actual initial temperature and the value used for input to the model.

3.2.2 Temperature-Dependent Thermal Conductivity of Granite

As mentioned in Chapter 1, Pratt et al. (1977) measured the thermal conductivity of Stripa granite in the laboratory and found it to be temperature dependent. To investigate the effect of this temperature dependency, we considered three models; two used constant thermal conductivities of 3.2 and 3.6 W/m°C (the former is the conductivity used in the preliminary calculation), and the third used a temperature-dependent thermal conductivity based on the formula given by Pratt et al.:

$$k(t) = 3.6 - 0.0037\ T\ (W/m°C).$$

The radial variation of temperatures in the midplane (Z = 0) is shown in Fig. 35 for two values of time, 10 and 100 days, for three cases. The actual

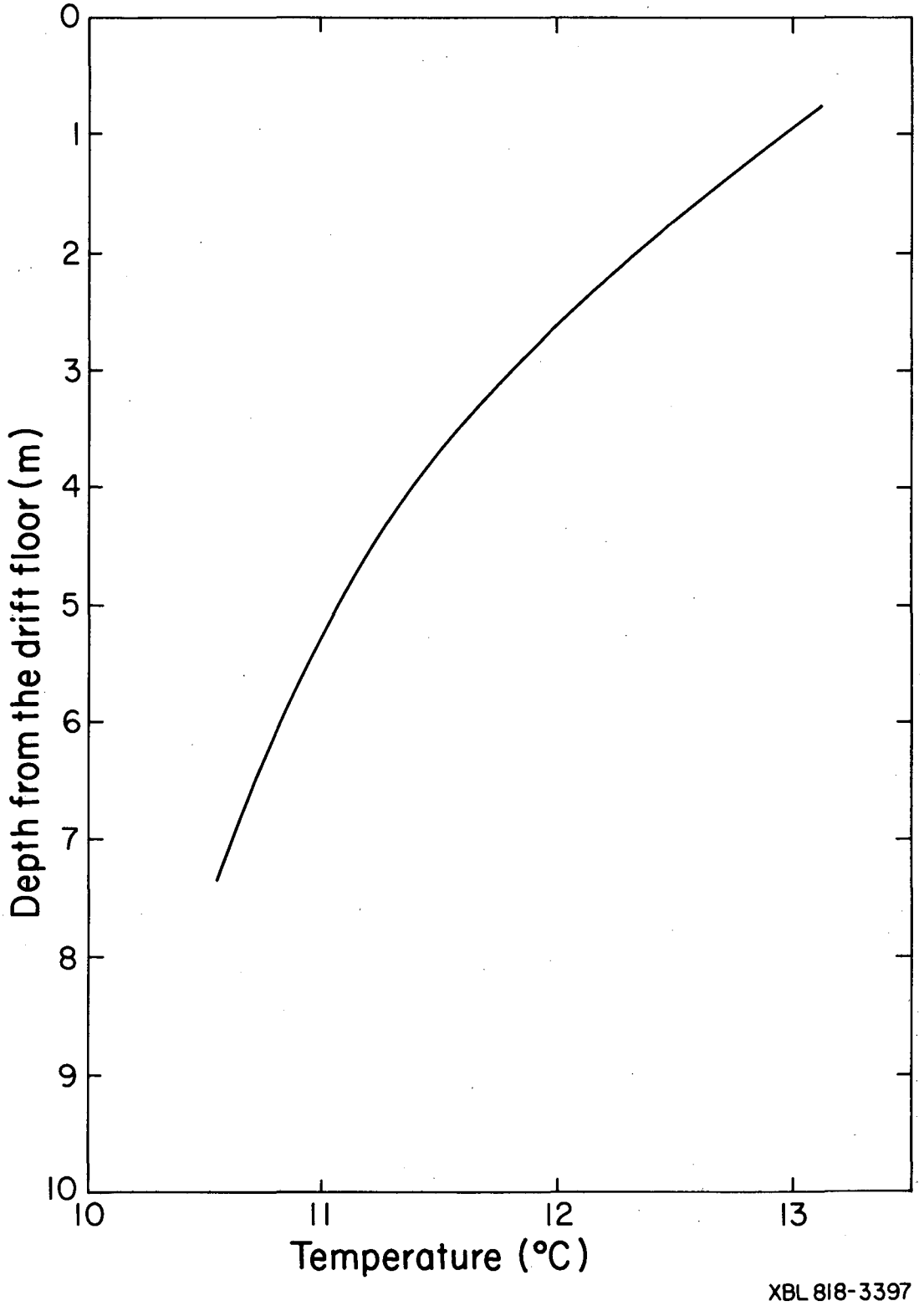

Fig. 33. Vertical distribution of temperature before the start of the experiment, measured at T-16.

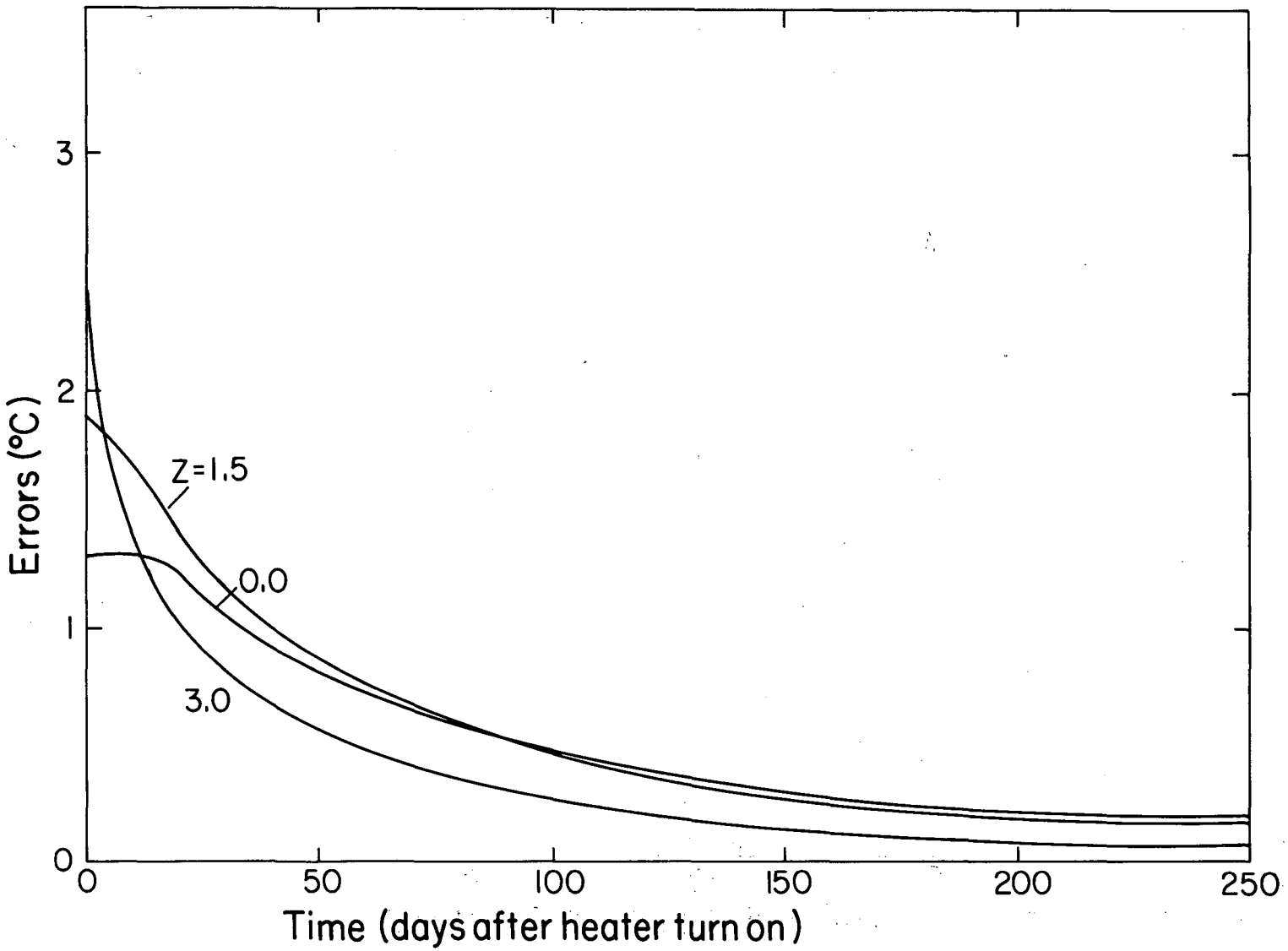

Fig. 34. Errors due to the assumption of a uniform initial temperature (10°C) and its variation with time at R = 0.4 m.

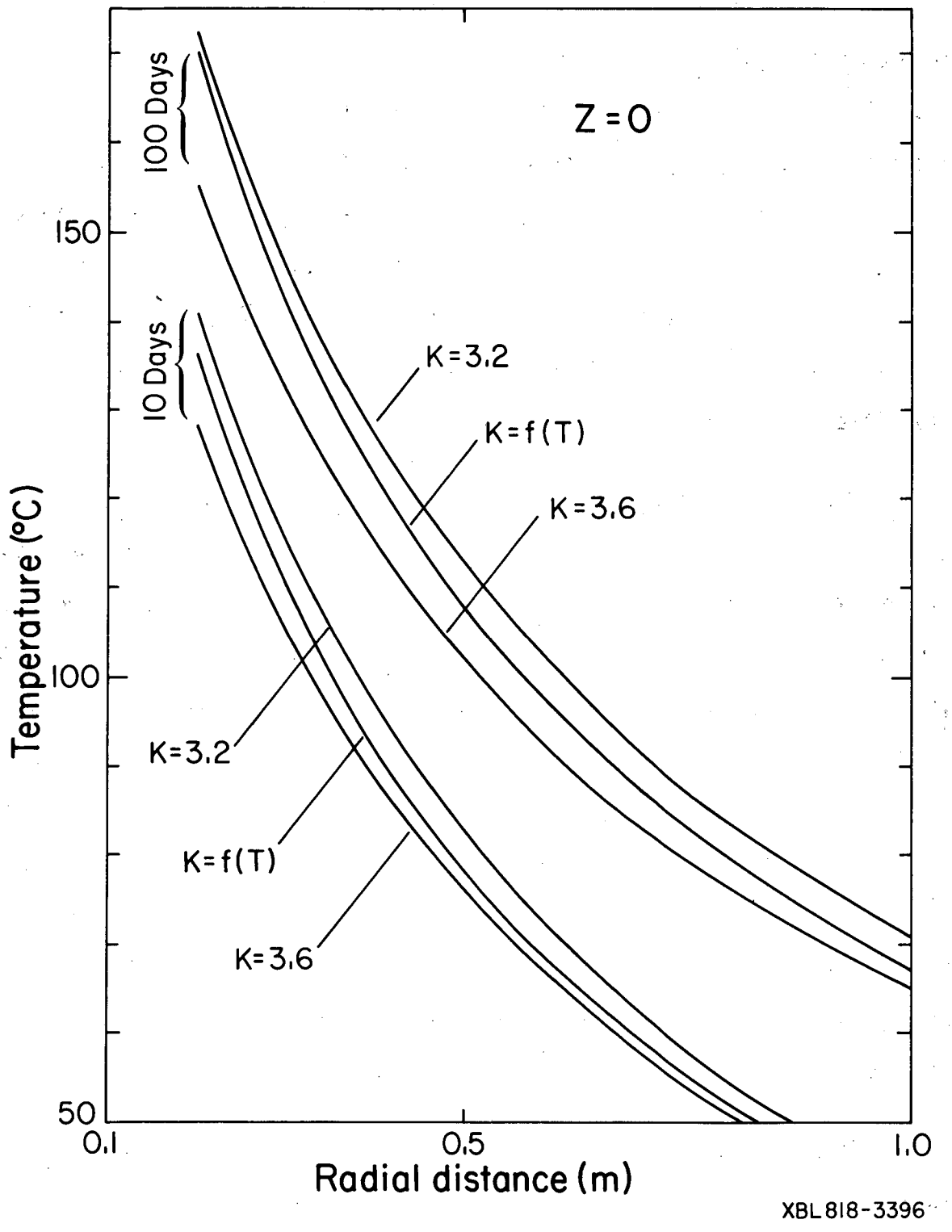

Fig. 35. Calculated radial variation of temperature in the midplane of 3.6 kW heater, at 10 and 100 days.

response of the rock, as given by the thermal-dependent model, seems to fall between the results of the two models with constant thermal conductivities. Thus closer to the heater, where the rock is warmer, the "actual" temperature seems to be closer to that predicted by the model with k = 3.2 W/m°C, while at distances beyond 1 or 2 m, where the rock is cooler, the model with k = 3.6 appears more accurate. The differences in calculated temperatures between these two models range from 2 to 5°C, depending on time and the distance from the heater. These results were obtained for the 3.6-kW heater; the differences are not expected to be larger for the 5 kW heater.

3.2.3 Effect of Boundary Conditions

In the early stages of the experiment, when the wave of rock heating had not yet reached the floor of the heater drift, both isothermal and adiabatic boundary conditions would have given the same results at the thermocouple positions. Once heating reached the floor of the drift, however, either a natural or a forced convection condition would seem more logical, depending on the velocity of air flow in the drift. The rate of heat loss by convection also depends on the drift air temperature. Drift air temperature was not closely controlled during the heater tests. Because of the distance of the heaters from the drift floor and the small increase of rock temperature there, one would expect the rock temperature to more or less follow of the variation in air temperature.

Values of the measured temperature at the floor of the heater drift are shown in Fig. 13. This figure shows that, in spite of oscillation, the average temperature is around 14°C, with a couple of degrees variation, so that an

isothermal condition on the drift floor would also be quite reasonable. Nevertheless, it is of interest to examine the influence of different heat transfer conditions at the drift on the temperature distribution in the rock.

To investigate the effect of a convection boundary condition, two sets of calculations, based on different heat transfer coefficients, were conducted. The first calculation used a coefficient of h = 3 $W/m^2°C$, corresponding to an air velocity of 1.1 m/sec. The calculated temperature at a representative point at the floor (R = 1.3 m, Z = 4.25 m) rose to 18.2°C in 40 days and 20.8°C in 200 days. These calculated temperatures are obviously warmer than the actual measured temperatures (Fig. 13). To achieve a smaller temperature rise at the floor, a larger coefficient of heat transfer, h = 8 $W/m^2°C$, corresponding to an air velocity of 3.9 m/sec, was employed for the second example. In this case, the maximum rock temperature at the floor is predicted to be a more reasonable 18.9°C. In comparison with the isothermal boundary condition model, the model with a heat transfer coefficient of h = 8 $W/m^2°C$ predicts generally higher rock temperatures. The maximum difference at elevation Z = 3 m is about 2°C. Both models predict identical temperatures below the heater midplane.

To examine the influence of the extensometer drift on temperature prediction, we employed two models with only one difference: one had no opening at the site of extensometer drift, and the other had an opening the size of that drift with its wall kept at 11°C. The interesting part of the results of these two models at an arbitrary point (R = 0.5 m, Z = 0) is shown in Fig. 36, which also includes the measured temperatures. To show the significance

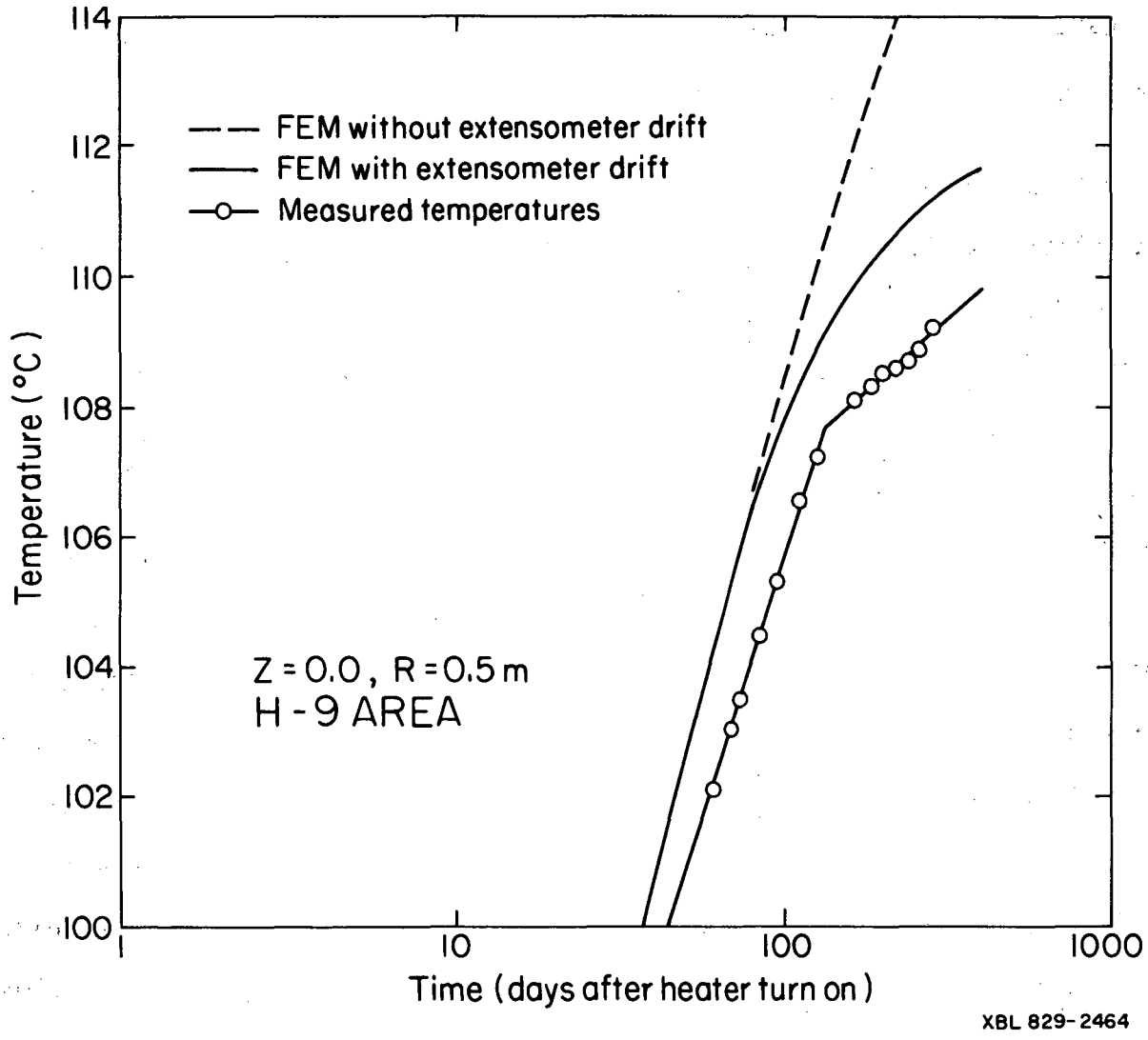

Fig. 36. Effect of extensometer drift on the temperature variation at R = 0.5 m, Z = 0.0, H-9 area.

of the effect, the temperature scale has been arbitrarily magnified. This figure shows that, up to about 130 days after the H-9 heater turn-on at 3.6 kW, a semi-log plot of measured temperatures versus time follows a straight line. Later, these data fall on another straight line with a smaller slope, indicating the presence of some sort of constant temperature boundary.

The results from the model without the extensometer drift also lie on a straight line, but no change in slope is visible. However, after the extensometer drift was included in the model, the calculated results followed the same trend as the measured data. In short, since the extensometer drift is relatively far from the heater, its effect is not felt by the rock mass in the near field until about 100 days after heater turn-on. After that, small amounts of cooling effects build up. At 400 days after heater turn-on, the error due to ignoring the extensometer drift is of the order of 3 to 4°C.

3.3 Mechanism of Heat Transfer Within the Heater Hole

The mechanism of heat transfer within the heater hole is probably one of the most important factors in understanding the thermal field around the heater. The arrangement of equipment in the hole is shown in Fig. 3. The canister, a steel cylinder with a diameter of 0.324 m and a height of 2.6 m, sits on a steel plate supported by a layer of pea gravel at the bottom of the hole. The exact thickness of gravel is not known but was supposed to be 0.084 m. The borehole diameter is 0.406 m, and the annulus between the canister and the rock wall was filled with air. At the top, the canister was covered with 1.05 m of vermiculite for thermal insulation.

Three pairs of thermocouples measured temperatures on the inner side of the canister wall. These thermocouples were placed at elevations -0.51, 0.1 and 0.71 m relative to the midplane of the heater. The temperatures registered during the first few days reveal a temperature gradient from top to bottom. The upper half was warmer, indicating either uneven heating or some convection mechanism in the early days of the experiment. Later, however, this pattern changed and temperatures were more uniform, with the central temperature being somewhat warmer. This, in fact, was also the reaction of the thermal field in the rock.

About 100 days after the 5 kW heater turn-on, the temperature of the canister was measured to be about 310°C. Unfortunately, no thermocouple was on the wall of the hole, but calculations show that the maximum temperature after 100 days was about 245°C. This was the midplane temperature; points away from the midplane were cooler.

This result raises the important question of the actual modes of heat transfer between the canister and the rock: radiation, convection, conduction, or a combination of these. Understanding the contribution of each mode is necessary to develop a correct model of the thermal field.

As a first step, let us consider the effects of radiation. The net exchange of the radiant energy between the canister of the 5 kW heater and the rock may be given by:

$$Q = \varepsilon \sigma (T_1^4 - T_2^4) A_1 F_{A_1-A_2} \qquad (1)$$

Where Q is the net rate of heat transfer in watts;

ε is the surface emissivity, which for the material of the canister (AISI 304 stainless steel) is about 40% at 310°C (Wong, 1977);

σ is the Stefan-Boltzmann constant (5.67×10^{-8} W/m^2·K^4);

A_1 is the surface area of the canister in m^2;

T_1 and T_2 are the absolute temperatures of the canister surface and the rock, respectively, in degrees K; and

$F_{A_1-A_2}$ is a configuration factor, which in this case is 0.98.

Since the exposed surface area of the canister is:

$$A_1 = \pi D\ell = \pi(0.324)(2.6) = 2.65 \text{ m}^2$$

then at a surface temperature of 310°C, the radiant heat transfer is:

$$Q = 0.4(5.67 \times 10^{-8})(583^4-518^4)(2.65)(0.98) = 2564 \text{ W.}$$

To calculate the rate of energy transmitted by conduction, one must break down the sources of conduction into three parts. Part one is from the side of the canister in contact with the air. The rate of heat transferred from this side may be approximated by:

$$Q = kA \frac{\Delta T}{L} \qquad (2)$$

where k is the thermal conductivity of the air in W/m°C (which for air at 250°C is about 0.0405 W/m°C), and A is the surface area, in this case the area of the cylinder between the canister and the rock.

$$A = \pi \left(\frac{0.324 + 0.406}{2}\right)(2.6) = 2.98 \text{ m}^2$$

ΔT is the temperature difference between the canister and the rock, and L is the distance between canister and rock. Thus:

$$Q = 0.0405\ (2.98)\ \frac{65}{0.041} = 191\ W$$

One may also calculate Q for conduction from the following formula:

$$Q = \frac{2\pi k l \Delta T}{\ln\ r_2/r_1} = \frac{2\pi(0.0405)(2.6)(65)}{\ln\ \frac{0.406}{0.324}} = 190.2\ W$$

which is not much different.

Part two is the heat transmitted from the bottom of the canister. This part could also be approximated from Eq. (2). Here k here would be the thermal conductivity of the pea gravel. We do not know the exact value of k for the kind of pea gravel used in the heater hole, but its thermal conductivity should be less than 3, and more than 0.04 W/m°C. No large error should be introduced if we assume k = 0.44 W/m°C for pea gravel with a porosity of 0.20. Then:

$$Q = \frac{0.44\ (\pi)\ (0.406)^2\ (310 - 160)}{4\ (0.084)} = 102\ W$$

Estimated from the model, 160 is the temperature of the rock just beneath the gravel.

Part three of this mode is the heat conduction from the top of the canister. That part theoretically should not transmit any energy, but actually the rate of heat transmitted is not zero. For the sake of simplicity, let us ignore the heat loss from the top. The total rate of energy transmitted from the canister to the rock by conduction is therefore about

$$191 + 102 = 293 \text{ W}$$

Thus the sum of the heat transmitted by radiation and by conduction is estimated to be about

$$2564 + 293 = 2857 \text{ W}$$

This means that the balance of the heat, about 2143 W or approximately 2/5 of the energy input, was transmitted by convection.

Although this is a rough calculation, using data for the one hundredth day after heater turn-on, it at least sheds light on the way heat was transmitted to the rock. In addition, it seems to explain the asymmetric nature of temperature measurement in the space between the heater canister and the rock, such as is shown in Fig. 37 for the 3.6 kW heater.

3.4 Modeling of 3.6 kW Heater Experiment

After all the information discussed above was considered, together with the capabilities of the code, a model was constructed to calculate the thermal field around the 3.6 kW heater. Its geometry is shown in Fig. 38. It incorporates the following conditions.

(a) Thermal conductivity of the rock was temperature-dependent.

(b) Initial temperature distribution was nonuniform and was based on the actual measurement in the field before the start of the experiment.

(c) A heat plug with the dimensions and thermal properties of the vermiculite was considered to be above the heater.

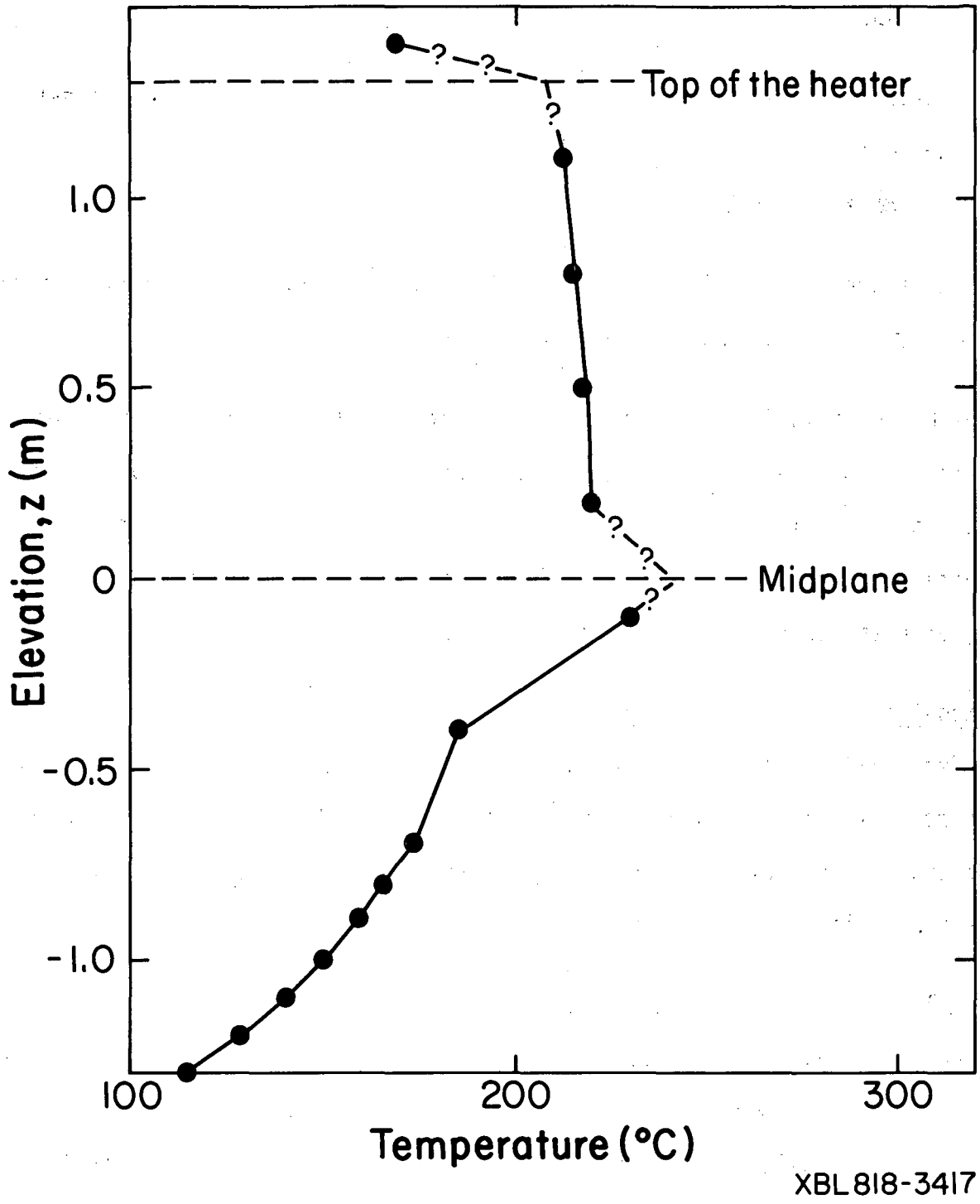

Fig. 37. Vertical profile of temperature measured in the air gap of 3.6 kW heater hole.

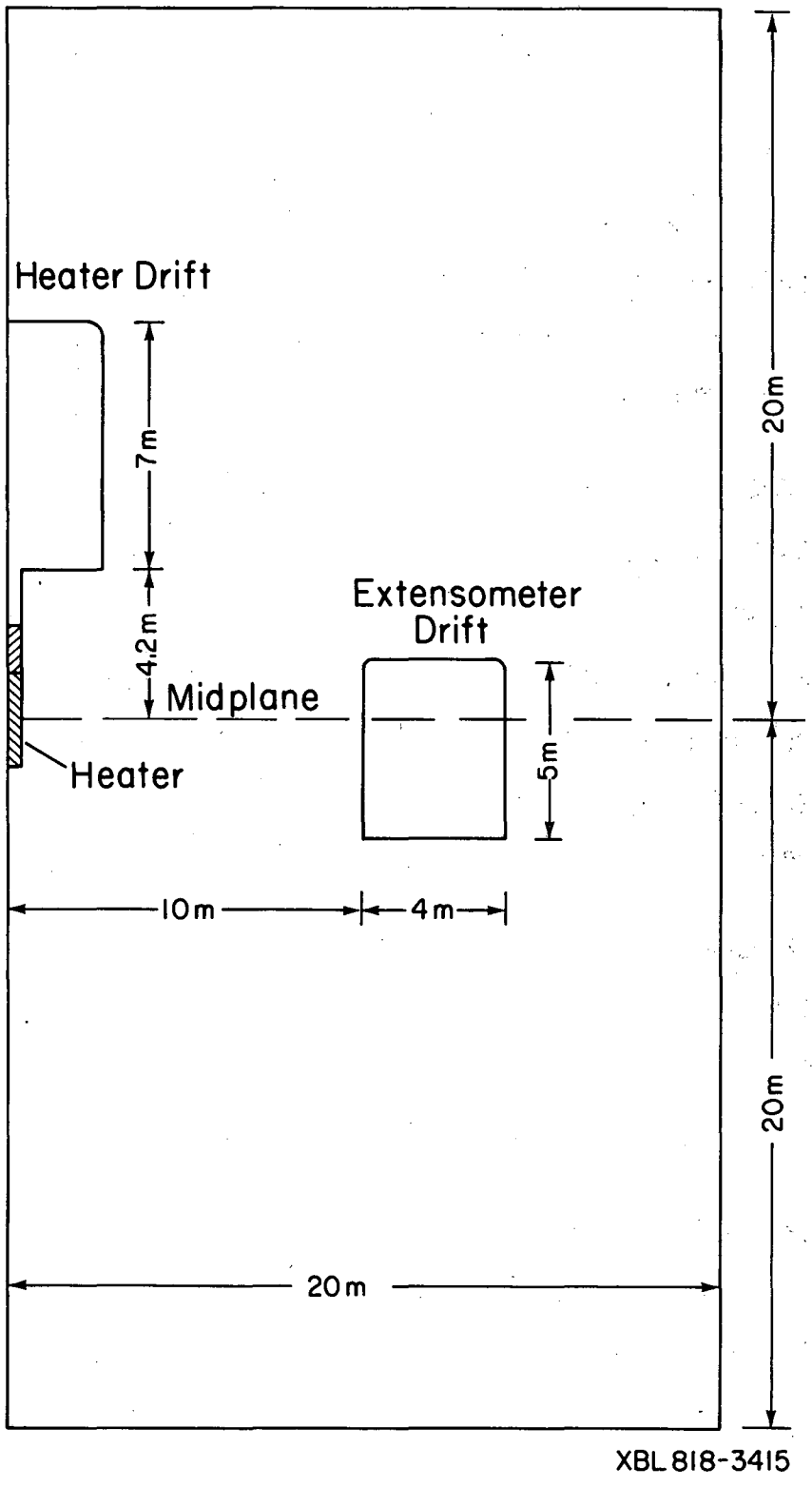

Fig. 38. Geometry of the model used for 3.6 kW heater experiment, vertical section.

(d) A layer of pea gravel was considered to be beneath the heater. Thermal properties which were used for vermiculite and pea gravel are given in Table 1.

(e) Rock temperature adjacent to the heater drift was kept at 14°C. Adjacent to the extensometer drift, the rock was kept at 11°C.

(f) The heater was considered to be in direct contact with the rock, thus ignoring the gap between the canister and the rock.

(g) The outside boundary was assumed to be adiabatic.

Calculated temperatures on the midplane (Z = 0) for two values of R = 0.4 and 0.89 m are shown in Fig. 39; values of measured temperatures at these points are also exhibited. Except for very early times, when the measured temperatures are slightly warmer than the calculated ones, we have a perfect match between the measured and calculated data. That slight deviation during the first two days could be due to the energy consumed in heating the total volume of rock assumed to be occupying the heater hole in the model.

Figure 40 shows calculated and measured temperatures at the elevation Z = 1.5 m. As in Fig. 39, temperature variations are for the radial distances R = 0.4 and 0.89 m, but unlike the previous figure, the calculated temperatures are much cooler than the measured ones (over 10°C at R = 0.4 m).

Below the midplane, at Z = -1.5 m we have the reverse condition: Fig. 41 shows measured temperatures cooler than calculated ones (over 10°C at R = 0.4 m). This difference starts at an early stage and continues throughout the experiment.

Table 1. Thermal properties of vermiculite and pea gravel.

Materials	Density (kg/m^3)	Specific heat (J/kg-°C)	Thermal conductivity (W/m-°C)
Vermiculite	168	921	0.06
Pea gravel	2080	862	0.44

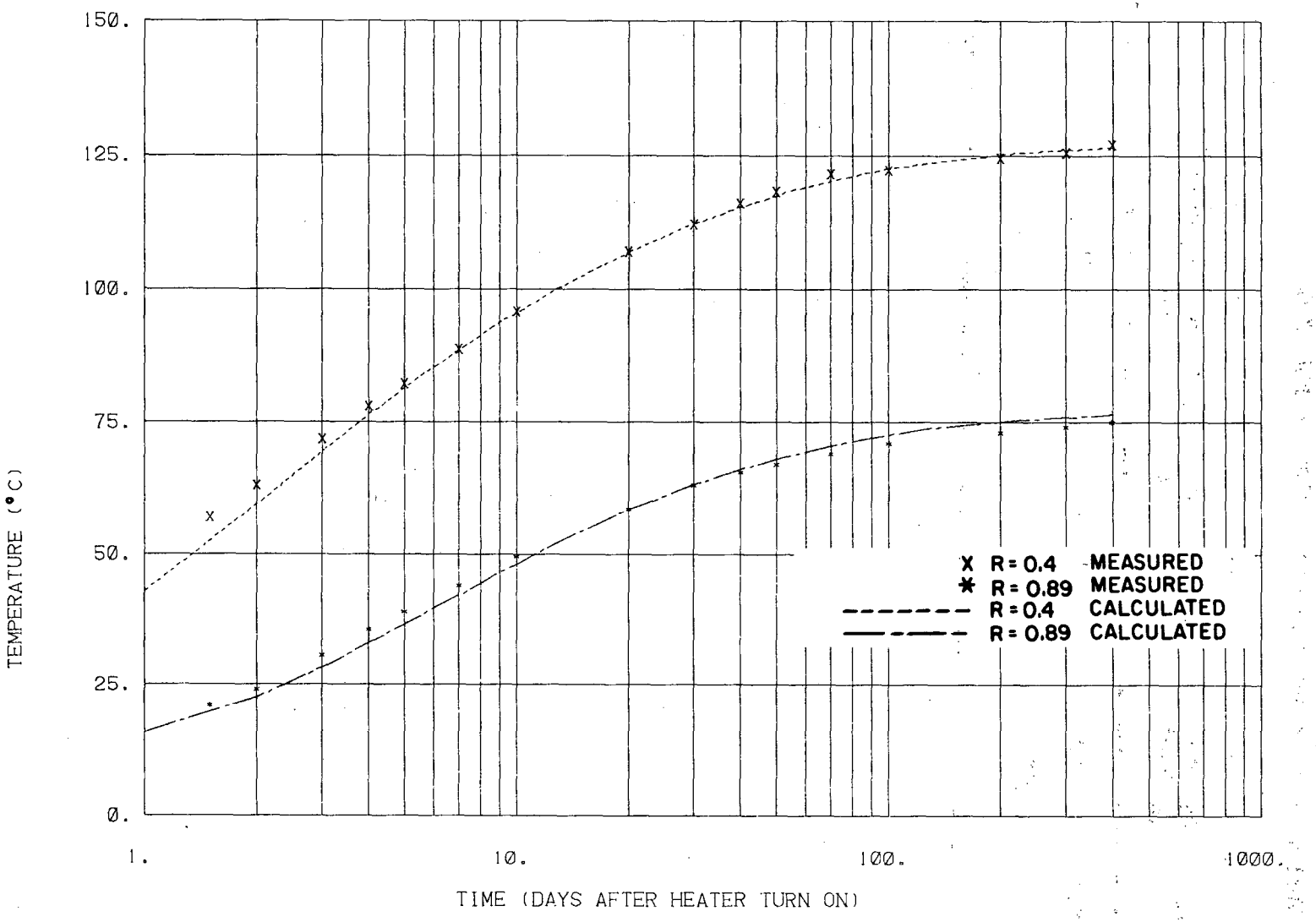

Fig. 39. Variation in calculated and measured temperatures with time on the midplane (Z = 0) in H-9 area.

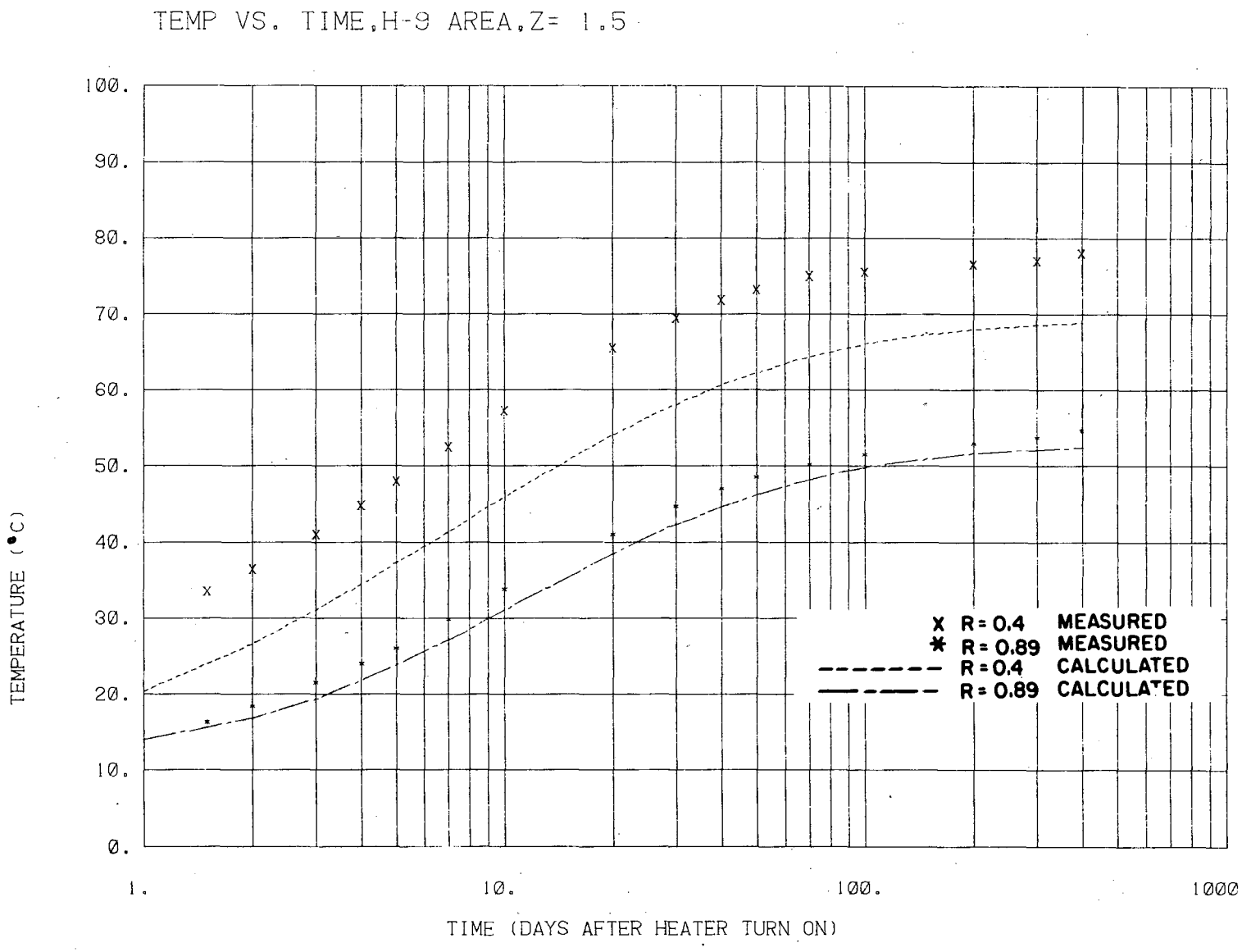

XBL 817-3338

Fig. 40. Variation in calculated and measured temperatures with time at Z = 1.5 m, H-9 area.

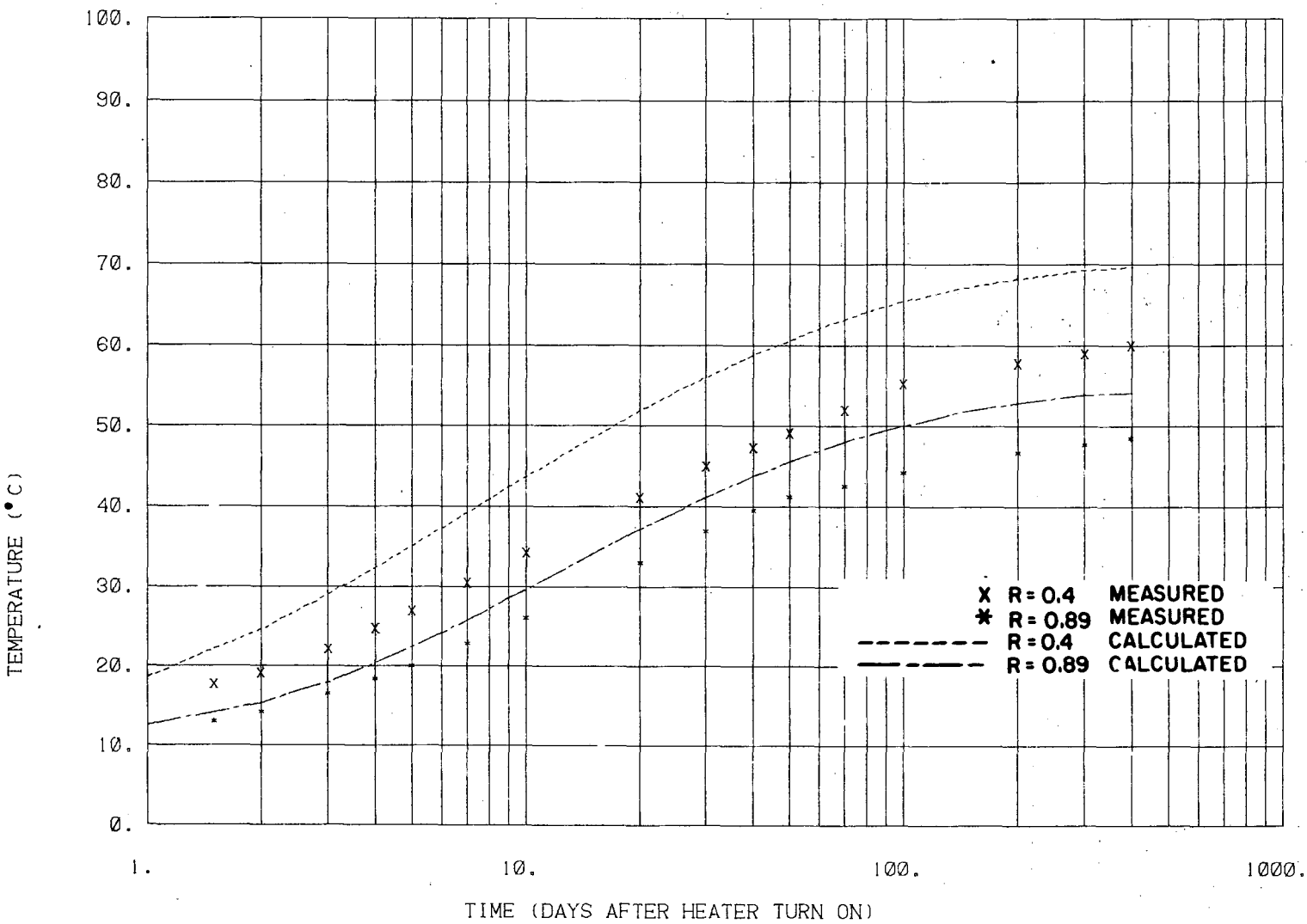

Fig. 41. Variation in calculated and measured temperatures with time at Z = -1.5 m, H-9 area.

Figures 42 and 43 present the same information for the levels 3 m above and below the midplane, and exactly the same trend can be seen: calculated temperatures are cooler above the midplane and warmer below.

Two factors could be responsible for these discrepancies:

(a) The heater may actually be a few centimeters above its planned position.

(b) Convection cells in the air gap between the heater canister and the rock may cause more heat to be transferred to the upper part of the rock.

A combination of these factors is also possible. In any case, neither would affect the temperature measurements at the midplane because of its very small vertical temperature gradient (Fig. 39).

In situ measurement during the experiment showed that the 3.6 kW heater was indeed installed about 10 to 13 cm above the planned position. However, some uncertainty about the exact position remains because of the irregular relief of the drift floor.

There is a way to gain further information about the position of the heater. Comparison of Figs. 40 and 41 indicates that, at any given time, the calculated temperature difference between R = 0.4 and 0.89 m is almost equal at both Z = 1.5 and -1.5 m. Measured temperatures, however, do not look like this. At any given time, the temperature difference between R = 0.4 and 0.89 m is larger at the elevation of Z = 1.5 m than that at Z = -1.5 m. This discrepancy has prompted us to study it further.

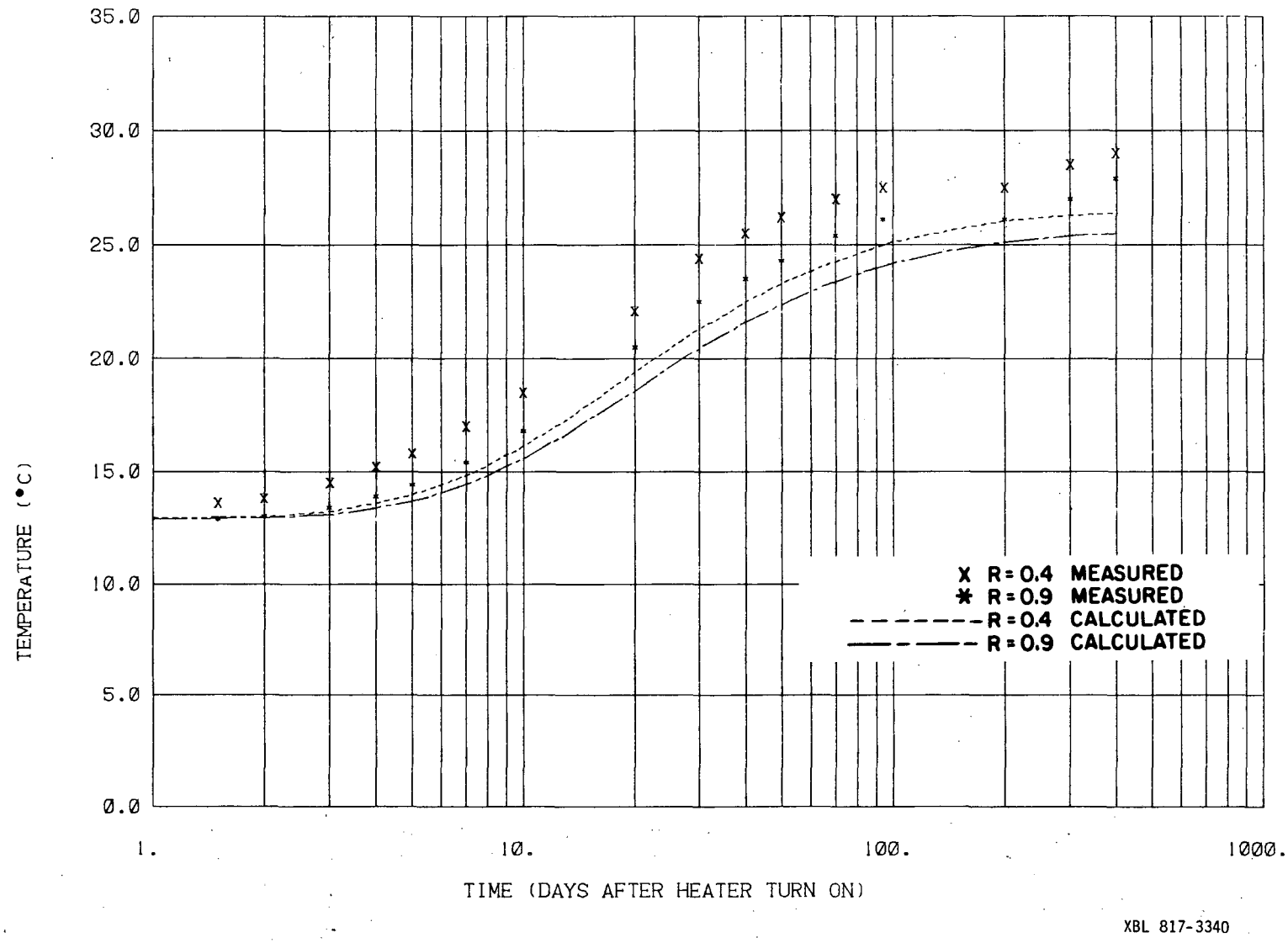

Fig. 42. Variation in calculated and measured temperatures with time at Z = 3.0 m, H-9 area.

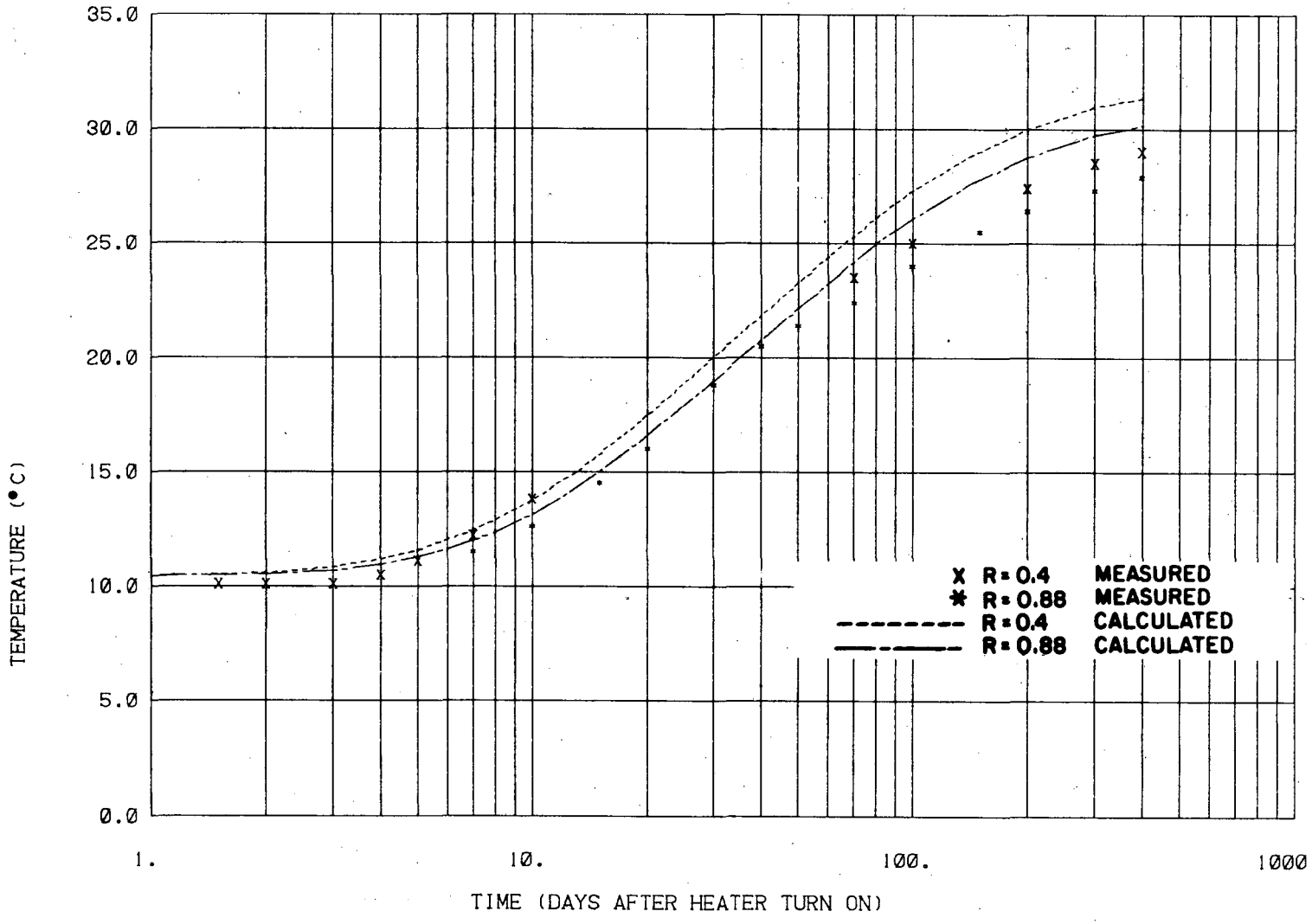

Fig. 43. Variation in calculated and measured temperatures with time at Z = -3.0 m, H-9 area.

Figure 44 presents the vertical profile of the calculated temperatures at the radii R = 0.4 and 0.9 m 40 days after turn-on of the 3.6-kW heater. It is apparent that the temperature difference between these two radii is a function of elevation. Variation with elevation of the calculated temperature difference between R = 0.4 and 0.9 m, shown by $(T_{0.4} - T_{0.9})$, has been plotted in Fig. 45. This figure has been used to estimate the magnitude of the vertical dislocation of the 3.6 kW heater. Comparing the measured differences of the two radii (i.e., $T_{0.4} - T_{0.9}$) at 40 days with Fig. 45 suggests that thermocouples supposed to be 1.5 m above the heater midplane are actually at the elevation of 1.36 m, and those designed to be at Z = -1.5 m are actually 1.63 m below the present heater midplane. These results suggest that the 3.6-kW heater was about 13 to 14 cm above its designed position.

Although this procedure independently confirms the field measurements, one should keep in mind that it was based on the results of the Model B, which has ignored the effect of convection heat transfer in the air gap adjacent to the heater.

3.4.1 Modified Model

The above model was then modified for the 13-cm dislocation of the 3.6 kW heater. Figures 46 through 50 present the comparison between the newly calculated and the measured temperatures at five different elevations. Although we still have some differences between the calculated and the measured values of temperatures, results have improved considerably, compared with the previous calculation. In fact, the magnitude of differences between the calculated and the measured data is within 2°C at Z = 3, 1.5, 0.0, and -3 m. The maximum deviation at Z = -1.5 m is about 3°C.

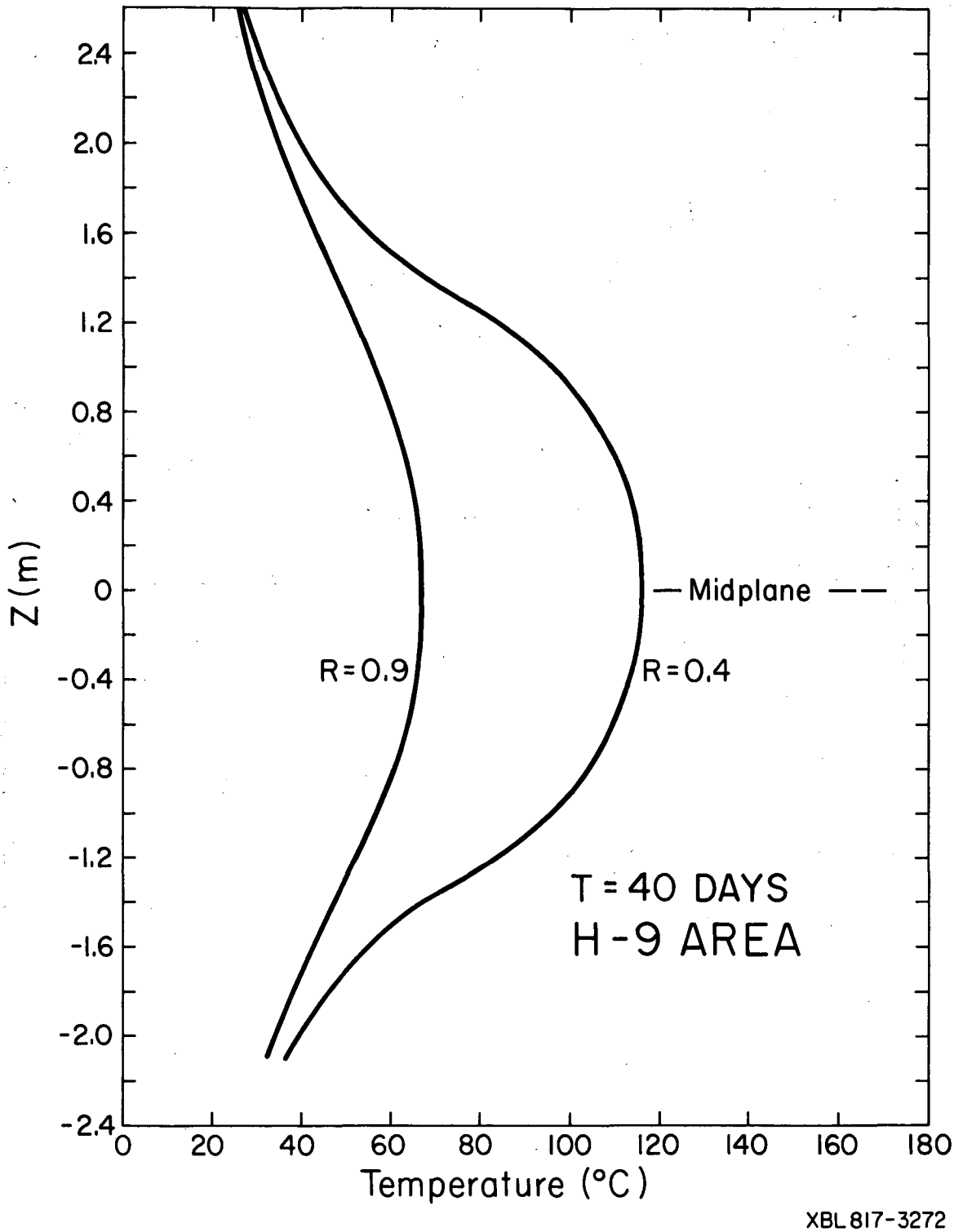

Fig. 44. Vertical profile of calculated temperature at the radii R = 0.4 and 0.9 m, 40 days after turn-on of the 3.6 kW heater.

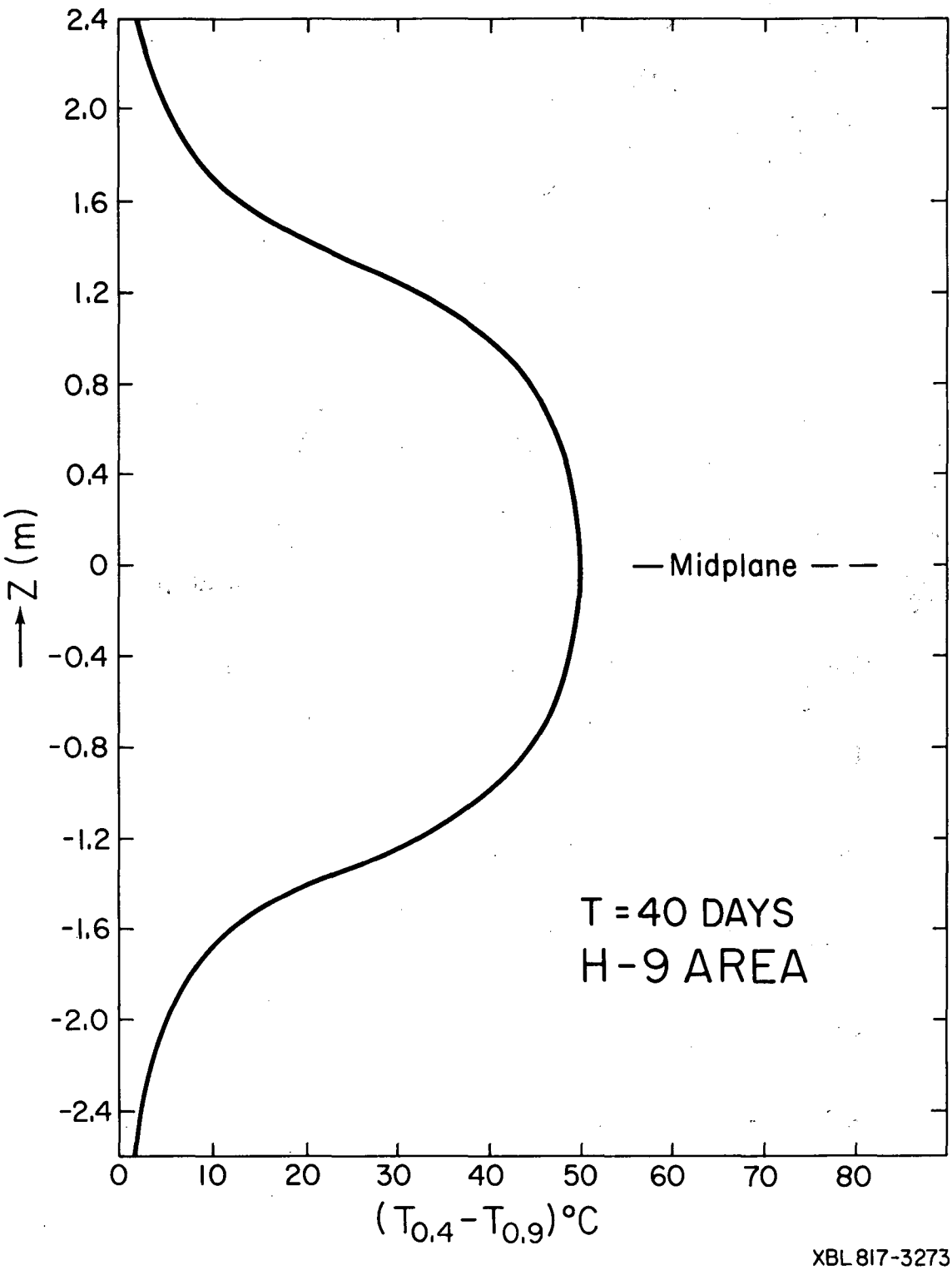

Fig. 45. Variation of ($T_{0.4}$ - $T_{0.9}$) with elevation around the 3.6 kW heater.

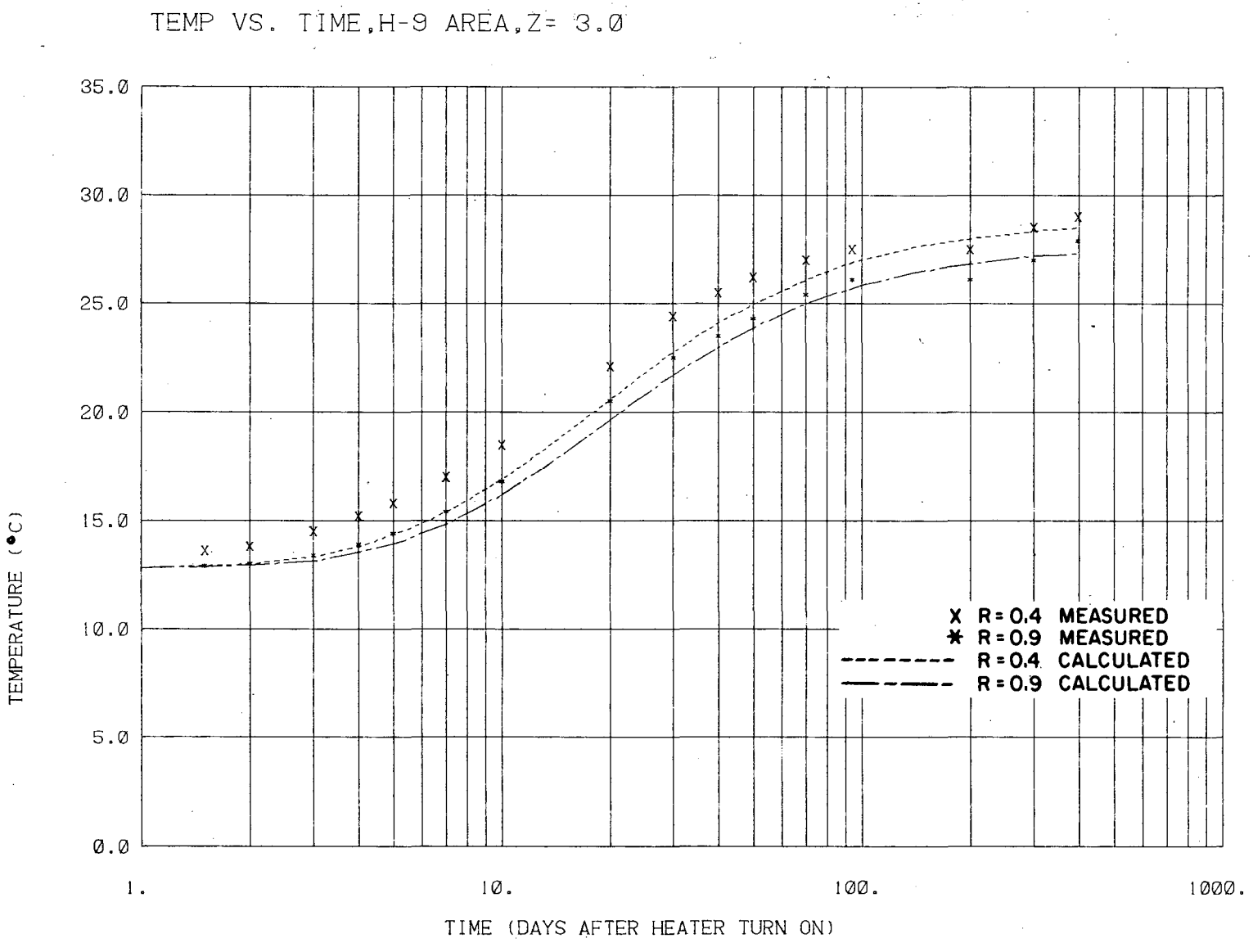

Fig. 46. Calculated and measured temperatures at Z = 3 m of H-9 area after adjusting heater location.

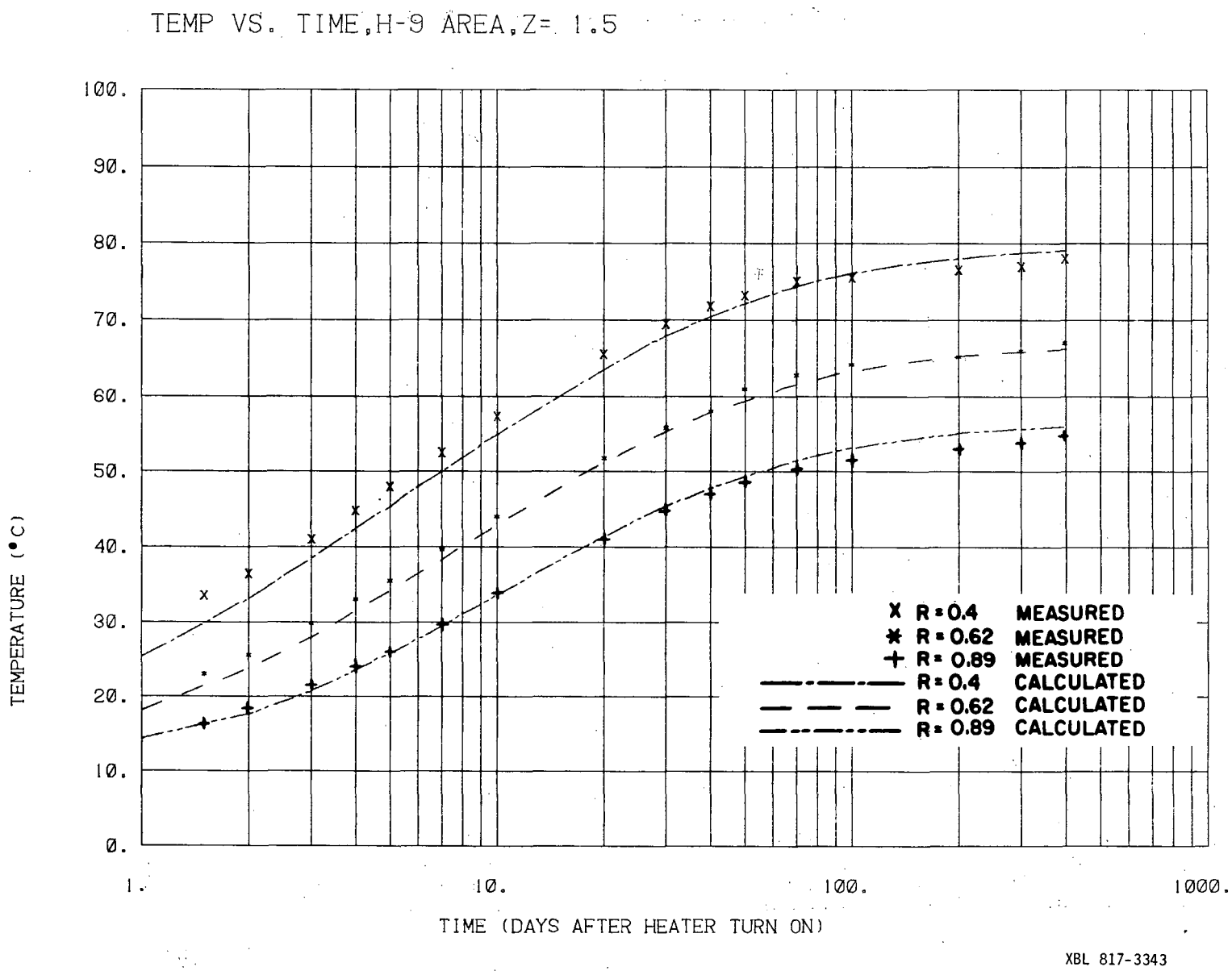

Fig. 47. Calculated and measured temperatures at Z = 1.5 m of H-9 area after adjusting heater location.

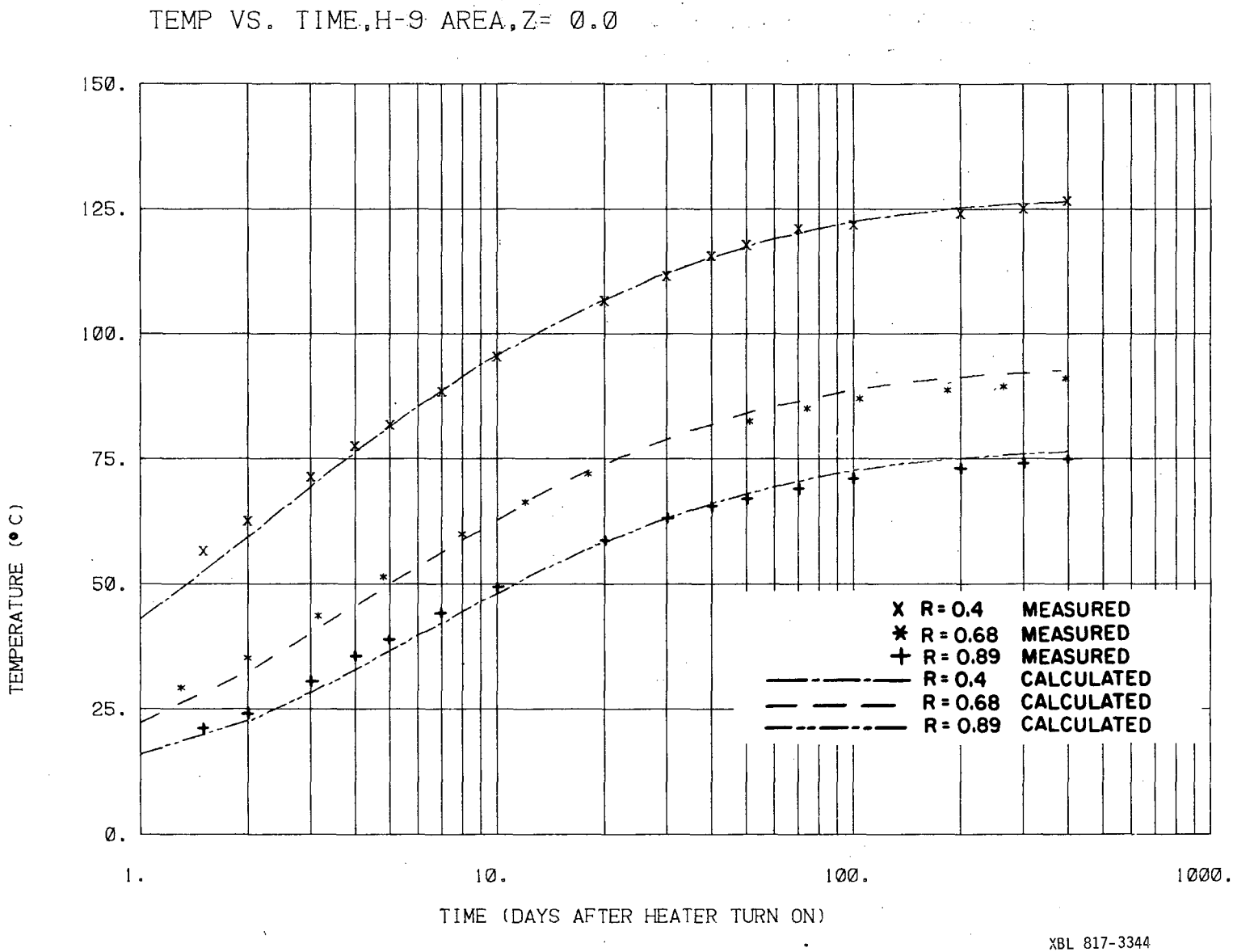

Fig. 48. Calculated and measured temperatures at Z = 0.0 of H-9 area after adjusting the heater location.

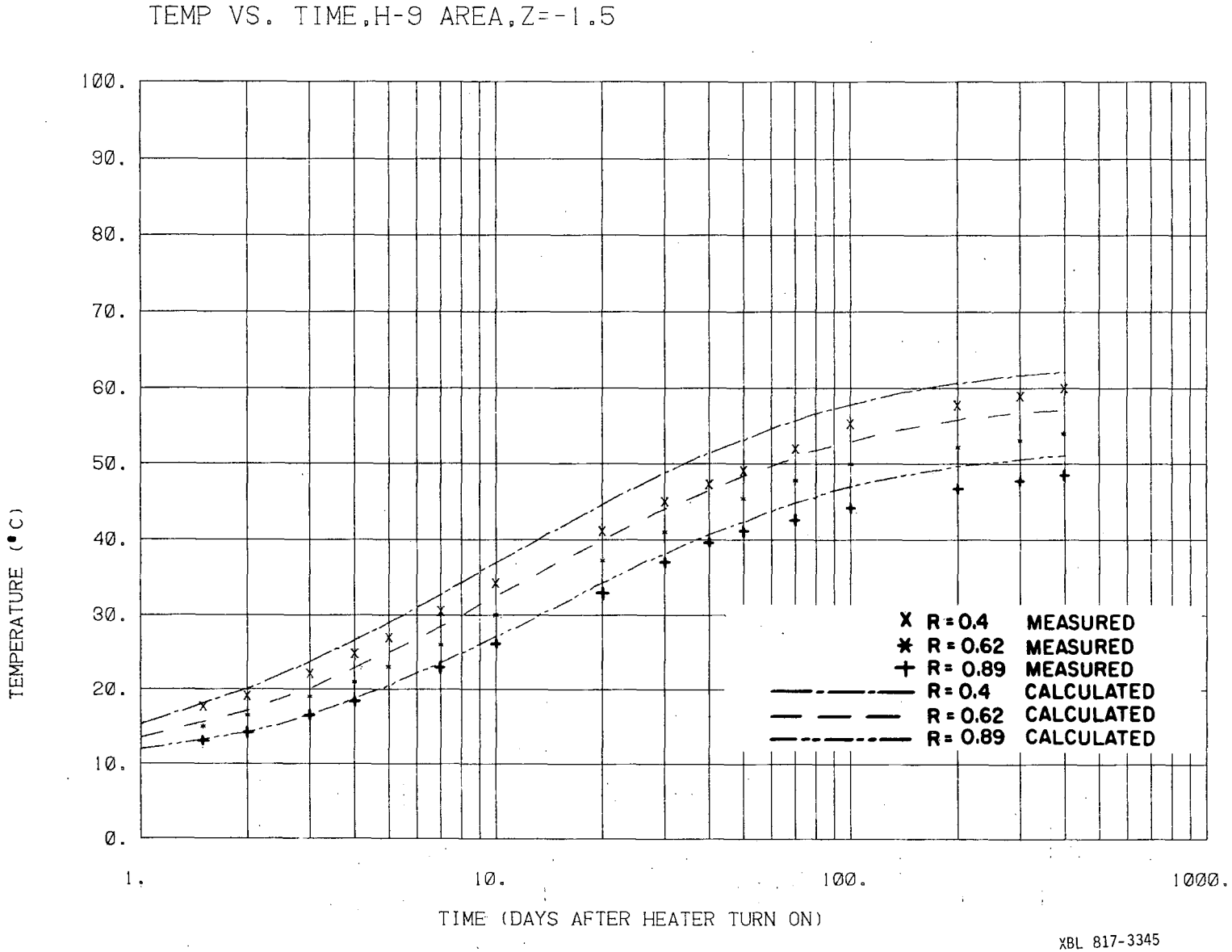

Fig. 49. Calculated and measured temperatures at Z = -1.5 m of H-9 area, after adjusting heater location.

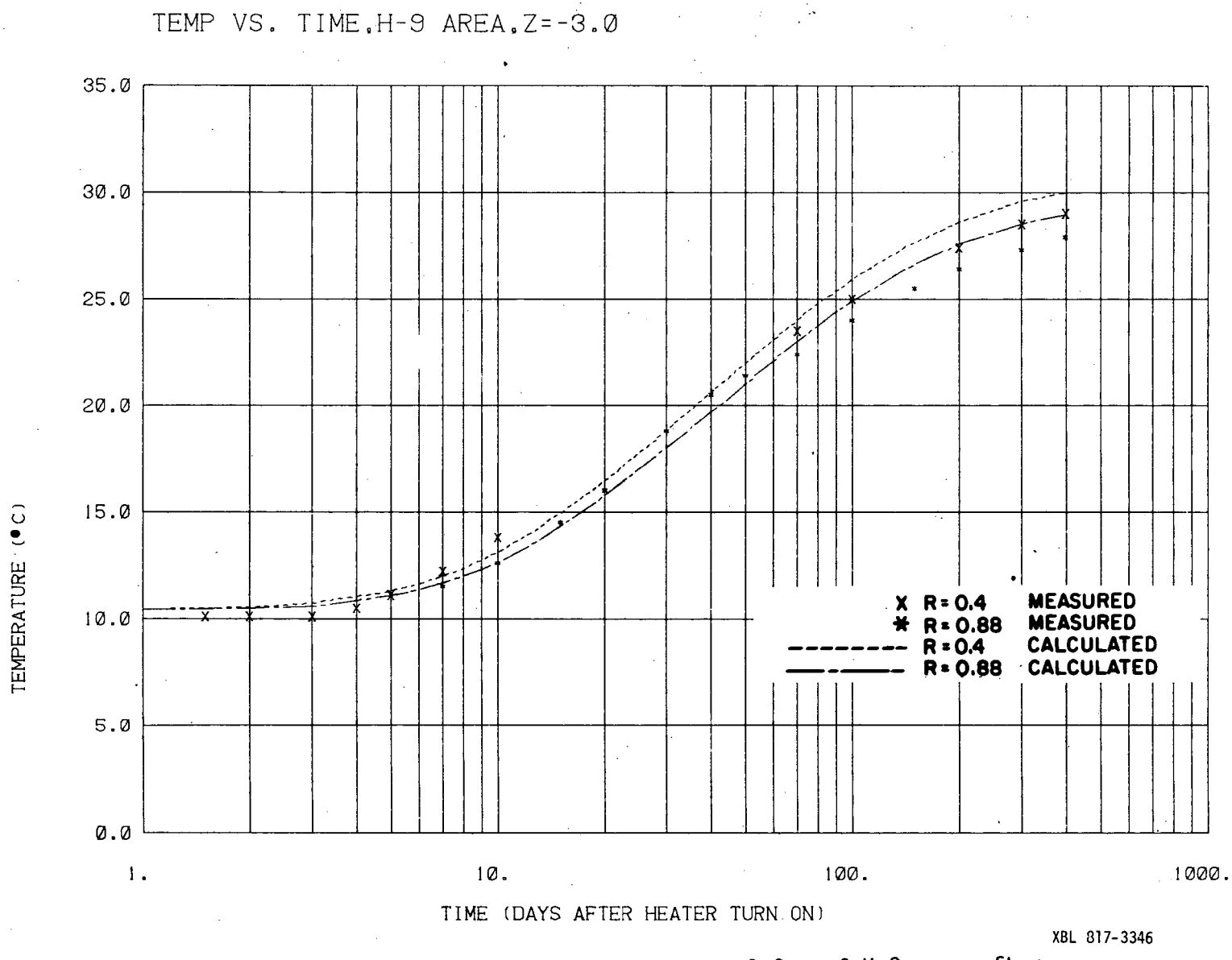

Fig. 50. Calculated and measured temperatures at Z = -3.0 m of H-9 area after adjusting heater location.

We had thus far focused our attention on the thermal field close to the heater, where temperatures had been measured by thermocouples in the T-holes, and ignored temperatures measured by thermocouples in the E-holes because those thermocouples were not intended to monitor rock temperature.

At this point, however, it seemed useful to examine the temperature data from the E-holes. Unfortunately, thermocouples in these holes were not set at regular distances, as was planned for the T-holes. Nevertheless, we have tried to consider as many of them as possible. They are on approximately these elevations: Z = 2.26, 0.0, and -2.25 m. Figure 51 presents a comparison between the calculated and measured temperatures at 3 different radii ranging from 2 to 3 m at the elevation of 2.26 m above the midplane. It is apparent that we have a very good match at these locations. Errors are within 1°C.

Figure 52 compares the measured and calculated temperatures at five radii, ranging from 1 to 3 m, on the midplane. The matching is very good at radii of 2.5 and 3 m whereas a difference of 1 to 2°C can be observed at points with higher temperatures. One explanation for this discrepancy is that the thermocouples at R = 1 and 1.5 m are not exactly on the midplane, but are respectively 18 and 15 cm above it. In addition, as described in Section 2.1.2, these thermocouples were not in touch with the rock. We should thus expect them to be somewhat cooler than the rock in their vicinity. Naturally, this difference increases slightly at higher temperatures.

Figure 53 shows a comparison of the measured and calculated temperatures at radii of 2 and 3 m, at elevation Z = -2.25 m. The calculated results seem to match the measured data very well.

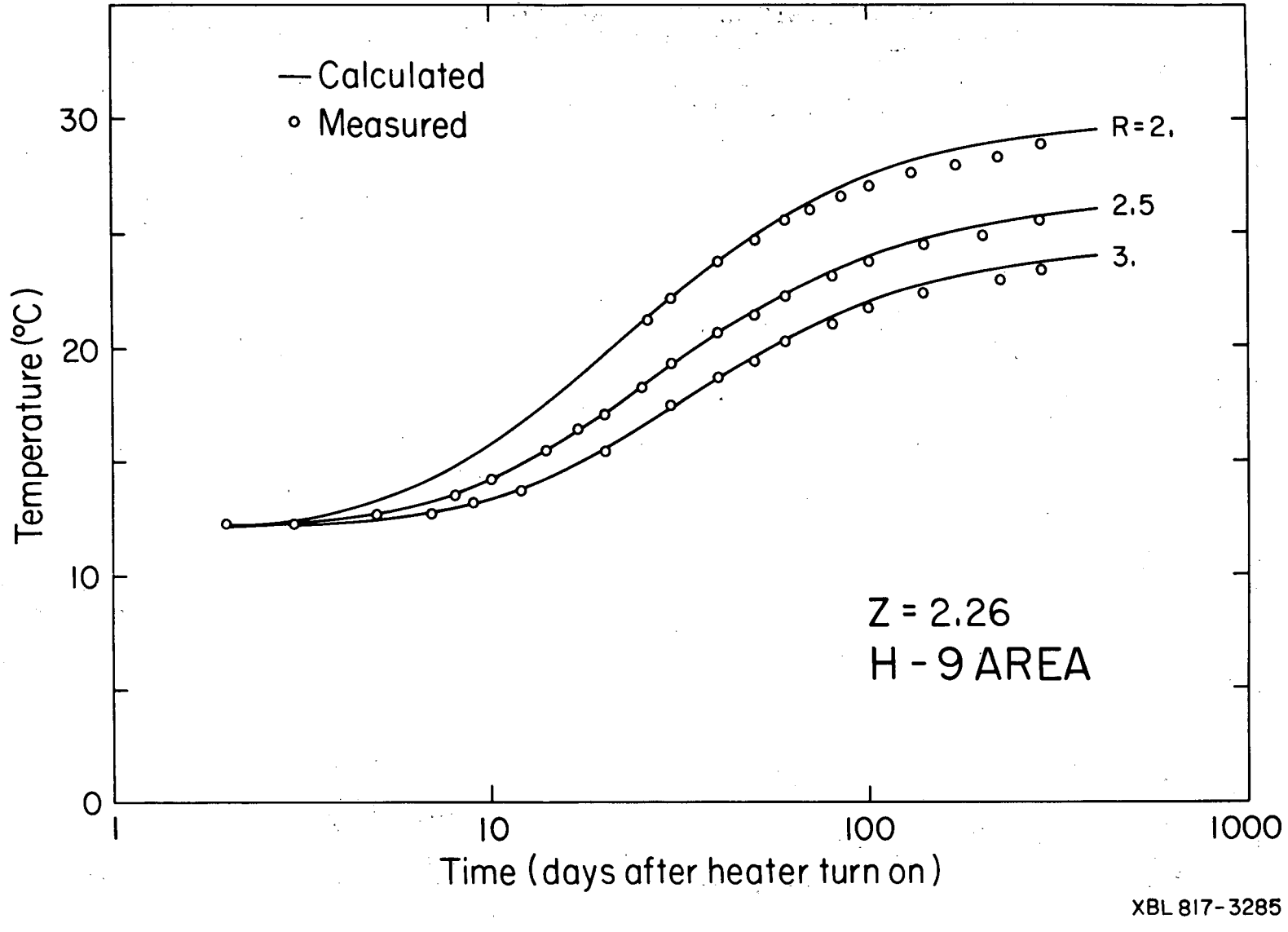

Fig. 51. Measured and calculated temperatures at three radii ranging from 2 to 3 m at Z = 2.26 m, of H-9 area.

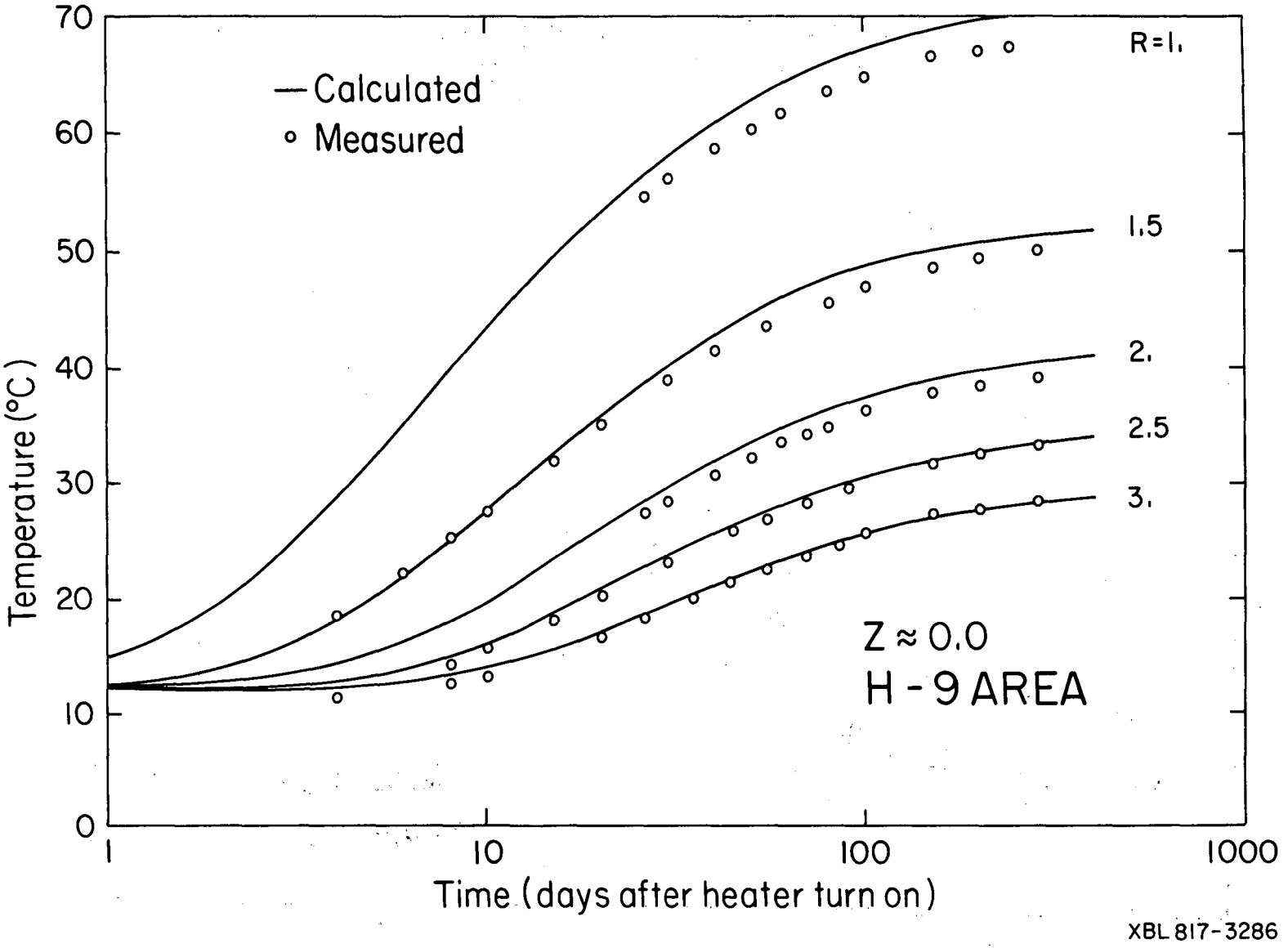

Fig. 52. Measured and calculated temperatures at five radii ranging from 1 to 3 m, on the midplane of H-9 area.

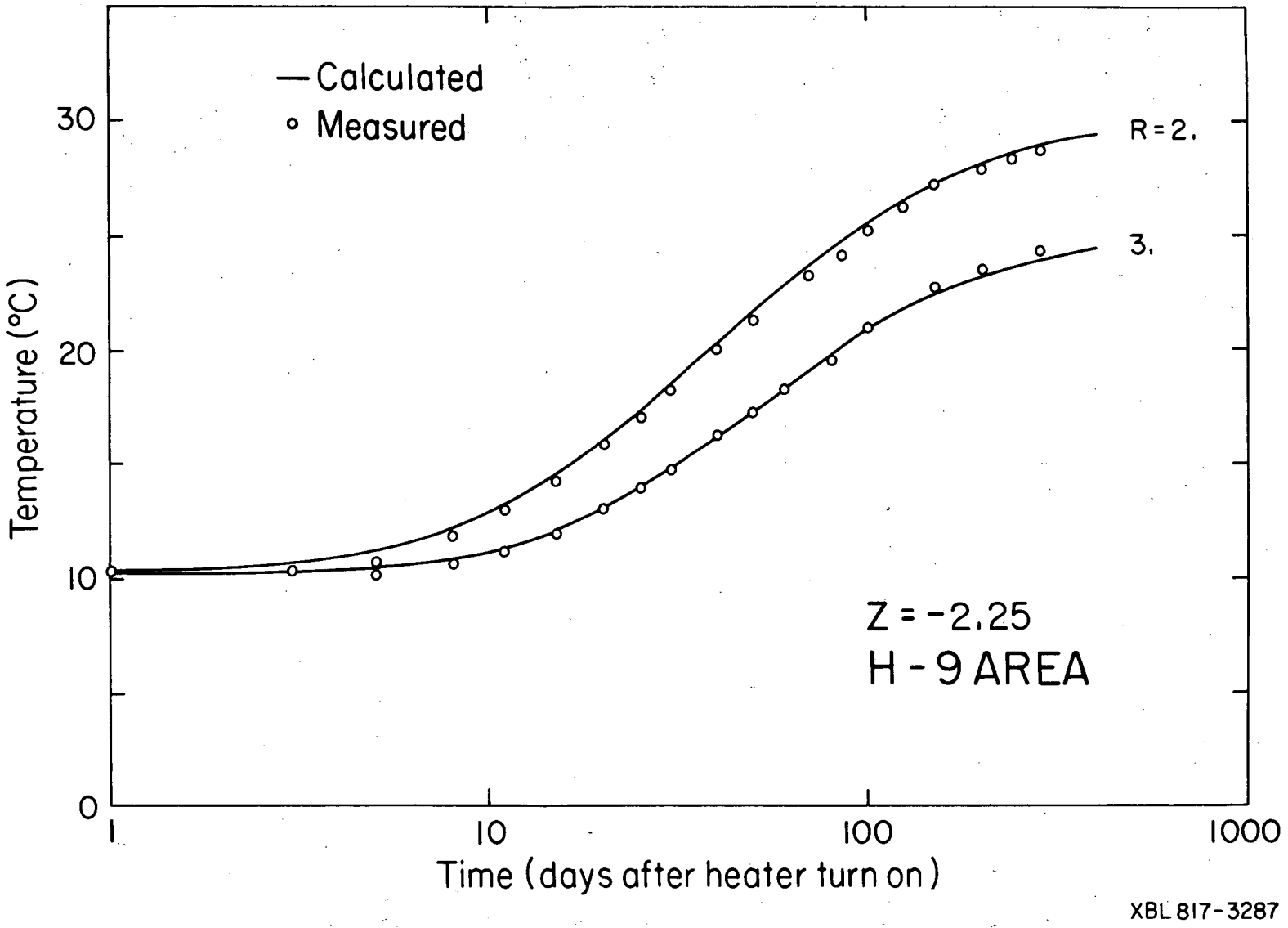

Fig. 53. Measured and calculated temperatures at radii of 2 and 3 m, at elevation Z = -2.25 m, of H-9 area.

3.4.2 Cooling Period

To calculate the temperature field after the 3.6 kW heater was turned off, we simply reduced the magnitude of heat generation in the model to zero level. The values of temperature calculated by the model, after converting the corresponding time into the dimensionless form of t/t', have been compared with the measured values of the temperature at respective points. t' designates the time after the heater was turned off. Figures 54 through 56 exhibit the comparison of measured and calculated temperatures after the heater turn-off at the levels of $Z = +1.5$, 0.0, and -1.5 m.

In general, all three figures suggest that the rock was cooling slightly faster than what our model has calculated. The temperature difference, at a given time, is a function of the rock temperature; for warmer zones, however, this difference is larger, the maximum difference being on the order of 3°C.

The larger deviations that exist between the measured and calculated temperatures at $Z = -1.5$ m are due to the differences that existed at heater turn-off, a completely different situation.

3.5 Modeling of 5 kW Heater Experiment

As far as modeling is concerned, this experiment consists of three parts. The first part, which lasted 204 days and was energized by one 5 kW heater, is an axisymmetric problem that can be easily solved by the "DOT" code. The second part begins after 204 days, when the peripheral heaters were also activated; the problem now becomes three-dimensional. The exact solution requires a 3-D code that can solve nonlinear heat conduction. The third part includes

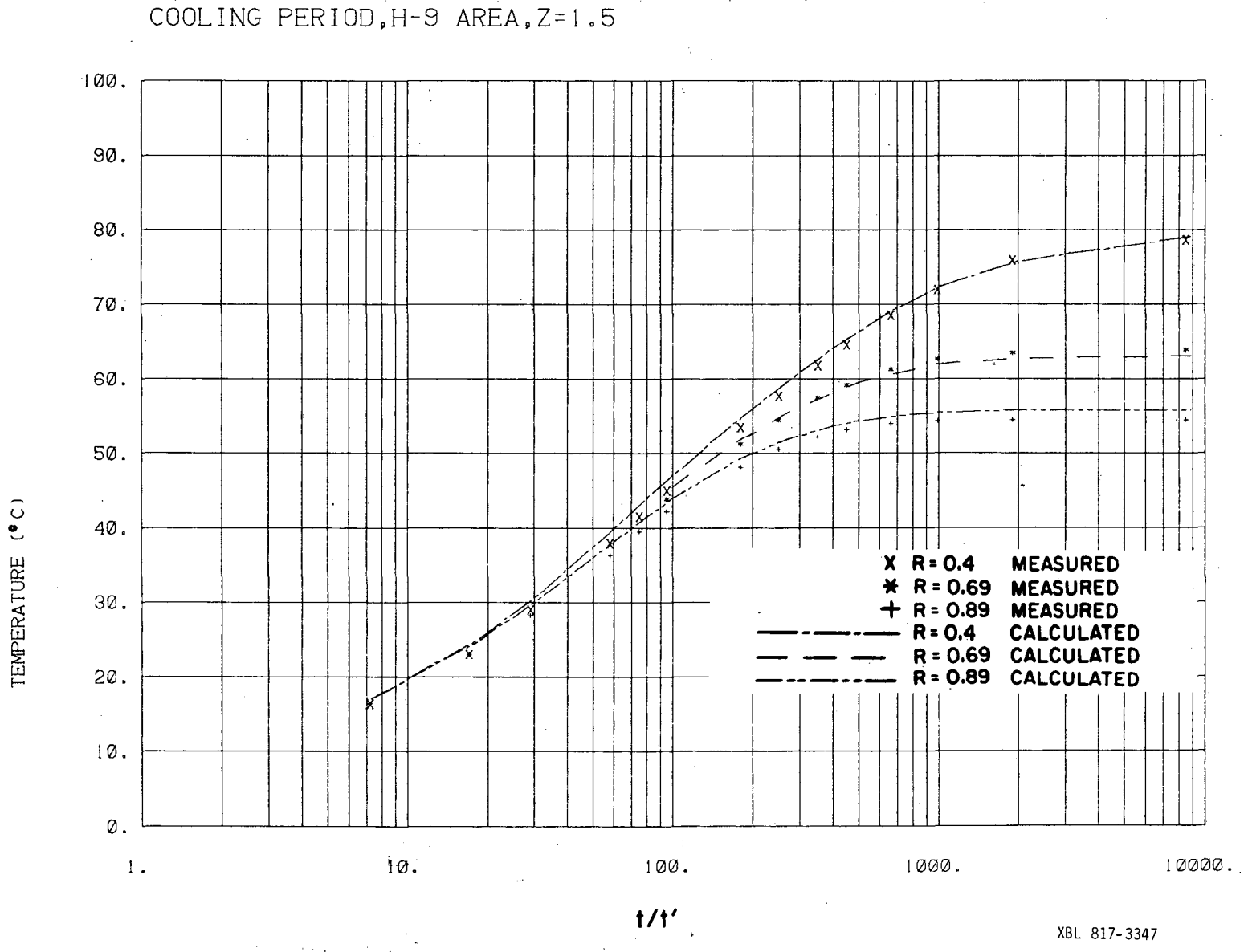

Fig. 54. Measured and calculated temperatures at Z = 1.5 m of H-9 area after heater turn-off.

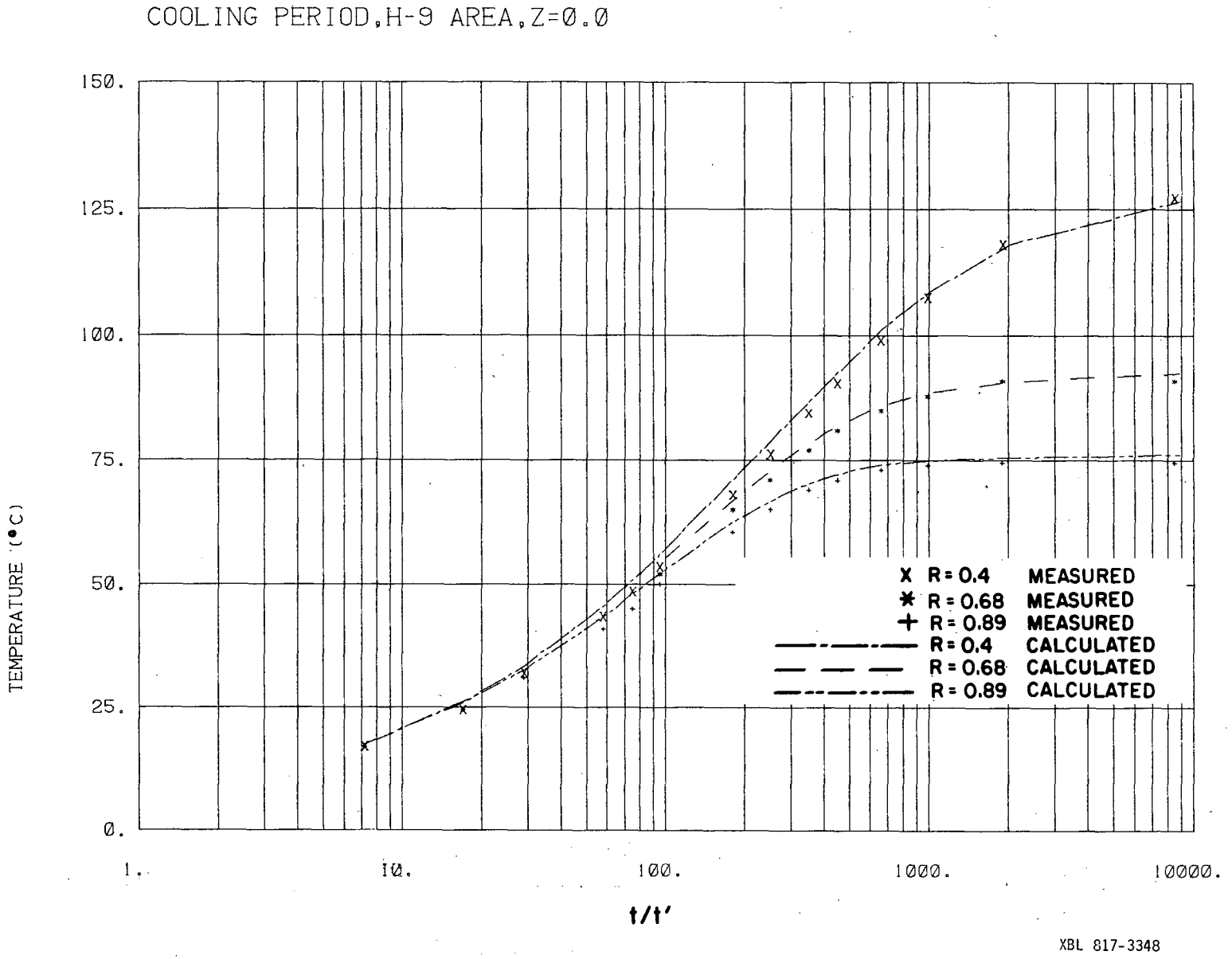

Fig. 55. Measured and calculated temperatures at Z = 0.0 of H-9 area after heater turn-off.

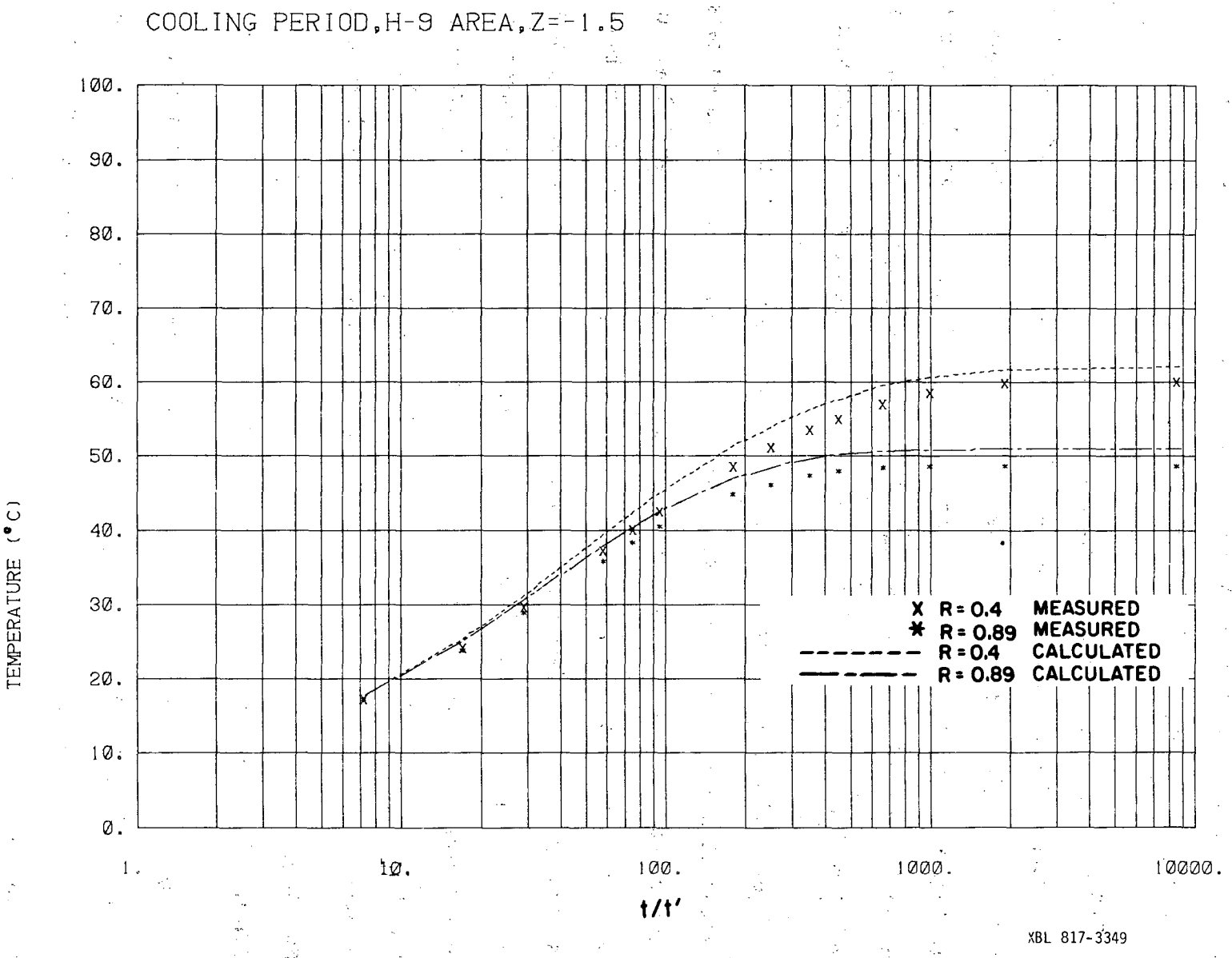

Fig. 56. Measured and calculated temperatures at Z = -1.5 m of H-9 area after heater turn-off.

the cooling period, again a three-dimensional case. We shall now study the first two parts separately.

3.5.1 Part 1: Rock is Heated by the 5 kW Heater Only

Except for the heater power, which is changed to 5 kW, the model for this part is a copy of that used for the 3.6 kW heater. The calculated and measured temperatures over time at radii of 0.4 and 0.91 m on the midplane are given in Fig. 57. The measured data that were obviously wrong have been deleted. The rest of the data seem to be relatively close to the calculated values.

Figures 58 and 59 exhibit the calculated values of temperature for two radii at Z = 1.5 and -1.5 m, respectively. Here again, the measured data are warmer above the midplane than the calculated ones, and cooler below. In spite of higher input power, the magnitude of the deviations is smaller than those observed in the 3.6 kW experiment, but the trend is the same, and the argument used in that experiment can also explain the discrepancies observed here. Variation with the elevation of the temperature differences between two particular radii, i.e. $(T_{0.4} - T_{0.9})$, 10 days after the start of the experiment, is presented on Fig. 60. Note that the magnitude of this parameter, $(T_{0.4} - T_{0.9})$, changes very rapidly in elevations between 1.2 to 1.6 m and -1.2 to -1.6 m, our areas of interest.

Once again, if one associates these deviations with mislocation of the heater, then Fig. 60 could be used to estimate the magnitude of this mislocation. In this case, while the heater was in place, no in situ measurement was performed to verify any vertical disclocation of the heater.

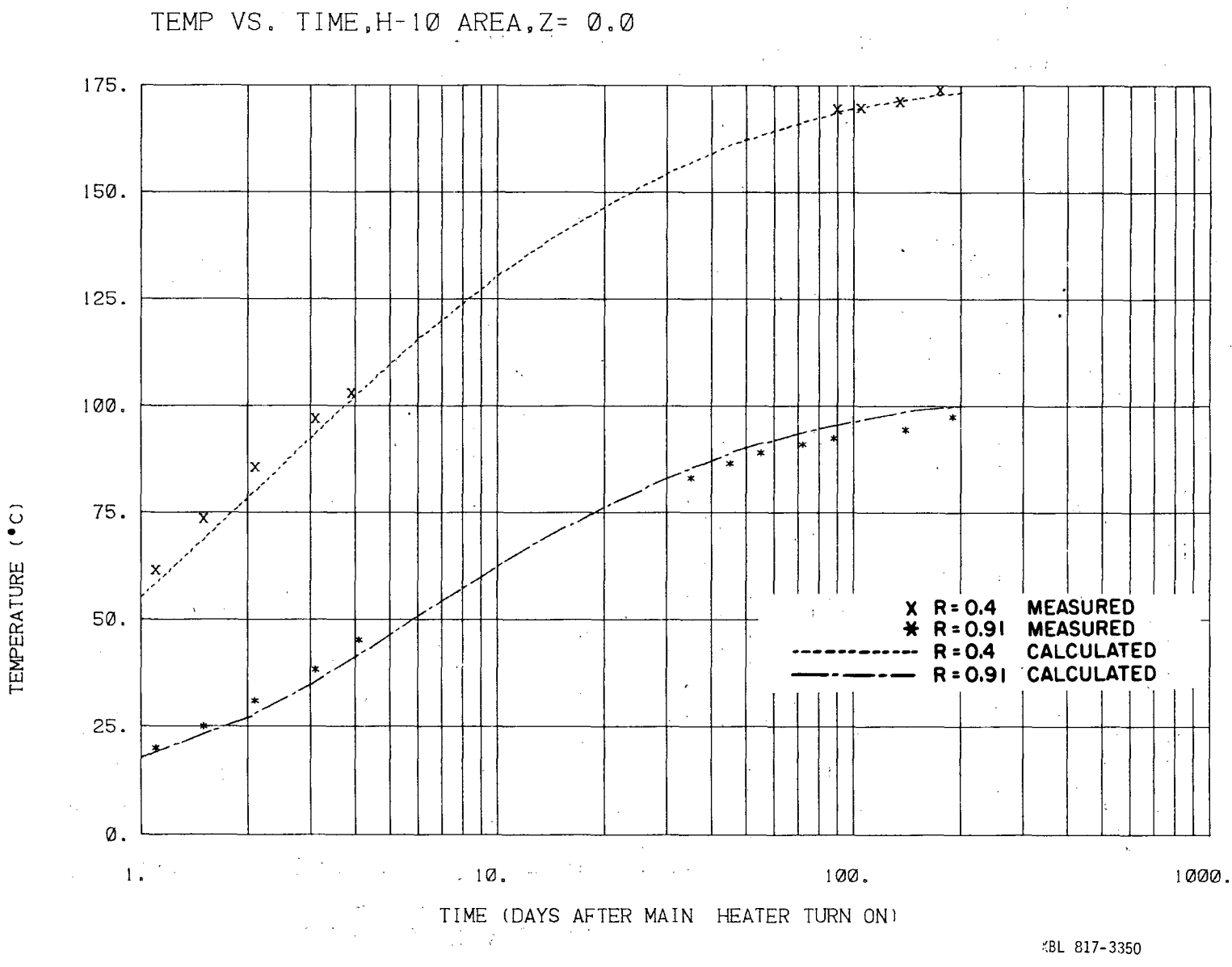

Fig. 57. Variation of measured and calculated temperatures with time at at Z = 0.0, H-10 area.

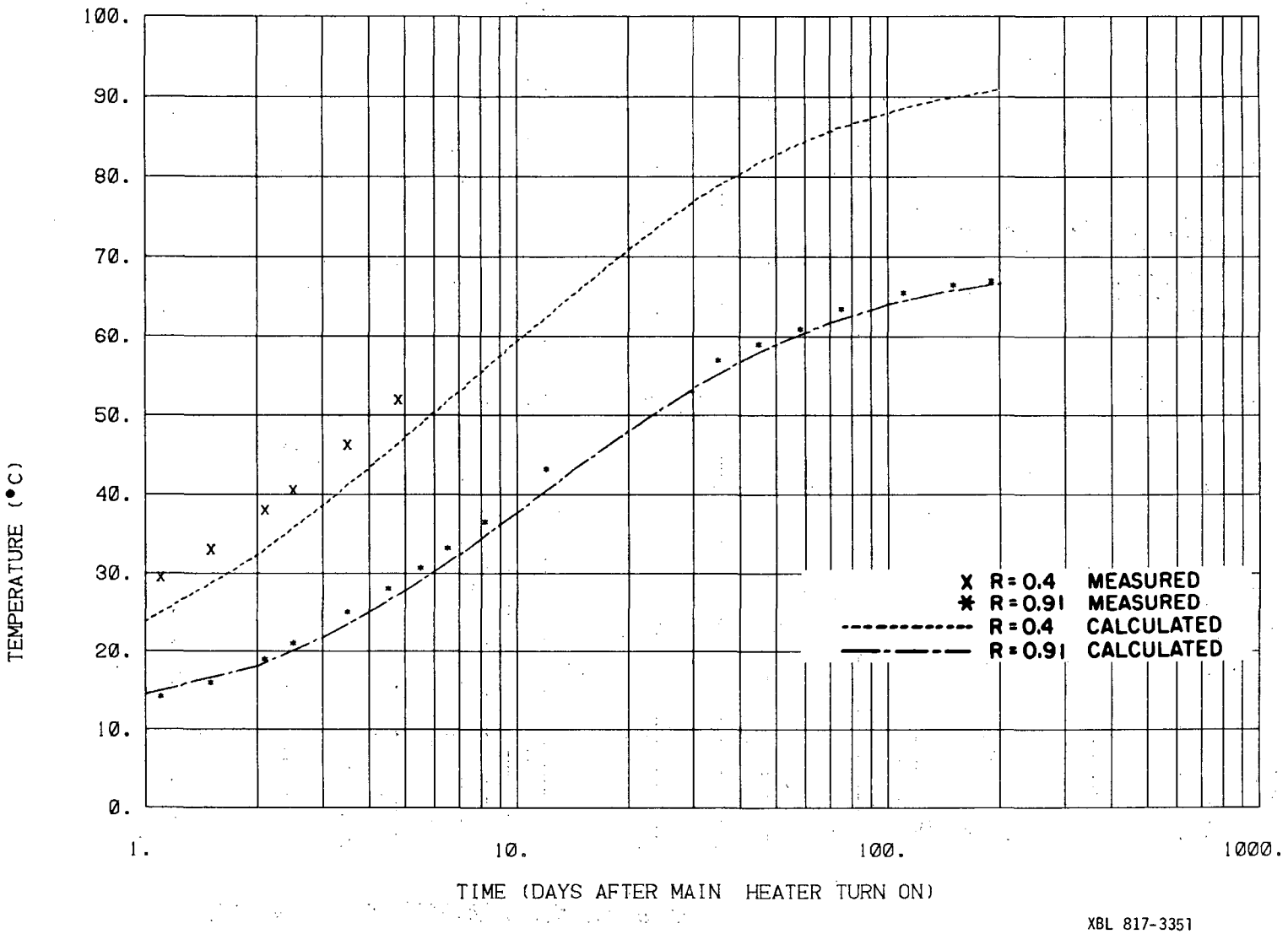

Fig. 58. Variation of measured and calculated temperatures with time at Z = 1.5 m of H-10 area.

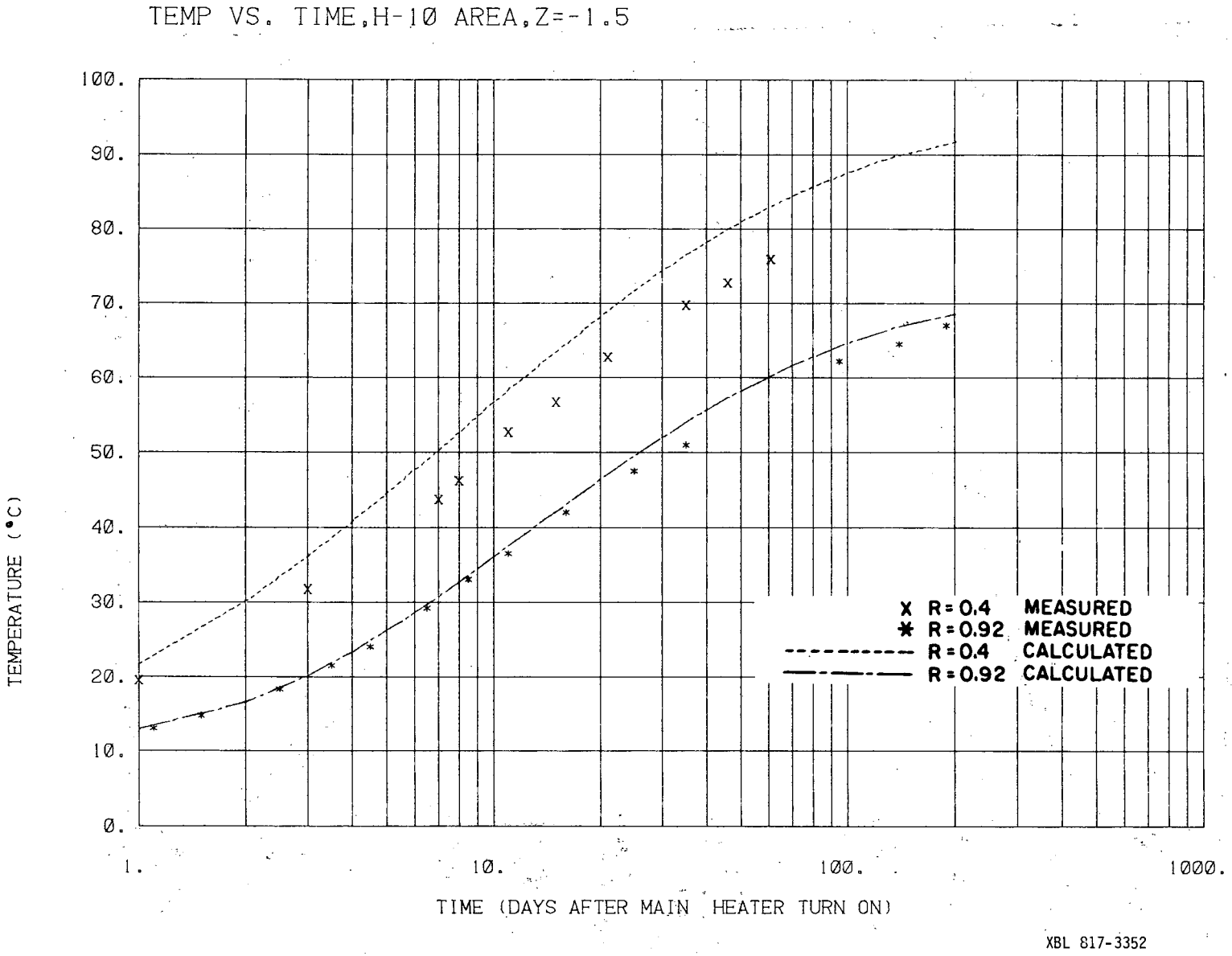

Fig. 59. Variation of measured and calculated temperatures with time at Z = -1.5 m of H-10 area.

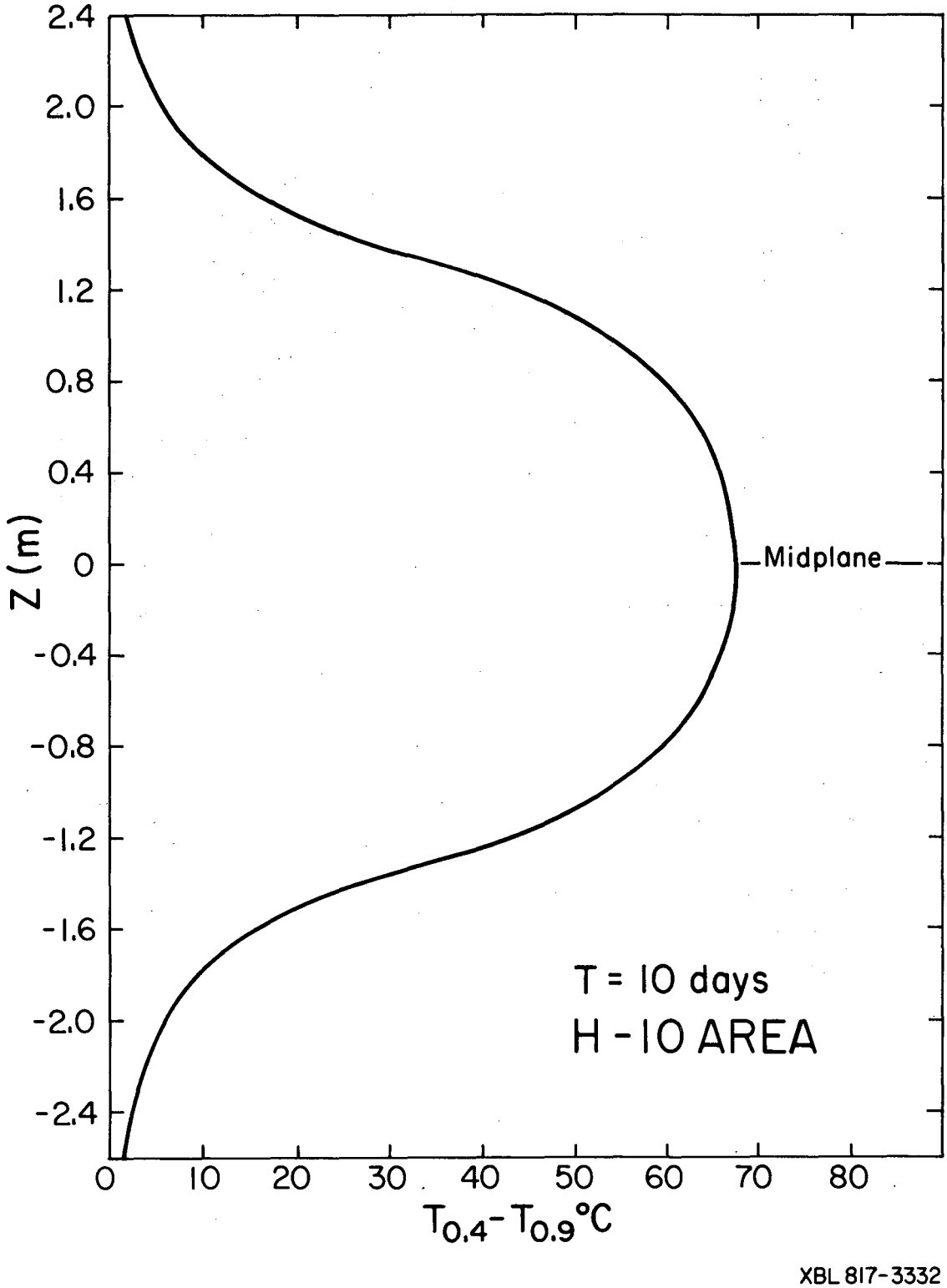

Fig. 60. Variation of ($T_{0.4}$ - $T_{0.9}$) with elevation around 5.0 kW heater.

The comparison of the measured parameter of $(T_{0.4} - T_{0.9})$ at around 10 days with Fig. 60 suggests that the thermocouples supposed to be 1.5 m above the heater midplane are actually at 1.42 m elevation and those planned to be at -1.5 m are actually 1.58 m below the present heater midplane, indicating that the heater is about 8 cm above its designed position.

The model was accordingly modified, and Figs. 61 through 63 are the results. Measured temperatures seem to verify the calculated ones very well.

3.5.2 Part 2: Peripheral Heaters Are Also Activated

As mentioned earlier, this part of the problem is a 3-dimensional case. As a first step approximation, we shall use the theory of superposition. If the thermal conductivity of the rock were in fact independent of temperature, this method would provide accurate results.

The essence of this well-known method is that temperature rise at any given time and space is the sum of the values of temperature rise at that point from all individual heaters. In this case, since the power levels of all the peripheral heaters are the same, we have constructed only one extra model for calculation of the temperature field around one of the peripheral heaters, in effect assuming that that was the only heater operating. Each thermocouple in the T-holes has a fixed distance from each one of the peripheral heaters. Thus, for any given time and any thermocouple location, one can easily calculate the temperature rise due to each peripheral heater. Adding up the effect of all eight plus that of the main 5 kW heater would give the temperature of that point at that time.

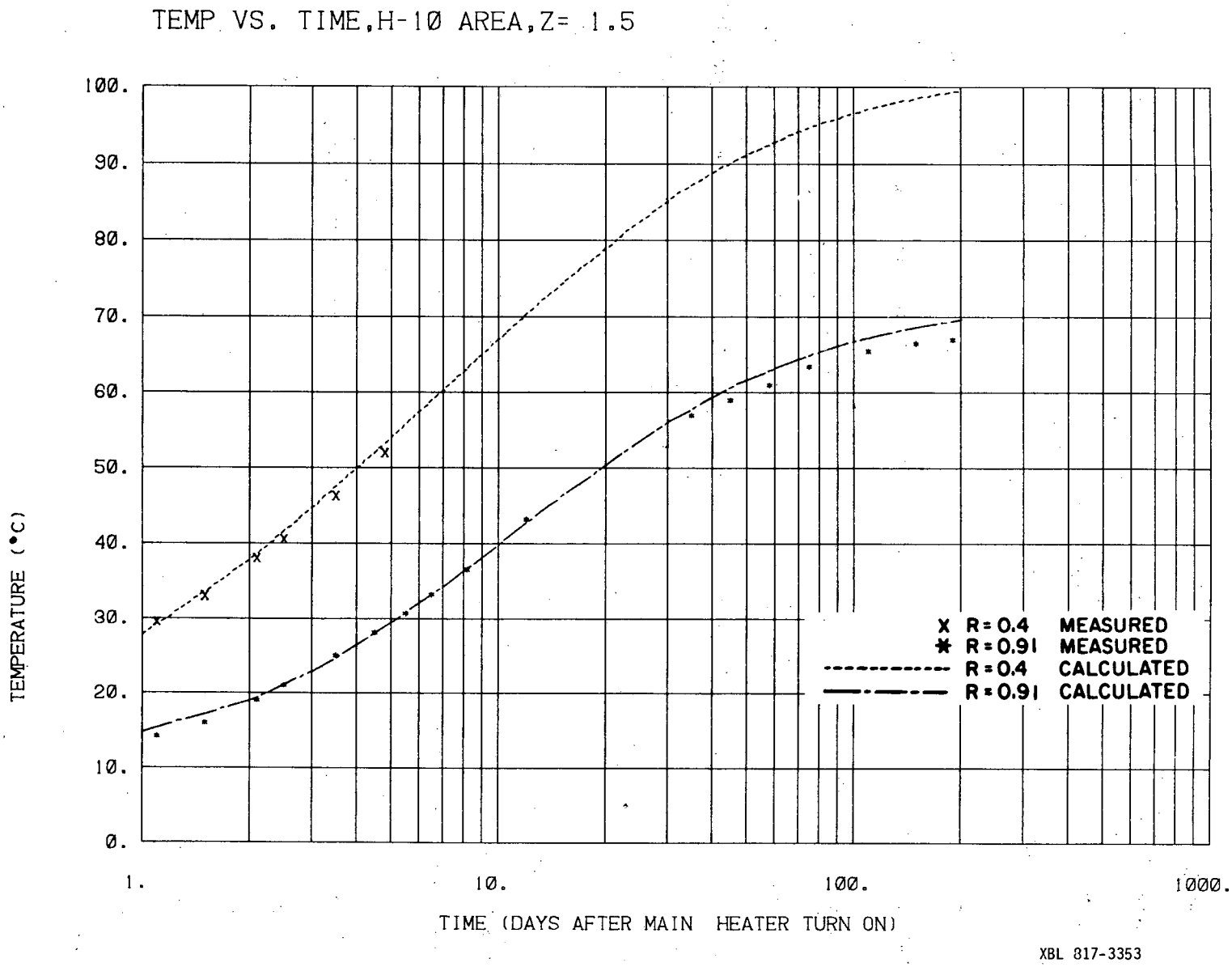

Fig. 61. Calculated and measured temperatures at Z = 1.5 m of H-10 area after adjusting heater location.

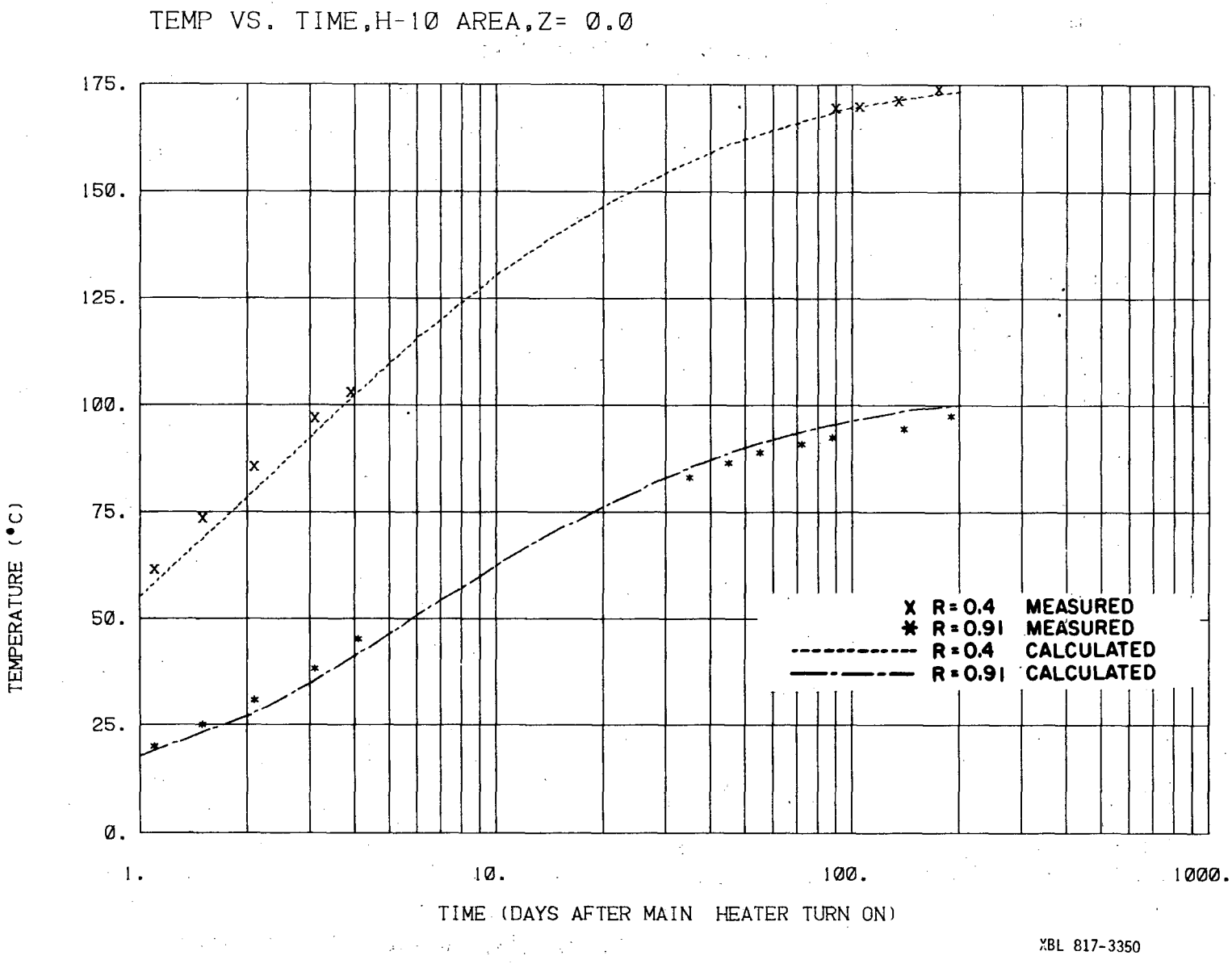

Fig. 62. Calculated and measured temperatures at Z = 0.0 of H-10 area after adjusting heater location.

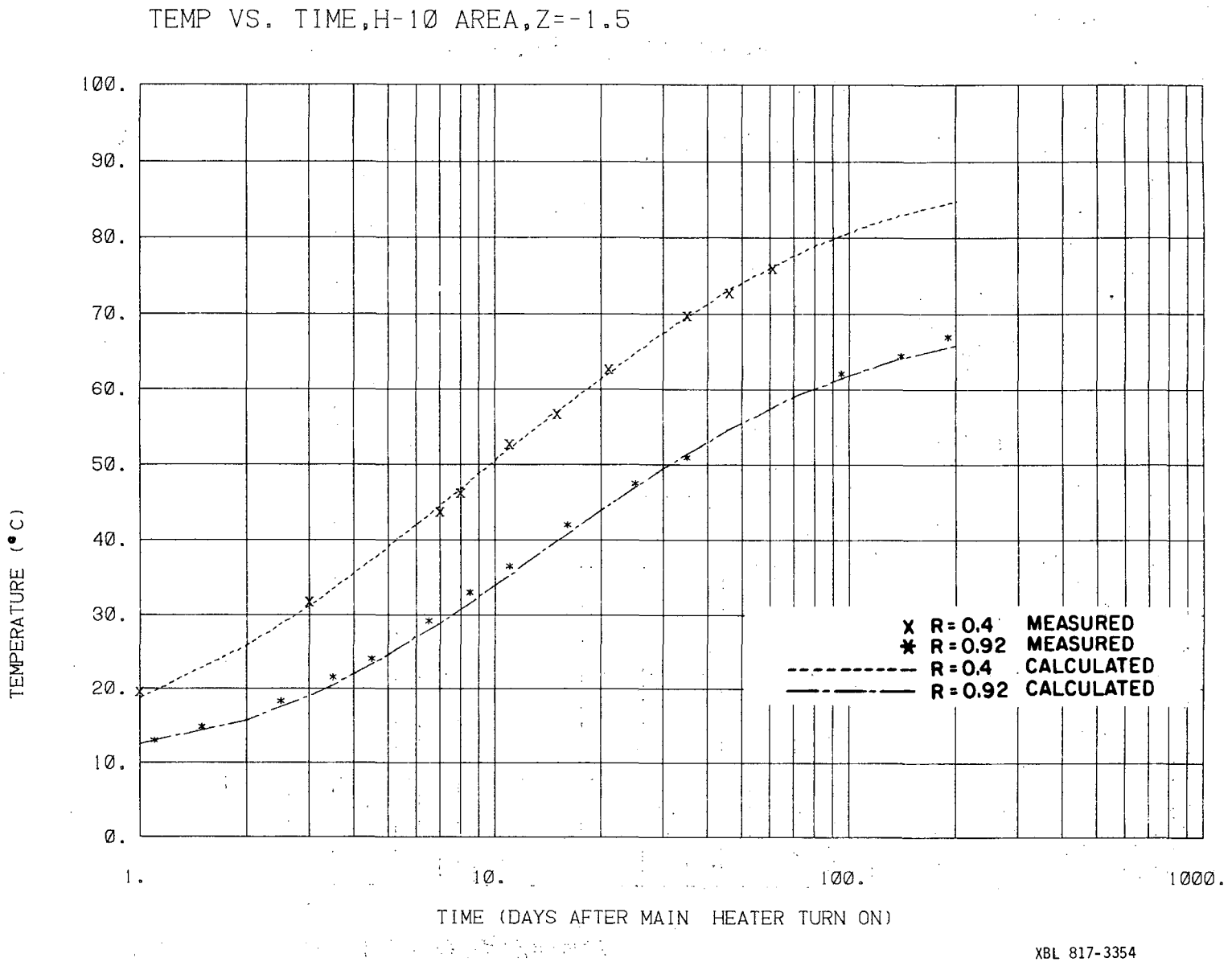

Fig. 63. Calculated and measured temeratures at Z = -1.5 m of H-10 area adjusting heater location.

The asymmetry of the problem stems from the fact that when the peripheral heaters were activated, temperature distribution in the rock around them was not axisymmetric and thus the thermal conductivity of the rock varies with the angle around each peripheral heater. The present code cannot handle either of these problems of temperature distribution and thermal conductivity. Fortunately, as we saw before, as long as variation of temperature with space is not very significant, the amount of error introduced is moderate. Thus, a constant thermal conductivity of 3.2 W/m°C, corresponding to a temperature of 108°C, was assigned to the peripheral heater model.

Another problem is the form of the boundary conditions at the heater drift as well as the extensometer drift. The solution is to assign 0°C to the temperature of the rock adjacent to the drifts when modeling the peripheral heaters. Temperature variations so calculated for levels Z = 0.0 and -1.5 m are plotted in Figs. 64 and 65, as are corresponding measured temperatures.

To avoid errors due to mislocation of the thermocouples after replacement, the temperatures actually registered by the thermocouples at turn-on of the peripheral heaters were considered as the contribution of the main heater at that time. Since the peripheral heaters are longer than the main 5 kW heater, the small vertical dislocation of the thermocouples around Z = $\pm$ 1.5 m does not introduce any significant error into the calculation of temperature rise from the peripheral heaters.

In general, the calculated temperatures for this period are in very close agreement with measured data for locations that are relatively cooler, such

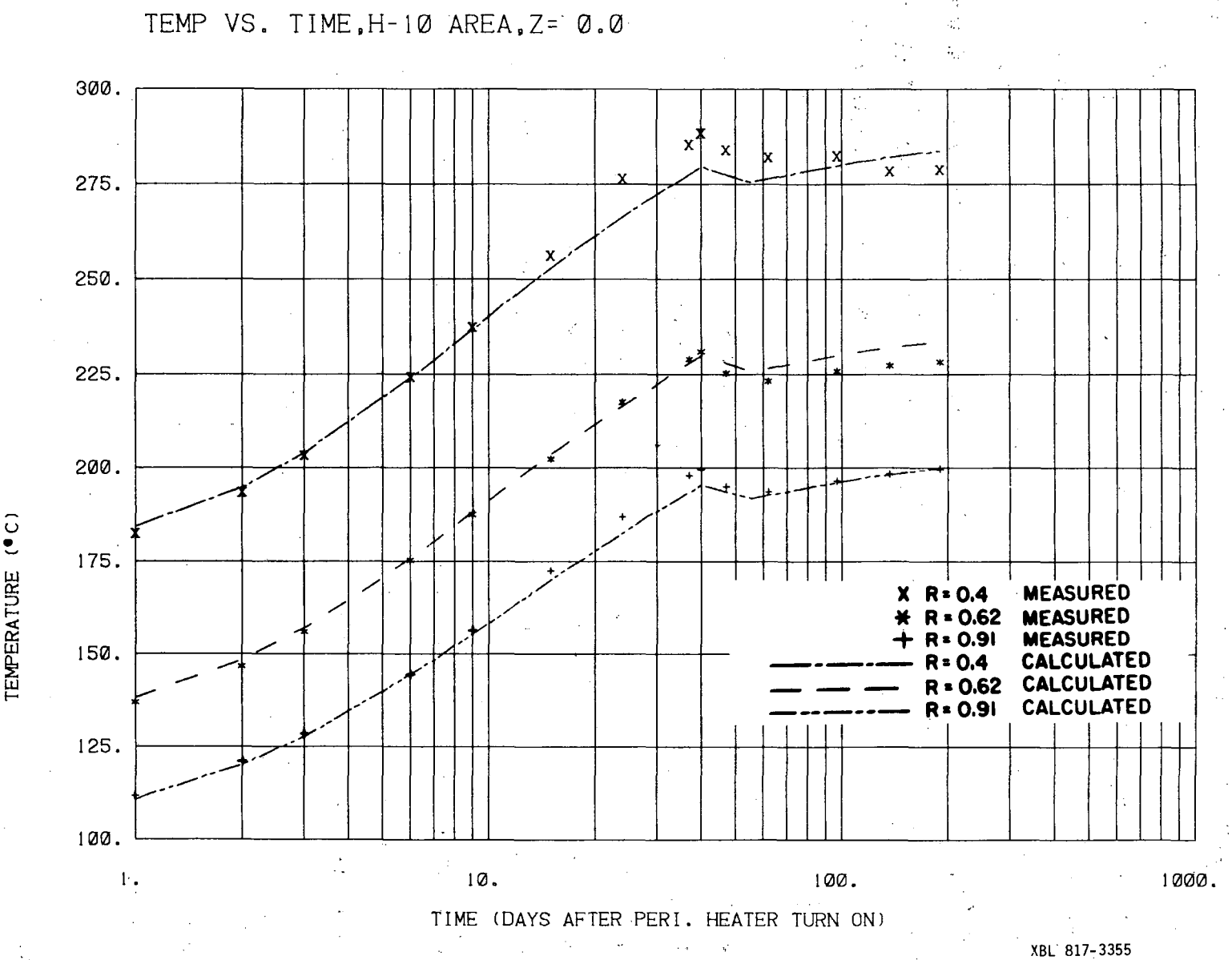

Fig. 64. Semilog plots of measured and calculated temperatures at Z = 0.0 of H-10 area, after peripheral-heater turn-on.

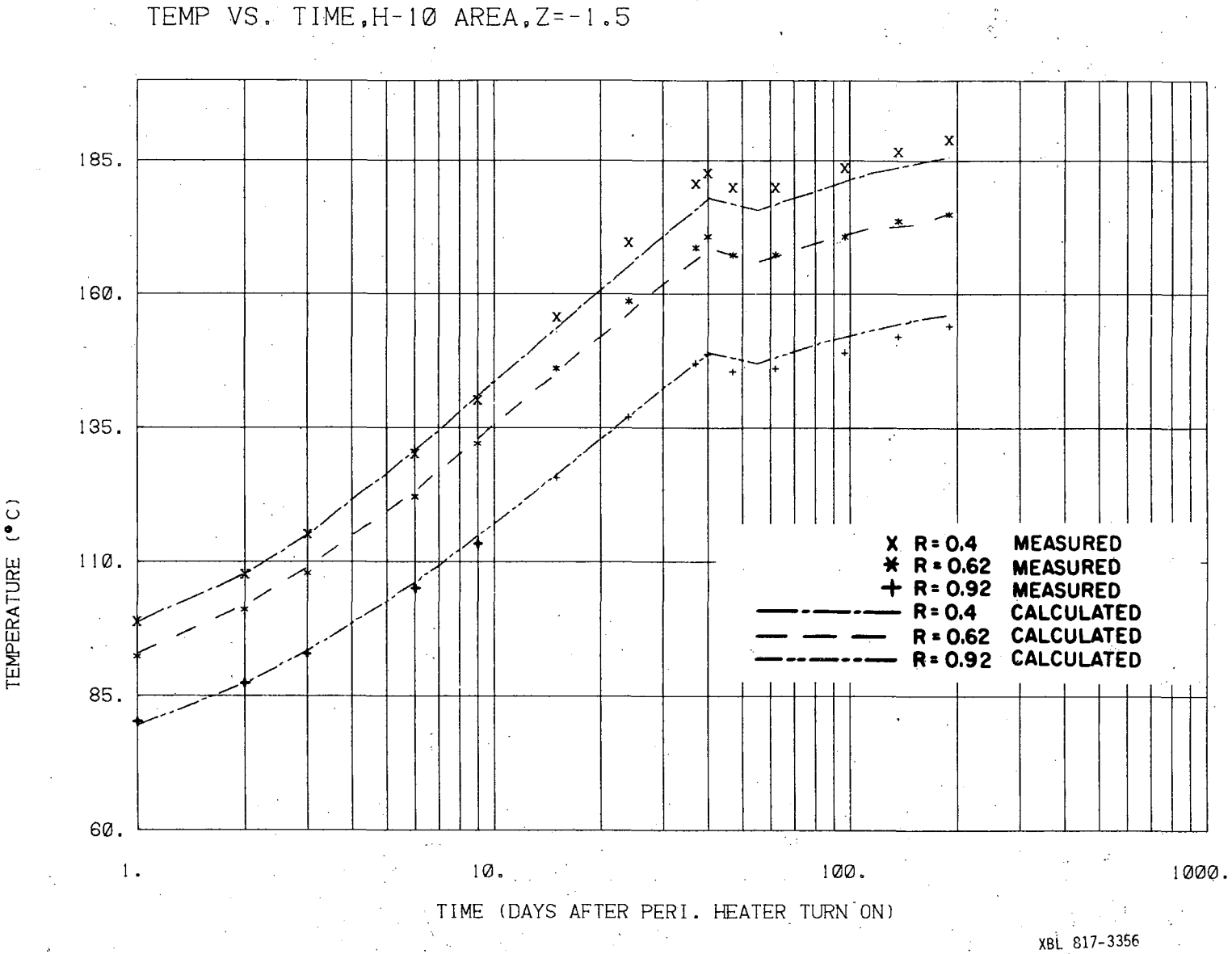

Fig. 65. Semilog plots of measured and calculated temperatures at Z = -1.5 m of H-10 area after peripheral-heater turn-on.

as those at R = 0.91 m. In warmer zones, however, measured temperatures are higher than calculated. This is because the thermal conductivity of the rock decreases with increase of temperature. As mentioned before, a fixed value of 3.2 W/m°C corresponding to the temperature of 108°C was arbitrarily assigned to the rock for calculation of the effects of the peripheral heaters. However, it is clear that, close to the main heater (around R = 0.4 m), temperatures are well over 108°C. In fact, around the midplane, temperatures after 3 days are over 200°C. Reduction of thermal conductivity from the assigned value of 3.2 W/m-°C would slow down the transfer of heat from those warmer areas, which in effect raises the temperature there.

To demonstrate this effect, we made another run of the model with the following thermal conductivity values:

K = 3.2 W/m°C corresponding to 108°C for the first 10 days and

K = 2.9 W/m°C corresponding to 190°C for the next 30 days.

Figures 66 and 67 illustrate the effect, of this change on the calculated values of temperature. These figures show that the calculated temperatures match more closely the temperatures measured at the warmer zone, i.e. R = 0.4 m. But an increase of difference between the measured and calculated temperatures is observed at relatively cooler areas, such as those at R = 0.92 of Z = -1.5 m.

Data from thermocouples above the midplane have not been compared with calculations because most of these data were distributed by the entry of water into the T-holes.

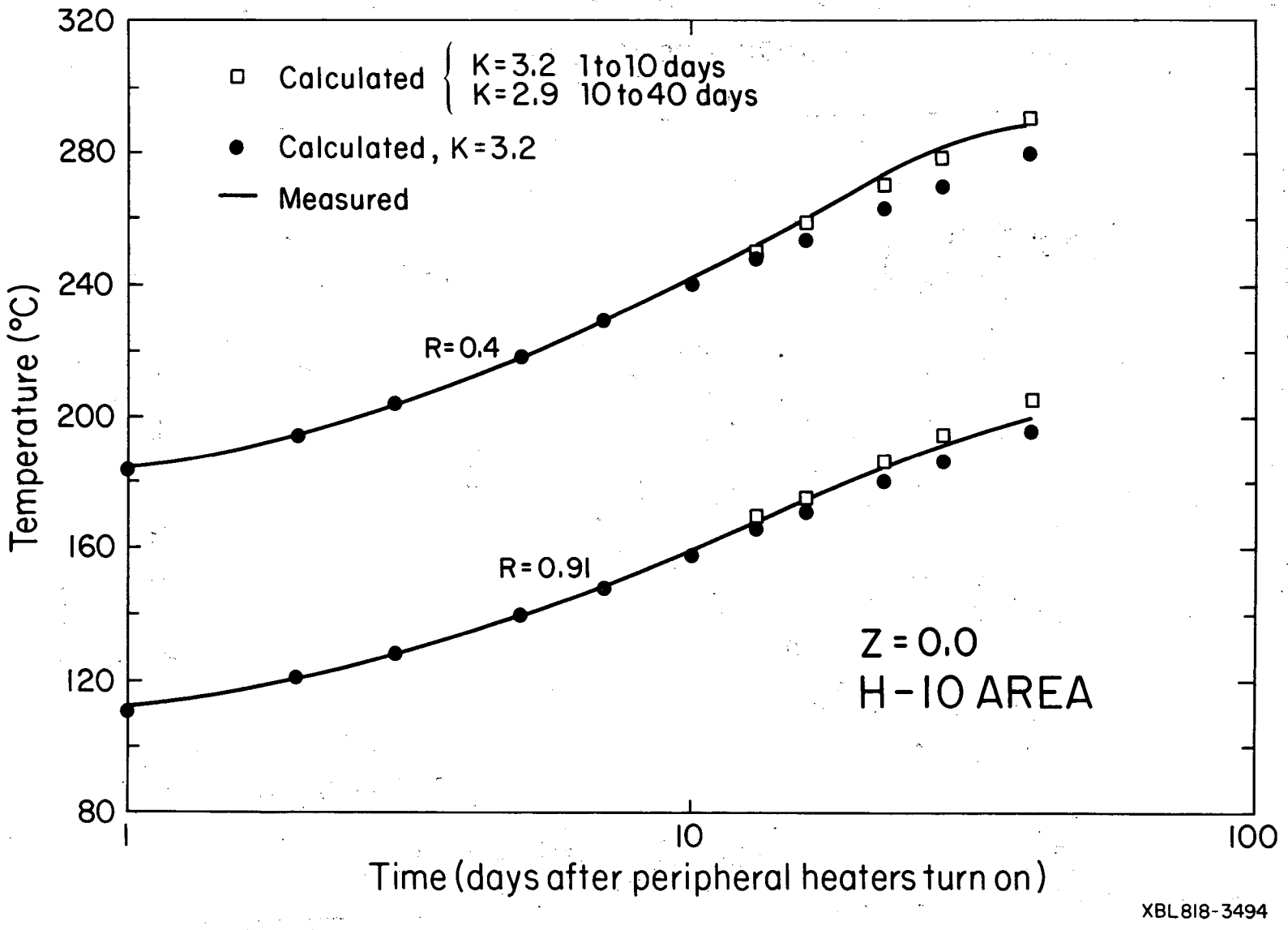

Fig. 66. Comparison of measured and calculated temperatures, based on two values of thermal conductivity, at Z = 0.0 of H-10 area, after peripheral-heater turn on.

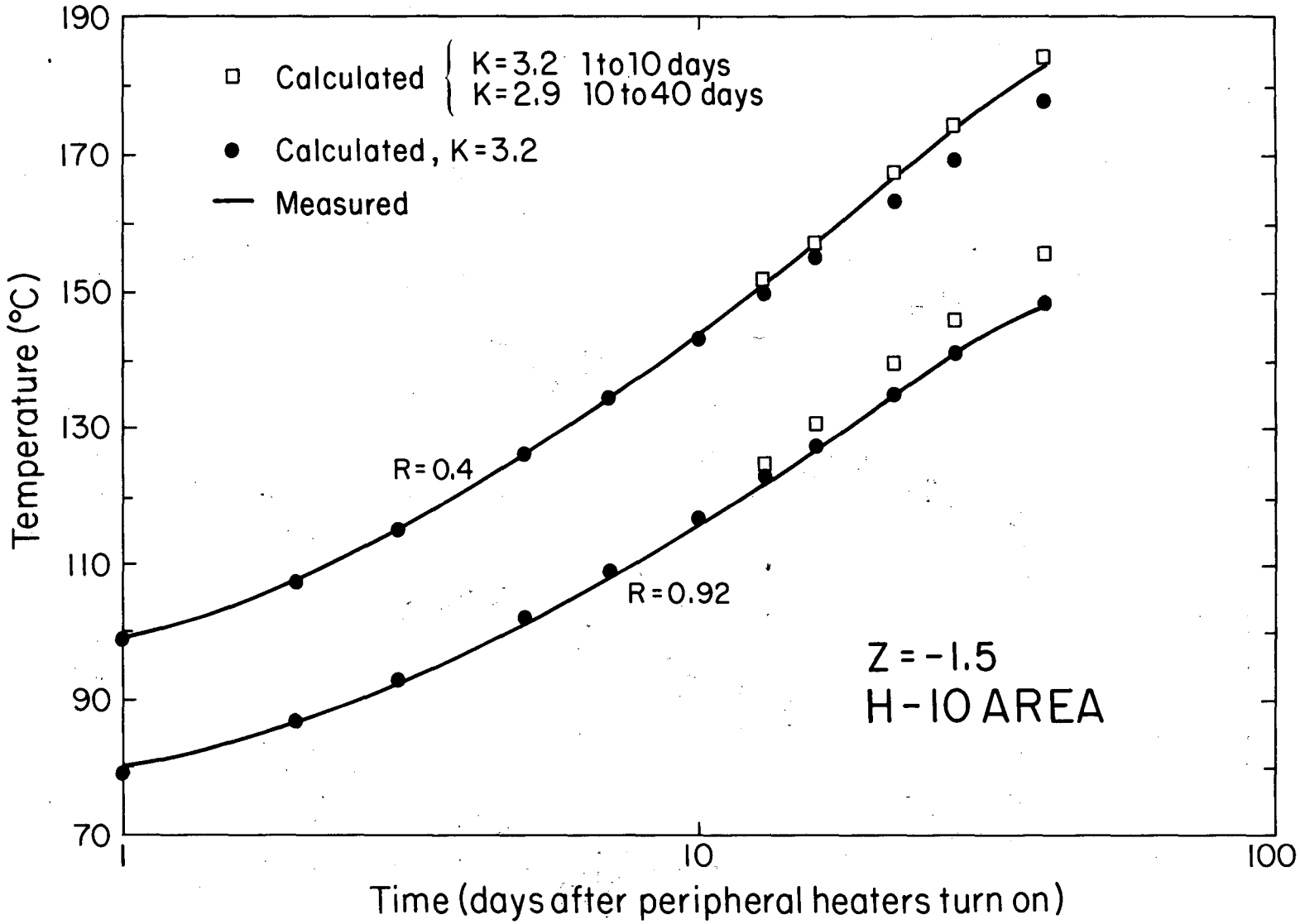

Fig. 67. Comparison of measured and calculated temperatures based on two values of thermal conductivity, at Z = -1.5 m of H-10 area, after peripheral-heater turn-on.

4. DISCUSSION

The amount of temperature data lost because of corrosion of the stainless steel sheath of the thermocouples in the 3.6 kW heater experiment is relatively small. In the 5 kW heater experiment, however, a considerable portion was lost during the first month or so.

Because of temperature anomalies observed in the measured data, we have suggested that some replacement thermocouples were not positioned in the same locations as the original thermocouples. In the H-10 area, some of the new data points did not coincide with the planned positions. In the H-9 area, recorded temperatures suggest that some of the original thermocouples were not at their designed positions, and temperature from these thermocouples were later corrected.

Temperature offsets as much as 10°C were recorded after the change of thermocouples. If we assume that vertical dislocation was the only reason for these offsets, then our studies, based on the modeling results, show that at most, 7 cm of vertical movement of the thermocouple string would cause a change of that magnitude.

Although study of temperatures at each level alone could suggest the presence of anisotropy in the thermal properties of the rock, looking at different levels together totally ruled out this possibility.

Horizontal movement of the thermocouples was also possible. The maximum extent to which a thermocouple in a T-hole could be horizontally displaced was 38 mm, assuming it was originally all the way to one side of the hole. This

amount of horizontal dislocation cannot be solely responsible for the temperature change observed.

Using the finite element code has enabled us to get a few steps closer to the solution of heat-transfer problems in rock storing high-level radioactive nuclear waste. Some areas, however, still need further improvement, as follows:

(a) As we estimated before, more than two-fifths of heat generated by the heater was transferred to the rock through convection. In the 3.6 kW heater experiment, after adjusting for the heater mislocation, some discrepancies still remained between measured and calculated temperatures. Figures 49 and 50 show that after correction for possible mislocation of the heater, measured temperatures below the midplane are still cooler than values calculated by ignoring convection in the air gap. Such convection possibly transferred heat from the lower to the upper part of the heater hole. Figures 46 and 47 seem to support this argument by showing that rock temperatures were warmer than measured values. This convection could also be responsible for the discrepancies we saw in the 5 kW heater experiment, discrepancies we had assumed might be due to vertical dislocation of the heater, a hypothesis that was not measured in the field while the experiment was running.

Since we could not handle convection with the "DOT" code we had to assume that the heater was in contact with the rock. For more accurate calculation, the effect of the air gap on the thermal

field in the rock should be correctly incorporated into the code.

(b) Modeling of the 5 kW heater experiment, after the peripheral heaters were turned on, could be further improved through application of a three-dimensional heat transfer code that can handle temperature-dependent thermal conductivity.

(c) Because of the axisymmetric nature of the code, we had to assume, in modeling both experiments, that the heater drift had a cylindrical shape with a diameter of 5.3 m and that the extensometer drift was a toroid with the heater axis as the axis of its symmetry. Although the magnitude of error introduced by these assumptions is not considerable near the heater, and appears only over long periods of time, more accurate results would be obtained through modeling the exact form of the drifts by a 3-D code.

Although the granite at the site of the experiment was fractured and intruded by diabase and pegmatite dikes, comparison of measured data from various T-holes located in different directions did not indicate any detectable heterogeneity or anisotropy in thermal properties of the rock. In addition, the model based on continuous media was suitable for predicting the thermal field around the heater, even though it gave no consideration to the joints and faults that were mapped in the area of study.

5. CONCLUSION

In general, heat transfer in the rock at the site of the heater tests in Stripa is predominantly by conduction. However, an annular air gap between the heater and the rock could generate convection cells that would affect the distribution of the heat flux to the rock.

The granite at the site of the experiments was fractured and faulted, but the results of this study indicate that, as far as the thermal field is concerned, modeling the rock as a continuous, homogeneous, and isotropic medium does not introduce noticeable errors.

Temperature distribution in the rock around the heaters has been calculated by a two-dimensional axisymmetric finite element code that employs a non-uniform initial condition as well as temperature-dependent thermal conductivity. The maximum difference between these results and the measured temperatures is about 5°C. More accurate results, if necessary, may be obtained by a 3-D code that can incorporate convection in the air gap around the heater.

Analysis of the measured data showed that the most sensitive parameter for accurate measurement of temperature in the area close to the heater is the relative position of the thermocouples with respect to the heater. An error of a few centimeters in the position of the thermocouple can easily lead to temperature differences of several degrees.

The experience gained in this study provides valuable insights that can be used in the design and analysis of future experiments for the study of nuclear waste storage.

ACKNOWLEDGMENTS

We would like to acknowledge the helpful discussions and comments provided by T. Chan, N.G.W. Cook, P. Nelson and H. Carlsson. Oliver Wan assisted in programming and provided a code for computer-aided plotting of some of the figures. Andy DuBois and E. Binnall were very helpful in providing information about Stripa instruments and problems related to them. Mark Kubacki helped in extracting some of the data from the data logger strips.

We also thank M. Bailey for drafting many of the figures for this report.

REFERENCES

Binnall, E.P. and M. McEvoy, 1982. Assessment of Thermocouple Temperature Measurements During In-Situ Heater Experiments at Stripa, Sweden. Lawrence Berkeley Laboratory report LBL-12670, Berkeley, California (in preparation).

Burleigh, R. H., E.P. Binnall, A.O. DuBois, D.O. Norgren, and A.R. Ortiz, 1979. Electrical Heaters for Thermomechanical Tests at the Stripa Mine. Lawrence Berkeley Laboratory report LBL-7063, SAC-13, Berkeley, California.

Carslaw, H.S. and J.C. Jaeger, 1959. Conduction of Heat in Solids. Oxford University press.

Chan, T., E.P. Binnall, P. Nelson, R. Stolzman, O. Wan, C. Weaver, K. Ang, J. Braley, and M. McEvoy, 1980a. Thermal and Thermomechanical Data from In Situ Heater Experiments at Stripa, Sweden. Lawrence Berkeley Laboratory report LBL-11477, SAC-29, Berkeley, California.

Chan, T., P.A. Witherspoon, and I. Javandel,.1980b. "Heat Transfer in Underground Heating Experiments in Granite, Stripa, Sweden." Heat Transfer in Nuclear Waste Disposal, ASME, HTD-Vol. 11, pp. 1-8.

Chan, T., N.G.W. Cook, and C.F. Tsang, 1978. Theoretical Temperature Fields for the Stripa Heater Project. Lawrence Berkeley Laboratory report LBL-7082, SAC-09, Berkeley, California.

Cook, N.G.W. and M. Hood, 1978. Full-Scale and Time-Scale Heating Experiments at Stripa: Preliminary Results. Lawrence Berkeley Laboratory report LBL-7072, SAC-11, Berkeley, California.

Cook, N.G.W. and P.A. Witherspoon, 1978. Mechanical and Thermal Design Considerations For Radioactive Waste Repositories In Hard Rock. Lawrence Berkeley Laboratory report LBL-7073, SAC-10, Berkeley, California.

Gale, J.E. and P.A. Witherspoon, 1979. An Approach to the Fracture Hydrology at Stripa: Preliminary Results. Lawrence Berkeley Laboratory report LBL-7079, SAC-15, Berkeley, California.

Jeffry, J., T. Chan, N.G.W. Cook, and P.A. Witherspoon, 1979. Determination of In-Situ Thermal Properties of Stripa Granite from Temperature Measurements in the Full-Scale Heater Experiments: Methods and Primary Results. Lawrence Berkeley Laboratory report LBL-8424, SAC-24, Berkeley, California.

Kurfurst, P.J., T. Hugo-Persson and G. Rudolph, 1978. Borehole Drilling and Related Activities at the Stripa Mine. Lawrence Berkeley Laboratory report LBL-7080, SAC-05, Berkeley, California.

Lowry, W.E., B.W. Davis, and H. Cheung, H., 1980. "The Effects of Annular Air Gaps Surrounding an Emplaced Nuclear Waste Canister in Deep Geologic Storage." Heat Transfer in Nuclear Waste Disposal, ASME, HTD-vol.11, pp-69-75.

McEvoy, M.G., 1979. Data Acquisition, Handling, and Display for the Heater Experiments at Stripa. Lawrence Berkeley Laboratory report LBL-7062, SAC-14, Berkeley, California.

Olkiewicz, A., J.E. Gale, R. Thorpe, and B. Paulsson, 1979. Geology and Fracture System at Stripa. Lawrence Berkeley Laboratory report LBL-8907, SAC-21, Berkeley, California.

Pratt, H.R., T.A. Schrauf, L.A. Bills, and W.A. Hustrulid, 1977. Summary Report Thermal and Mechanical Properties of Granite, Stripa, Sweden. TR-77-92, Terra Tek, Salt Lake City Utah.

Polivka, R.M. and E. L. Wilson, 1976. Finite Element Analysis of Nonlinear Heat Transfer Problems. Report No. UC SESM 76-2, Department of Civil Engineering, University of California, Berkeley, California.

Saad, K.F., 1960. None Steady Flow Toward Wells Which Partially Penetrate Thick Artesian Aquifers. M.S. thesis, New Mexico Institute of Mining and Technology, Socorro, New Mexico.

Schrauf, T.A., H. Pratt, E. Simonson, W. Hustrulid, P. Nelson, A. DuBois, E. Binnall, and R. Haught, 1979. Instrumentation Evaluation, Calibration and Installation for the Heater Experiments at Stripa. Lawrence Berkeley Laboratory report LBL-8313, SAC-25, Berkeley, California.

Witherspoon, P.A. and O. Degerman, 1978. Swedish-American Cooperative Program on Radioactive Waste Storage in Mined Caverns. Lawrence Berkeley Laboratory report LBL-7049, SAC-01, Berkeley, California.

Wong, H.Y., 1977. Handbook of Essential Formulae and Data on Heat Transfer for Engineers. Longman, London and New York.

This report is part of a cooperative Swedish-American project supported by the U.S. Department of Energy and/or the Swedish Nuclear Fuel Supply Company. Any conclusions or opinions expressed in this report represent solely those of the author(s) and not necessarily those of The Regents of the University of California, the Lawrence Berkeley Laboratory, the Department of Energy, or the Swedish Nuclear Fuel Supply Company.

TECHNICAL INFORMATION DEPARTMENT
LAWRENCE BERKELEY LABORATORY
UNIVERSITY OF CALIFORNIA
BERKELEY, CALIFORNIA 94720